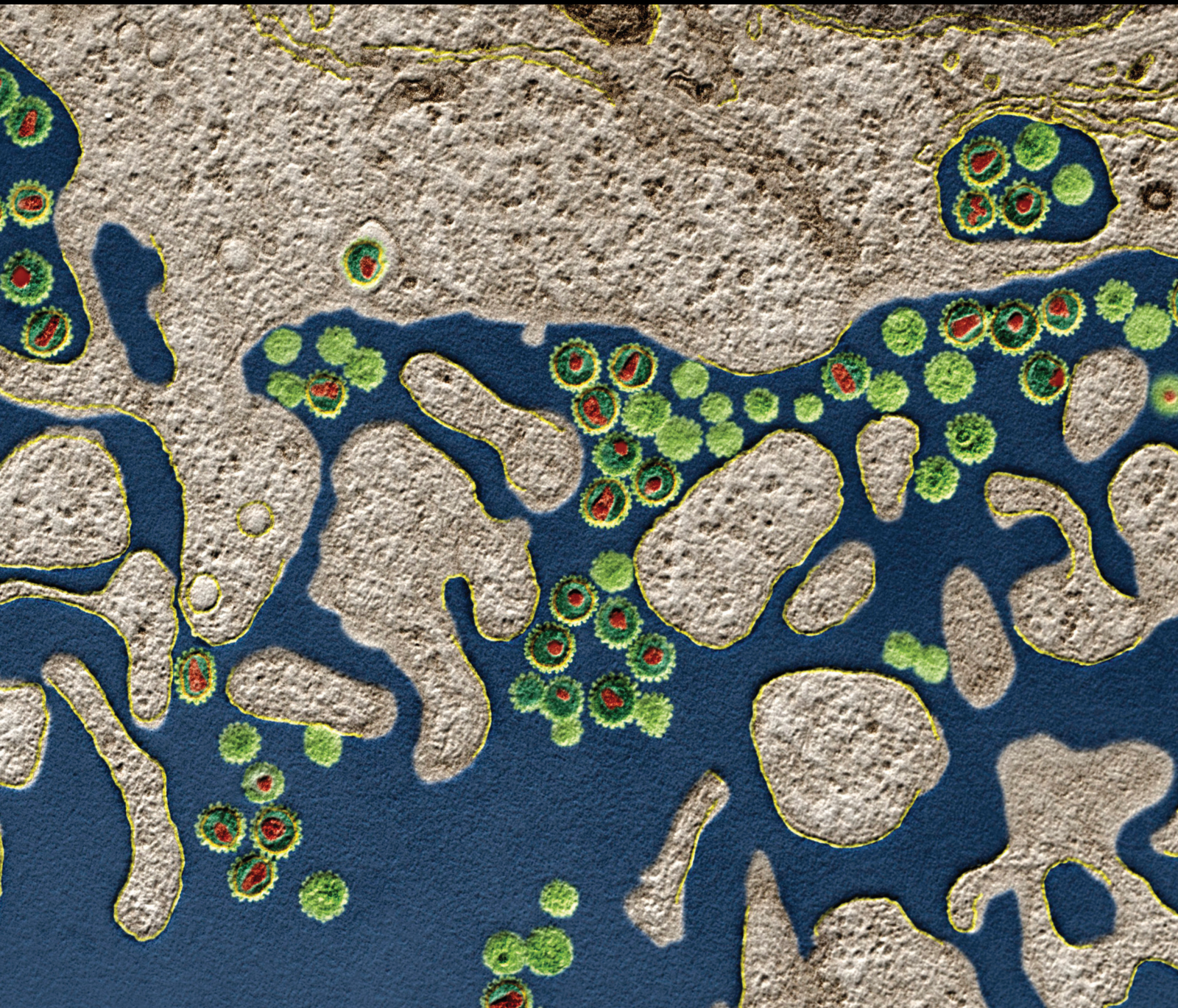


Epigenetics: a Growing Regulator in Immunology

Lead Guest Editor: Xianfeng Wang

Guest Editors: Vidula Vachharajani and Yanning Liu





Epigenetics: a Growing Regulator in Immunology

Journal of Immunology Research

Epigenetics: a Growing Regulator in Immunology

Lead Guest Editor: Xianfeng Wang





Guest Editors: Vidula Vachharajani and Yanning Liu



Copyright © 2021 Hindawi Limited. All rights reserved.

This is a special issue published in "Journal of Immunology Research." All articles are open access articles distributed under the Creative Commons Attribution License, which permits unrestricted use, distribution, and reproduction in any medium, provided the original work is properly cited.

Associate Editors

Douglas C. Hooper , USA
Senthamil R. Selvan , USA
Jacek Tabarkiewicz , Poland
Baohui Xu , USA

Academic Editors









Nitin Amdare , USA
Lalit Batra , USA
Kurt Blaser, Switzerland
Dimitrios P. Bogdanos , Greece
Srinivasa Reddy Bonam, USA
Carlo Cavaliere , Italy
Cinzia Ciccacci , Italy
Robert B. Clark, USA
Marco De Vincentiis , Italy
M. Victoria Delpino , Argentina
Roberta Antonia Diotti , Italy
Lihua Duan , China
Nejat K. Egilmez, USA
Theodoros Eleftheriadis , Greece
Eyad Elkord , United Kingdom
Weirong Fang, China
Elizabeth Soares Fernandes , Brazil
Steven E. Finkelstein, USA
JING GUO , USA
Luca Gattinoni , USA
Alvaro González , Spain
Manish Goyal , USA
Qingdong Guan , Canada
Theresa Hautz , Austria
Weicheng Hu , China
Giannicola Iannella , Italy
Juraj Ivanyi , United Kingdom
Ravirajsinh Jadeja , USA
Peirong Jiao , China
Youmin Kang , China
Sung Hwan Ki , Republic of Korea
Bogdan Kolarz , Poland
Vijay Kumar, USA
Esther Maria Lafuente , Spain
Natalie Lister, Australia

Daniele Maria-Ferreira, Saint Vincent and the Grenadines

Eiji Matsuura, Japan
Juliana Melgaço , Brazil
Cinzia Milito , Italy
Prasenjit Mitra , India
Chikao Morimoto, Japan
Paulina Niedźwiedzka-Rystwej , Poland
Enrique Ortega , Mexico
Felipe Passero, Brazil
Anup Singh Pathania , USA
Keshav Raj Paudel, Australia
Patrice Xavier Petit , France
Luis Alberto Ponce-Soto , Peru
Massimo Ralli , Italy
Pedro A. Reche , Spain
Eirini Rigopoulou , Greece
Ilaria Roato , Italy
Suyasha Roy , India
Francesca Santilli, Italy
Takami Sato , USA
Rahul Shivahare , USA
Arif Siddiqui , Saudi Arabia
Amar Singh, USA
Benoit Stijlemans , Belgium
Hiroshi Tanaka , Japan
Bufu Tang , China
Samanta Taurone, Italy
Mizue Terai, USA
Ban-Hock Toh, Australia
Shariq M. Usmani , USA
Ran Wang , China
Shengjun Wang , China
Paulina Wlasiuk, Poland
Zhipeng Xu , China
Xiao-Feng Yang , USA
Dunfang Zhang , China
Qiang Zhang, USA
Qianxia Zhang , USA
Bin Zhao , China
Jixin Zhong , USA
Lele Zhu , China









Contents

Corrigendum to “miR-183-5p Is a Potential Molecular Marker of Systemic Lupus Erythematosus”

Shaolan Zhou , Jing Zhang, Pengfei Luan , Zhanbing Ma , Jie Dang , Hong Zhu , Qian Ma , Yanfeng Wang , and Zhenghao Huo 


Corrigendum (2 pages), Article ID 9818203, Volume 2021 (2021)

miR-183-5p Is a Potential Molecular Marker of Systemic Lupus Erythematosus

Shaolan Zhou , Jing Zhang, Pengfei Luan , Zhanbing Ma , Jie Dang , Hong Zhu , Qian Ma , Yanfeng Wang , and Zhenghao Huo 

Research Article (11 pages), Article ID 5547635, Volume 2021 (2021)

IL-13 Augments Histone Demethylase JMJD2B/KDM4B Expression Levels, Activity, and Nuclear Translocation in Airway Fibroblasts in Asthma

Khuloud Bajbouj , Mahmood Y. Hachim , Rakhee K. Ramakrishnan , Huwaida Fazel , Jumana Mustafa , Shahed Alzaghari , Mahmoud Eladl , Jasmin Shafarin , Ronald Olivenstein, and Qutayba Hamid 

Research Article (10 pages), Article ID 6629844, Volume 2021 (2021)

Identification of a New Prognostic Risk Signature of Clear Cell Renal Cell Carcinoma Based on N⁶-Methyladenosine RNA Methylation Regulators

Yan Zhang, Yao Yao, Xiaochen Qi, Jianyi Li, Meihong Liu, Xiangyu Che , Yingkun Xu , and Guangzhen Wu 

Research Article (23 pages), Article ID 6617841, Volume 2021 (2021)

Corrigendum

Corrigendum to “miR-183-5p Is a Potential Molecular Marker of Systemic Lupus Erythematosus”

Shaolan Zhou ^{1,2} **Jing Zhang** ^{1,3,4} **Pengfei Luan** ^{1,3} **Zhanbing Ma** ^{1,3} **Jie Dang** ^{1,3}
Hong Zhu ² **Qian Ma** ^{1,3} **Yanfeng Wang** ^{1,3} and **Zhenghao Huo** ^{1,3,5}

¹Department of Medical Genetics and Cell Biology, College of Basic Medicine, Ningxia Medical University, Yinchuan, Ningxia, China

²Department of Rheumatology, General Hospital of Ningxia Medical University, Yinchuan, Ningxia, China

³Key Laboratory of Fertility Preservation and Maintenance (Ningxia Medical University), Ministry of Education, Yinchuan, Ningxia, China

⁴Ningxia Key Laboratory of Cerebrocranial Diseases, Ningxia Medical University, Yinchuan, Ningxia, China

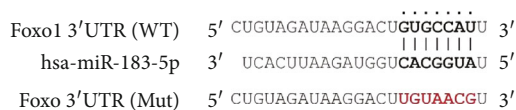
⁵Department of Biology, Gansu Medical College, Pingliang, Gansu, China

Correspondence should be addressed to Zhenghao Huo; huozhh@163.com

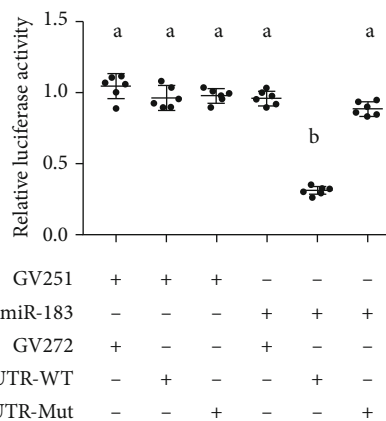
Received 14 August 2021; Accepted 14 August 2021; Published 11 September 2021

Copyright © 2021 Shaolan Zhou et al. This is an open access article distributed under the Creative Commons Attribution License, which permits unrestricted use, distribution, and reproduction in any medium, provided the original work is properly cited.

In the article titled “miR-183-5p Is a Potential Molecular Marker of Systemic Lupus Erythematosus” [1], Figure 8 was formatted incorrectly. The authors have corrected this error and provided the correct figure as follows:



(a)



(b)

FIGURE 8: miR-183-5p directly targets Foxo1 3'UTR. (a) The binding site of miR-183-5p and the position 226-242 of Foxo1 3'UTR wild type (WT) and mutant type (mut). (b) miR-183-5p ectopic expression significantly inhibited luciferase activity of the wild-type Foxo1 3'UTR reporter plasmid in comparison with the mutated counterpart. Groups labelled with different letters are statistically different from each other ($*p < 0.05$). Differences between groups were analyzed for statistical significance by ANOVA with Fischer's probable least-square difference post hoc test.

References

- [1] S. Zhou, J. Zhang, P. Luan et al., "miR-183-5p Is a Potential Molecular Marker of Systemic Lupus Erythematosus," *Journal of Immunology Research*, vol. 2021, 11 pages, 2021.

Research Article

miR-183-5p Is a Potential Molecular Marker of Systemic Lupus Erythematosus

Shaolan Zhou ^{1,2}, Jing Zhang ^{1,3,4}, Pengfei Luan ^{1,3}, Zhanbing Ma ^{1,3}, Jie Dang ^{1,3},
Hong Zhu ², Qian Ma ^{1,3}, Yanfeng Wang ^{1,3} and Zhenghao Huo ^{1,3,5}

¹Department of Medical Genetics and Cell Biology, College of Basic Medicine, Ningxia Medical University, Yinchuan, Ningxia, China

²Department of Rheumatology, General Hospital of Ningxia Medical University, Yinchuan, Ningxia, China

³Key Laboratory of Fertility Preservation and Maintenance (Ningxia Medical University), Ministry of Education, Yinchuan, Ningxia, China

⁴Ningxia Key Laboratory of Cerebrocranial Diseases, Ningxia Medical University, Yinchuan, Ningxia, China

⁵Department of Biology, Gansu Medical College, Pingliang, Gansu, China

Correspondence should be addressed to Zhenghao Huo; huozhh@163.com

Received 23 February 2021; Revised 19 April 2021; Accepted 26 April 2021; Published 8 May 2021

Academic Editor: Xianfeng Wang

Copyright © 2021 Shaolan Zhou et al. This is an open access article distributed under the Creative Commons Attribution License, which permits unrestricted use, distribution, and reproduction in any medium, provided the original work is properly cited.

Objective. To investigate microRNA (miRNA) expression profiles in individuals with systemic lupus erythematosus (SLE) and identify the valuable miRNA biomarkers in diagnosing and monitoring SLE. **Methods.** Next-generation sequencing (NGS) was performed to assess miRNA amounts in peripheral blood mononuclear cells (PBMCs) from four SLE cases and four healthy controls. Quantitative polymerase chain reaction (qPCR) was carried out for validating candidate miRNAs in 32 SLE cases and 32 healthy controls. In addition, receiver operating characteristic (ROC) curve analysis was completed to evaluate diagnostic performance. Finally, the associations of candidate miRNAs with various characteristics of SLE were analyzed. **Results.** A total of 157 miRNAs were upregulated, and 110 miRNAs were downregulated in PBMCs from SLE cases in comparison to healthy controls, of which the increase of miR-183-5p and decrease of miR-374b-3p were validated by qPCR and both showed good diagnostic performance for SLE diagnosis. Besides, miR-183-5p expression levels displayed a positive association with SLE disease activity index (SLEDAI) and anti-dsDNA antibody amounts. **Conclusion.** Our data indicated that miR-183-5p is a promising biomarker of SLE.

1. Introduction

Systemic lupus erythematosus (SLE) is an important chronic, inflammatory, and multisystem autoimmune pathology, featuring the production of autoantibodies against various nuclear self-antigens. The precise molecular mechanisms underlying the pathogenesis of SLE remain uncertain but encompass complex interactions of genetic, epigenetic, and environmental factors [1, 2]. Numerous reports have extensively focused on identifying susceptibility loci/genes in SLE [3–5]. Genome-wide association studies (GWAS) have revealed the major signaling pathways affected in SLE, but no single gene defect has been identified as the principal pathogenic factor contributing to SLE induction [6–8]. In

addition, SLE monozygotic twins harboring identical genes show a low concordance in disease phenotypes, suggesting that nongenetic factors such as epigenetic parameters play a critical role in SLE pathogenesis [9, 10].

MicroRNAs (miRNAs) constitute a group of small, single-stranded noncoding RNAs, which suppress genes posttranscriptionally through binding to specific seed sequences in their target genes, causing translation inhibition or target gene degradation [11]. miRNA is a typical type of epigenetic modification, which contributes to the pathogenesis of multiple autoimmune diseases [12]. Previous evidence indicates the potential role of miRNAs in regulating immune cell development and maintaining immune homeostasis [13–16]. Vinuesa and collaborators identified multiple target

sites for >140 conserved miRNAs in SLE susceptibility genes [17]. miRNAs are also known to have important functions in the molecular mechanisms of SLE by interacting with innate and adaptive immunity [18–21]. Furthermore, miRNAs represent potent biomarkers for the diagnosis and monitoring of diverse pathologies thanks to their high stability [22, 23]. However, the functions of miRNAs in the diagnosis and stratification of SLE remain undefined. Therefore, understanding the associations of miRNAs with SLE would provide novel insights into disease pathogenesis and help develop new diagnostic biomarkers [24].

The present study performed next-generation sequencing (NGS) to examine miRNA profiles in SLE cases and healthy subjects and to determine the values of select miRNAs in diagnosing and monitoring SLE.

2. Methods

2.1. Patients and Specimen Collection. In this study, SLE patients were enrolled in Rheumatology and Immunology Department, General Hospital of Ningxia Medical University. The subjects were included according to the criteria of the American College of Rheumatology (1997 revision) [25]. Subjects who had additional rheumatic pathologies, infectious diseases, or cancers were excluded. Disease activity was evaluated according to the SLE disease activity index-2000 (SLEDAI-2000) [26]. Age- and sex-matched healthy controls undergoing routine health exams were strictly assessed by two experienced rheumatologists and archived in parallel. All healthy controls with any medical histories (including rheumatic pathologies, infectious diseases, or cancers), family histories (including rheumatic pathologies), or rheumatic manifestations (including nephritis, arthritis, rash, and serositis) were excluded. The peripheral venous blood from each subject was collected in evacuated tubes containing EDTA as the anticoagulant and peripheral blood mononuclear cells (PBMCs) were isolated within 2 hours. This study was approved by the Ethics Committee of General Hospital of Ningxia Medical University. All participants signed written informed consent.

2.2. Study Flow. The study comprised two main phases, the exploration and validation. In the exploration phase, PBMC specimens from four SLE cases and four healthy controls were examined in NGS to detect miRNA expression profiles. In the validation phase, PBMC specimens from 32 SLE patients and 32 healthy controls were assessed by quantitative polymerase chain reaction (qPCR) to detect the expression levels of candidate miRNAs for NGS data validation.

2.3. Clinical and Laboratory Assessments. The features of SLE and control cases in the validation phase are displayed in Table 1. Clinical symptoms in SLE were lupus nephritis, arthritis (at least two joints involved), rash (including discoid or butterfly rash, oral ulcer, and photosensitivity), and serositis (including pleuritis and pericarditis). Laboratory features included erythrocyte sedimentation rate (ESR), hypersensitive C-reactive protein (CRP), complement 3 (C3), and

TABLE 1: Clinicopathological and laboratory data of SLE and control cases.

Parameters	SLE ($n = 32$)	Healthy controls ($n = 32$)
Age (years)	34.8 ± 10.6	33.5 ± 10.3
Gender (male/female), n	4/28	4/28
Arthritis, n (%)	19 (59.4%)	—
Lupus nephritis, n (%)	15 (46.9%)	—
Serositis, n (%)	10 (31.3%)	—
Rash, n (%)	17 (53.1%)	—
ANA, n (%)	32 (100%)	—
ESR (mm/h)	39.83 ± 32.45	—
CRP (mg/L)	18.57 ± 28.31	—
Complement 3 (g/L)	0.71 ± 0.29	—
Anti-dsDNA antibody (IU/mL)	98.84 ± 130.46	—
SLEDAI score	11.34 ± 5.97	—

The average data of age, ESR, CRP, complement 3, anti-dsDNA, and SLEDAI score are presented as the mean ± SD.

anti-dsDNA antibody. The SLEDAI was assessed for each patient.

2.4. PBMC Isolation and RNA Purification. PBMC isolation was performed from SLE and healthy control cases by the Ficoll-Paque density gradient centrifugation assay. Briefly, the diluted blood sample was carefully layer on Ficoll-Paque and centrifuged at 400 g for 30 min at 18°C to 20°C, the layers of mononuclear cells were transferred to a sterile centrifuge tube, and the isolated cells were washed with balanced salt solution [27]. Total RNA was purified with Trizol by the protocol as provided by the manufacturer. RNA quality and amounts were evaluated on a NanoDrop 2000 (Thermo, USA), by 1% agarose gel electrophoresis and Agilent 2100 Bioanalyzer (Agilent Technologies, USA).

2.5. Library Generation and Sequencing. The miRNA sequencing libraries were prepared from extracted miRNA samples using the Illumina small RNA sample prep kit according to instructions provided by the manufacturer. Small RNAs (18–30 nt) were isolated from total RNA to perform ligations with 5′ and 3′ adapters. Then, RT-PCR was completed taking the ligation products as templates. Finally, the PCR products were clustered, and the Illumina HiSeq™2500 platform (Illumina, USA) was utilized for sequencing.

2.6. Differential Expression Analysis. For miRNA sequencing, sequence reads were cleaned after library construction. Then, miRNAs in various groups were compared after raw read count normalization; the data were log-transformed according to the fold change (FC) formula [FC = log₂ (treatment/control)]. Statistical significance was defined as $p < 0.05$ and log₂ (FC) > 0.5.

2.7. Preparation of cDNA and qPCR. Complementary DNA (cDNA) was synthesized with the PrimeScript™ RT reagent kit (Takara Biotech, China) with miRNA stem loop primers. The qPCR reactions were carried out with TB Green® Premix Ex Taq™ II kit (Takara Biotech) on an ABI 7500 real-time PCR system (Applied Biosystems, USA). The PCR amplification procedure was as follows: denaturation at 95°C for 30s, followed by 40 cycles of 95°C for 5s and 34s at 60°C. Candidate miRNA and mRNA amounts were calculated by the $2^{-\Delta\Delta C_t}$ method, with U6 and GAPDH used for normalization, respectively. Primers for qPCR are shown in Supplementary Table 1.

2.8. Dual-Luciferase Reporter Assay. To develop the plasmid containing human Foxo1 3'UTR, plasmid GV272 was purchased from Shanghai Genechem Company and digested with *Xba*I. In this plasmid, the expression of firefly luciferase is driven by SV40 promoter; a multicloning site is located downstream of firefly luciferase. A fragment sequence of 454 bp was chemically synthesized containing either wild type human Foxo1 3'UTR (NM_002015) or the counterpart with mutations on miR-183-5p binding site (GTGCCAT), followed by the ligation into GV272, resulting in plasmid GV-Foxo1-3'UTR-WT or GV-Foxo1-3'UTR-Mut. To develop plasmid GV-hmiR-183-5p, a chemically synthesized DNA sequence was inserted into plasmid GV251, in which miR-183-5p will be translated under the promoter of human U6. All constructs were verified by sequencing. Renilla luciferase-expressing plasmid was ordered from Shanghai Genechem Company.

To verify the functional inhibition of miR-183 to human Foxo1 expression, dual-luciferase reporter assay was completed by cotransfection of miRNA plasmid (GV251 or GV-hmiR-183) and firefly luciferase plasmid (GV272, or GV-Foxo1-3'UTR-WT, or GV-Foxo1-3'UTR-Mut). Briefly, 293T cells were seeded into a 24-well plate in 1 mL complete medium. The next day, miRNA plasmid (0.4 μ g for each) was cotransfected with firefly luciferase plasmid (0.1 μ g for each). In each transfection, Renilla luciferase-expressing plasmid (0.02 μ g for each) was incorporated as the internal control. After 48 hours, the cells were lysed and dual-luciferase assay was performed based on the instruction of Promega kit (Cat# E1910). The firefly luciferase reading was corrected by Renilla luciferase. The data were presented by relative luciferase activity as the mean \pm standard deviation (SD).

2.9. Statistical Analysis. SPSS 23.0 (SPSS, USA) and GraphPad Prism 7.0 (GraphPad Software Inc., USA) were employed for data analysis. Data are presented as the mean \pm SD, from triplicate assays repeated at least thrice. Two-tailed Student's *t*-test or one-way analysis of variance (ANOVA) was performed for comparisons. The Spearman's test was carried out to assess associations of candidate miRNAs with continuous variables in SLE cases. Receiver operating characteristic (ROC) curve analysis was carried out to evaluate the performances of candidate miRNAs and to distinguish SLE cases from controls. $p < 0.05$ indicated statistical significance.

3. Results

3.1. Correlation Heat Map Analysis for Total miRNA Patterns. To investigate the distinct cluster of the miRNA expression profiles between the samples from SLE patients and healthy controls, Pearson correlation was performed. The correlation heat map demonstrated that SLE patients and controls had distinct clusters based on the miRNA expression profiles, except for SLE_F1 (Figure 1). Our data indicated that miRNA expression profiles were able to differentiate SLE patients from controls.

3.2. Volcano Plot and Heat Map Analyses. To identify the differentially expressed miRNAs between SLE and controls, the hierarchical cluster analysis was carried out. The volcano plot revealed 157 upregulated and 110 downregulated miRNAs in SLE cases in comparison to controls [\log_2 (FC) > 0.5 and $p < 0.05$] (Figure 2(a)). The detailed information of 267 differentially expressed miRNAs is displayed in Supplementary Table 2. Heat map analysis revealed that these differentially expressed miRNAs could clearly discern SLE patients from controls (Figure 2(b)).

3.3. GO and KEGG Enrichment Analyses. To assess the biological functions and pathways of the above differentially expressed miRNAs, GO and KEGG enrichment analyses were carried out. GO enrichment analysis revealed the involvement of the differentially expressed miRNAs in multiple biological processes such as molecular function, protein binding, and nucleotide binding activity (Figure 3(a)). KEGG enrichment analysis demonstrated that the differentially expressed miRNAs were involved in different pathways such as cancer, MAPK signaling, and Rap1 signaling (Figure 3(b)). Both enrichment analyses revealed that the differentially expressed miRNAs were implicated in inflammatory and immune activities.

3.4. Expression of Candidate miRNAs in SLE Cases and Healthy Controls in the Validation Phase. To further evaluate miRNA dysregulation in SLE, two upregulated miRNAs (hsa-miR-1-3p and hsa-miR-183-5p) and two downregulated miRNAs (hsa-miR-374b-3p and hsa-miR-19b-3p) were assessed by qPCR in 32 SLE and 32 healthy controls. Among the four candidate miRNAs, miR-183-5p was upregulated ($p = 0.005$) (Figure 4(a)) and miR-374-3p was downregulated ($p = 0.016$) (Figure 4(b)) in SLE cases in comparison with controls, while miR-1-3p ($p = 0.318$) (Figure 4(c)) and miR-19b-3p ($p = 0.115$) (Figure 4(d)) levels did not show significance between the two groups.

3.5. Diagnostic Values of miRNAs. To evaluate the potential diagnostic value of miR-183-5p and miR-374b-3p in SLE, ROC curve analysis was performed. Areas under the ROC curves (AUCs) for miR-183-5p and miR-374b-3p were 0.703 (95% CI: 0.574–0.833) and 0.681 (95% CI: 0.542–0.826), respectively. Meanwhile, miR-183-5p combination with miR-374b-3p yielded an AUC of 0.832 (95% CI: 0.727–0.937) (Figure 5). These results suggested that miR-183-5p and/or miR-374b-3p presented a good diagnostic

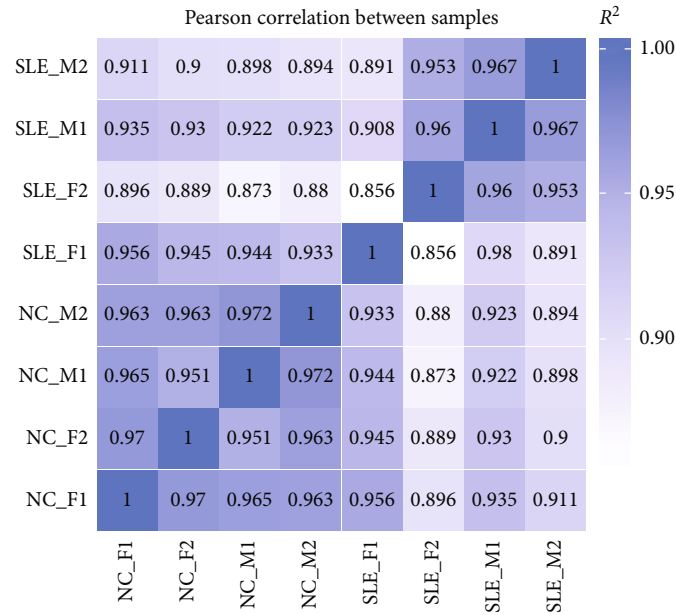


FIGURE 1: Correlation heat map analysis. SLE and controls presented distinct clusters based on the miRNA expression profiles of the eight specimens except for SLE_F1.

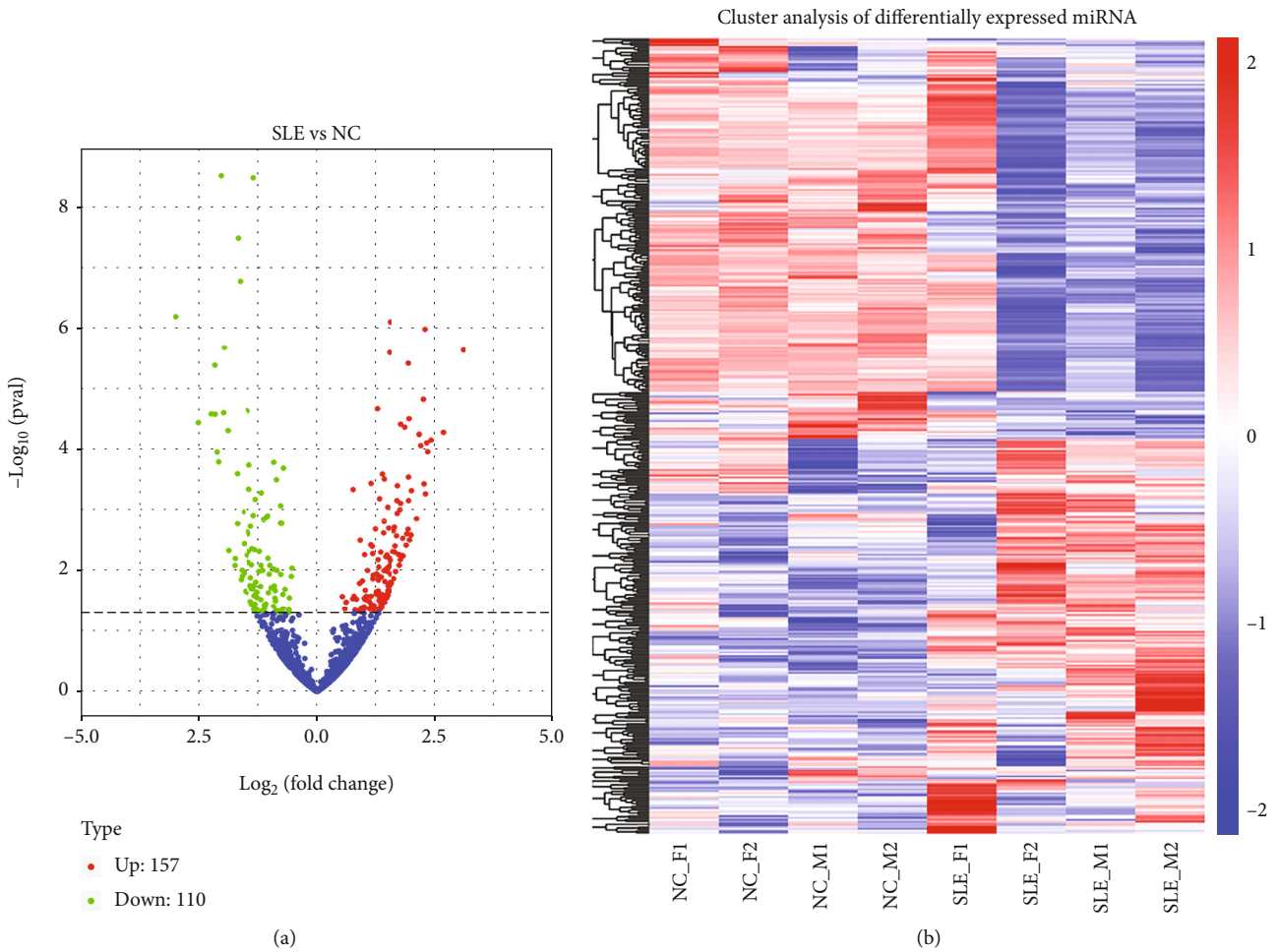
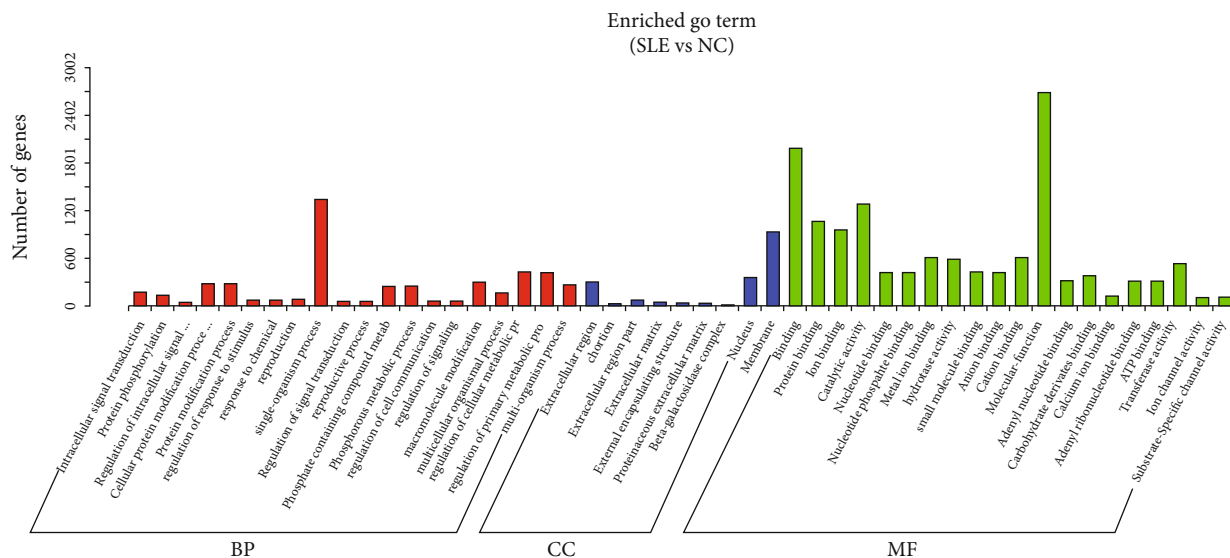
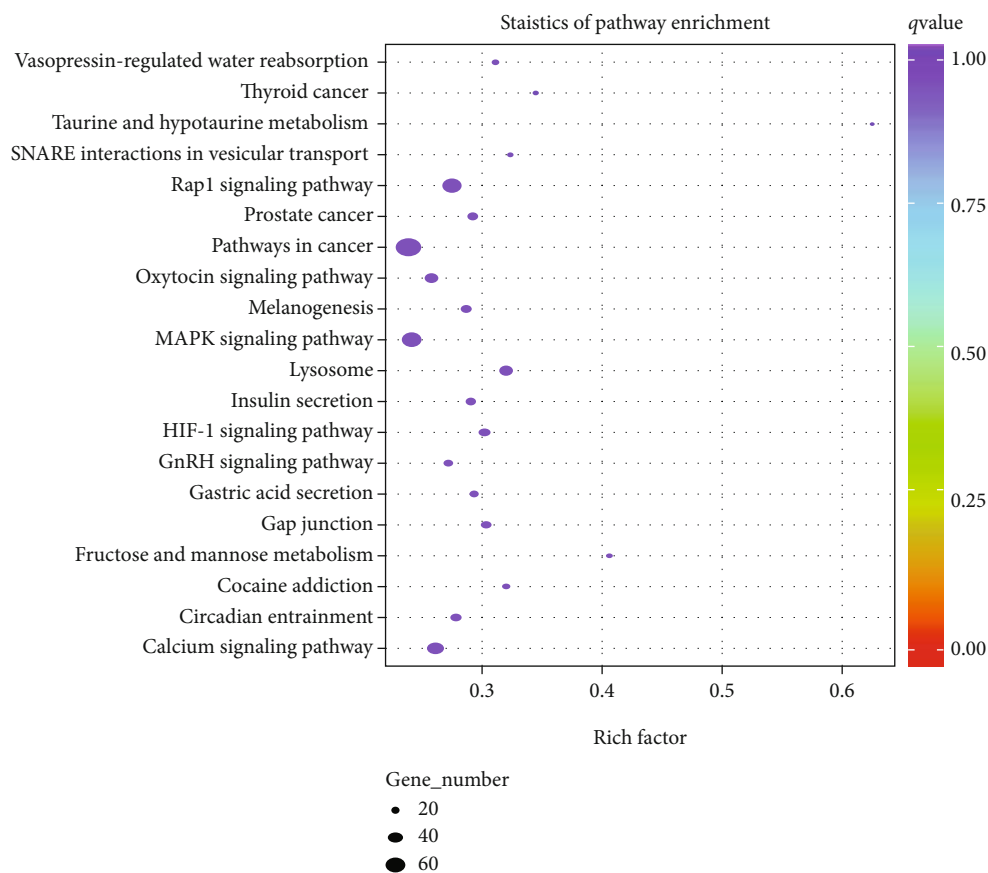


FIGURE 2: Volcano plot and heat map analyses. (a) Totally, 157 and 110 miRNAs were upregulated and downregulated, respectively, in SLE cases compared with controls. (b) The differentially expressed miRNAs well differentiated SLE cases from healthy controls.



(a)



(b)

FIGURE 3: GO and KEGG enrichment analyses of the differentially expressed miRNAs. (a) GO enrichment analysis showed that the differentially expressed miRNAs were correlated with various biological processes such as molecular function, protein binding, and nucleotide binding activity. (b) KEGG enrichment analysis revealed the involvement of the differentially expressed miRNAs in various pathways such as cancer, MAPK signaling, and Rap1 signaling.

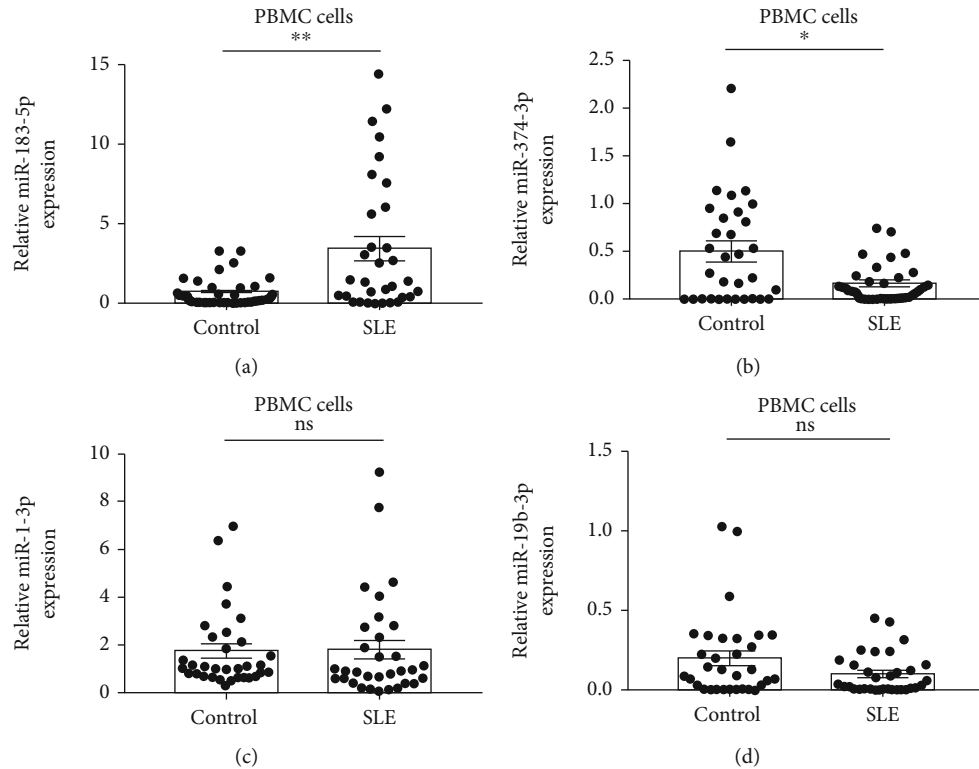


FIGURE 4: Expression levels of candidate miRNAs in SLE cases and controls in the validation phase. The expression level of miRNA was determined using qPCR from each group. Our data found that miR-183-5p was upregulated (a) and miR-374b-3p was downregulated (b). However, no significant difference was exhibited with regard to miR-1-3p (c) and miR-19b-3p (d). ns: $p > 0.05$; * $p < 0.05$; ** $p < 0.01$.

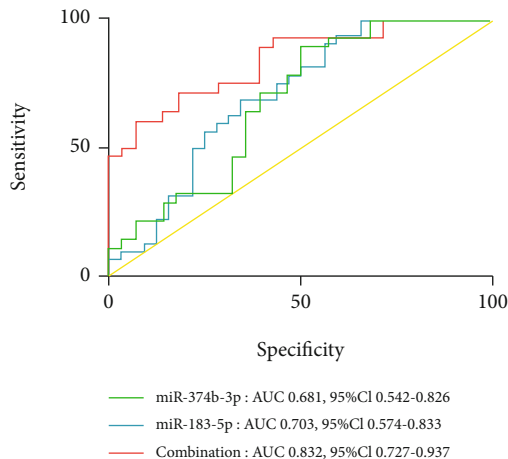


FIGURE 5: Diagnostic values of miR-183-5p and miR-374b-3p. ROC curve analysis indicated AUCs for miR-183-5p and miR-374b-3p of 0.703 (: 0.574–0.833) and 0.681 (95% CI: 0.542–0.82), respectively. Combination of miR-183-5p and miR-374b-3p yielded an AUC of 0.832 (95% CI: 0.727–0.937).

value for SLE detection, with the combination being superior to either miRNA used alone.

3.6. miR-183-5p Is Associated with Patient Data in SLE. To determine the potential functions of miR-183-5p and miR-374b-3p in SLE, the associations of miR-183-5p and miR-374b-3p with the characteristics of SLE patients were exam-

ined. miR-183-5p was elevated in SLE cases with nephritis compared to the counterparts without nephritis ($p = 0.018$) (Figure 6(a)). SLE cases with arthritis had increased miR-183-5p amounts compared with counterparts without arthritis ($p = 0.022$) (Figure 6(b)). In correlation analysis, miR-183-5p expression displayed significant positive associations with SLEDAI score ($p = 0.040$) (Figure 6(c)) and anti-dsDNA antibody levels ($p = 0.033$) (Figure 6(d)). Meanwhile, miR-374b-3p amounts in SLE cases were similar regardless of clinical features ($p > 0.05$), and no correlations of miR-374b-3p expression levels were observed with various clinical characteristics ($p > 0.05$).

3.7. Bioinformatics Analysis of the Potential Target Genes of miR-183-5p. To further explore the underlying molecular mechanisms, the potential target genes of miR-183-5p were predicted in Targetscan (<http://www.targetscan.org>), miRDB (<http://mirdb.org>), and miRTarBase (<http://mirtarbase.cuhk.edu.cn>) platforms (Figure 7(a)). The overlapped genes on these three platforms were evaluated for Protein-Protein Interaction (PPI) network analysis to discover the interactions between the predictive target genes. Finally, the network consisting of 40 nodes and 81 edges is shown in Figure 7(b). Foxo1 was chosen for further investigations due to the high degree of connectivity.

3.8. Functional Binding of miR-183-5p to Foxo1. To test whether miR-183-5p can directly target human Foxo1, we did bioinformatics analysis through the online tool,

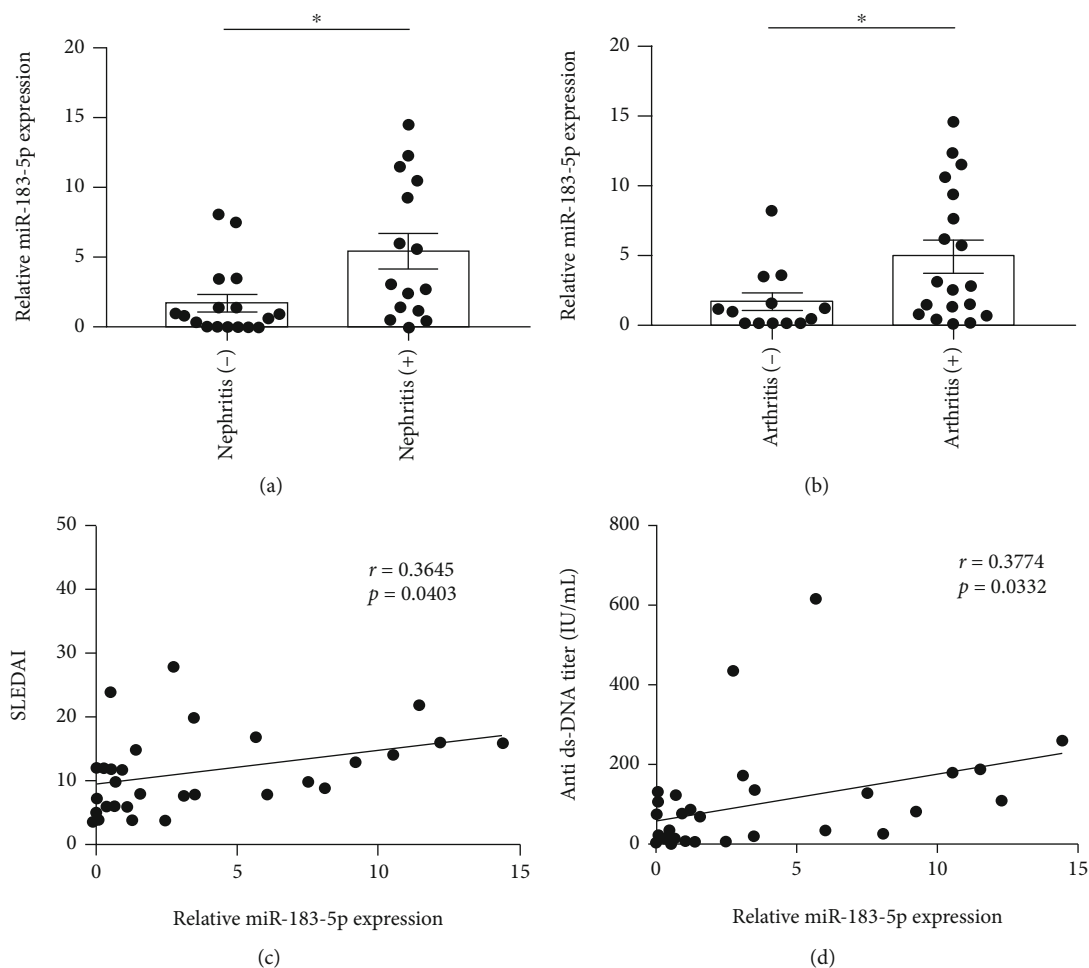


FIGURE 6: miR-183-5p is associated with patient data in SLE. The expression level of miR-183-5p was higher in SLE cases with nephritis (a) or arthritis (b) in comparison with negative SLE counterparts, showing significant positive associations with SLEDAI score (c) or anti-dsDNA antibody levels (d). * $p < 0.05$.

TargetScan platform (<http://www.targetscan.org>). We found miR-183-5p could directly bind to human Foxo1 3'UTR at sequences (GUGCCAU) (Figure 8(a)). To further verify the binding in cell culture study, luciferase reporter plasmid containing Foxo1 3'UTR (and the mutant version) and miR-183-5p expressing plasmid were developed. The luciferase mRNA will be degraded once miR-183-5p binds to Foxo1 3'UTR. The plasmids were cotransfected into 293T cells for dual-luciferase assay. The data showed that the cotransfection of miR-183-5p plasmid with wild type 3'UTR luciferase plasmid knocked down luciferase activity significantly (Figure 8(b)), while the combination of miR-183-5p plasmid with mutant 3'UTR luciferase plasmid displayed a similar luciferase level to the mock transfections. Collectively, our cell culture study functionally demonstrated the targeting and binding of miR-183-5p to the wild type of human Foxo1 3'UTR rather than the mutant version.

3.9. Decreased mRNA Expression Levels of the Target Gene Foxo1. To answer the importance that miR-183-5p can target and bind to Foxo1 3'UTR in patients, we compared the

expression level of Foxo1 between SLE cases and healthy controls and analyzed its correlation with miR-183-5p amounts in SLE. The Foxo1 mRNA expression level was markedly decreased in SLE cases compared with healthy controls (Figure 9, $p < 0.0001$). In correlation analysis, miR-183-5p and Foxo1 showed the inverse correlation in SLE patients ($p = 0.049$). The results further indicated that miR-183-5p is involved in the mechanisms of SLE by inhibiting the expression of Foxo1.

4. Discussion

Growing evidence indicates that miRNAs have critical functions in immune homeostasis and are involved in the pathophysiological mechanisms of various autoimmune ailments such as SLE [28–30]. Next-generation sequencing is capable of identifying novel transcripts and detecting low-expression transcripts. Here, NGS was performed to analyze the miRNA profiles of PBMCs from SLE and healthy controls. A total of 157 and 110 miRNAs were upregulated and downregulated, respectively, in SLE cases in comparison with healthy controls. GO enrichment analysis revealed the

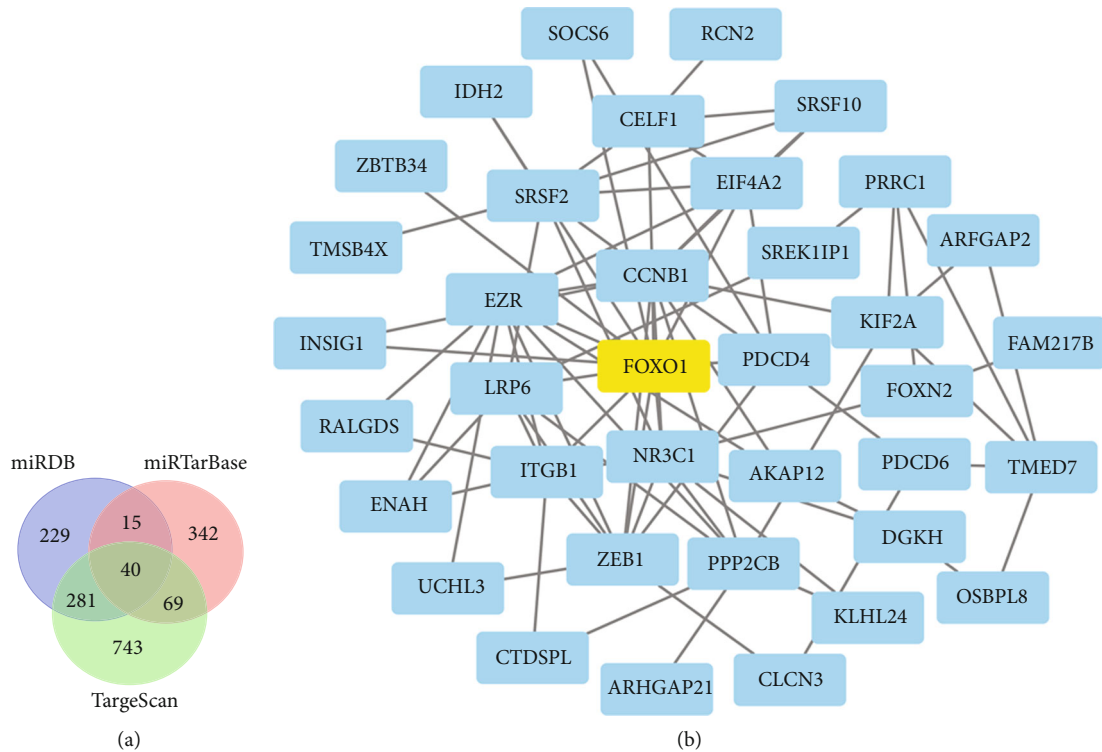


FIGURE 7: Bioinformatics analysis of the potential target genes of miR-183-5p. (a) The potential target genes of miR-183-5p were predicted in Targetscan7.1, miRDB, and miRTarBase platforms. (b) PPI network analysis showed the Foxo1 with high degrees of connectivity in potential target genes.

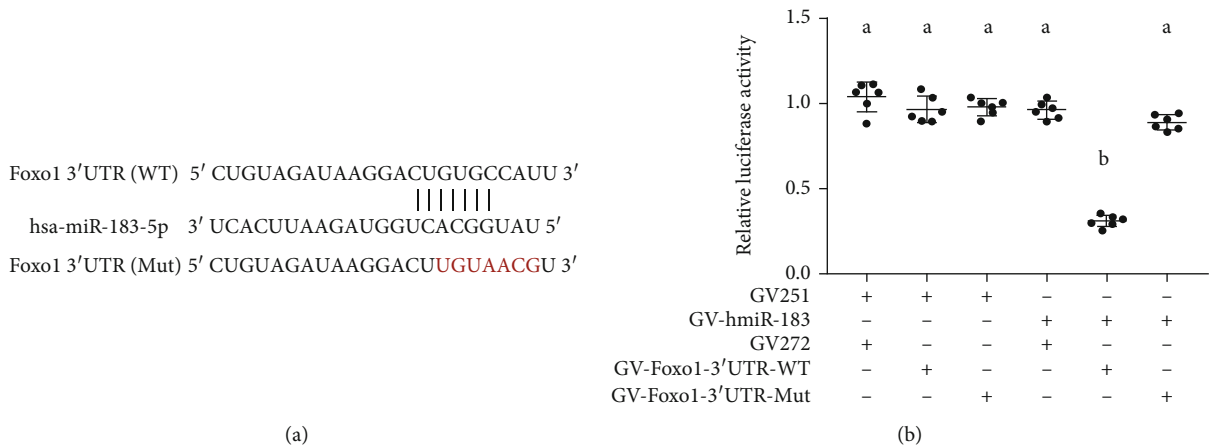


FIGURE 8: miR-183-5p directly targets Foxo1 3'UTR. (a) The binding site of miR-183-5p and the position 226-242 of Foxo1 3'UTR wild-type (WT) and mutant-type (mut). (b) miR-183-5p ectopic expression significantly inhibited luciferase activity of the wild-type Foxo1 3'UTR reporter plasmid in comparison with the mutated counterpart. Groups labeled with different letters are statistically different from each other. * $p < 0.05$. Differences between groups were analyzed for statistical significance by ANOVA with Fischer's probable least-square difference post hoc test.

involvement of the differentially expressed miRNAs in various biological processes such as molecular function, protein binding, and nucleotide binding activity. In addition, KEGG analysis demonstrated that the target genes of differentially expressed miRNAs participated in the MAPK and Rap1 pathways, which regulate inflammatory responses.

The complex manifestations of SLE make its diagnosis difficult. Therefore, further assessment of the above miRNAs

might help discover new diagnostic biomarkers of SLE. To this end, two upregulated and two downregulated miRNAs were selected and validated in 32 SLE cases and 32 controls. As depicted above, miR-183-5p and miR-374b-3p amounts were elevated and reduced, respectively, in SLE cases in comparison with controls. Meanwhile, the AUC for miR-183-5p combined with miR-374b-3p was 0.832 (95% CI: 0.727–0.937). These results demonstrated the diagnostic value of

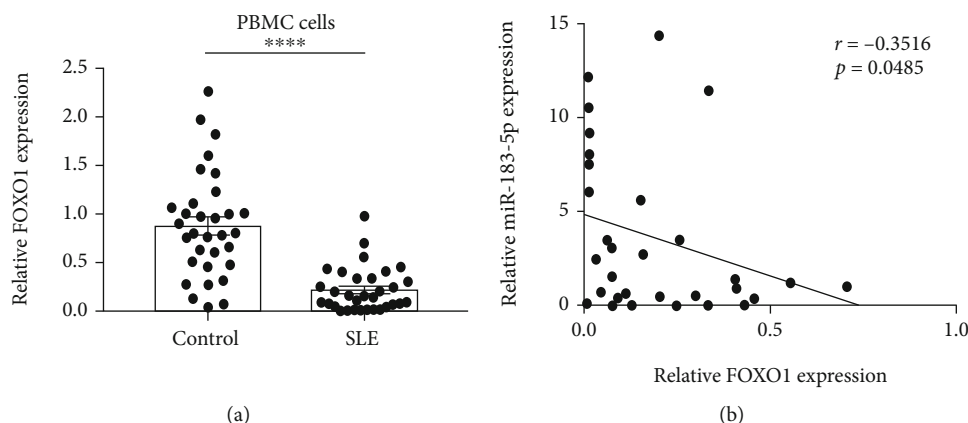


FIGURE 9: Expression of Foxo1 in subjects and with miR-183-5p levels (a) Foxo1 amounts are reduced in SLE cases ($n = 32$) in comparison with healthy controls ($n = 32$). (b) Spearman's rank correlation revealed a negative relationship between Foxo1 amounts and miR-183-5p expression levels. * $p < 0.05$; **** $p < 0.0001$.

miR-183-5p and miR-374b-3p combination in SLE. Moreover, SLE cases with nephritis and arthritis had elevated miR-183-5p amounts compared with counterparts without these clinical features, indicating miR-183-5p might be involved in the destruction of the kidneys and joints. Next, the associations of miR-183-5p and miR-374b-3p with clinical characteristics of SLE cases were examined. As demonstrated above, miR-183-5p amounts displayed positive correlations with SLEDAI and anti-dsDNA antibody in SLE patients, indicating miR-183-5p could be a good indicator for evaluating SLE activity.

miR-374b was previously found to inhibit cell growth and promote apoptosis in T cell lymphoblastic lymphoma via suppression of AKT1 and Wnt-16 [31], which were correlated with immune activities in autoimmune diseases [32, 33]. In addition, miR-374b inhibits cell proliferation and enhances apoptosis via p38/ERK signaling by interacting with JAM-2 [34], suggesting miR-374b contributes to inflammation-associated pathways. Therefore, miR-374b may be involved in SLE-related inflammatory reactions.

miR-183-5p represents the main member of the miR-183 cluster, which can be dramatically induced in immune cells after activation. Previous reports indicated that the miR-183 cluster has a critical function in immune cell functions by regulating several proinflammatory pathways [35]. Thiel et al. found that miR-183 and miR-96 amounts are elevated in CD4⁺ T cells obtained from the peripheral blood of Graves' orbitopathy (GO) cases, and adoptive transfer of miR-183 and miR-96 overexpressing antigen-specific T cells accelerates the onset of autoimmune diabetes, whereas transferring specific antagomirs in CD4⁺ T cells prolongs disease onset [36]. miRNAs perform biological functions by inhibiting their target genes. We found Foxo1 was the potential functional target genes of miR-183-5p by bioinformatics analysis, and the direct targeting relationship was validated by dual-luciferase reporter assay in our study. Foxo1 activation is critical in autoimmune diseases [37, 38]. Furthermore, Foxo1 is also tightly correlated with the immune response. As shown above, Foxo1 amounts were significantly reduced in PBMCs from SLE cases in comparison with healthy controls,

and miR-183-5p and Foxo1 showed an inverse correlation in SLE patients. This could reflect a potential mechanism wherein suppression of Foxo1 by miR-183-5p contributes to SLE pathogenesis. Ichiyama and colleagues reported that Foxo1 downregulation by miR-183 cluster constitutes one of the important mechanisms by which Th17 cells become pathogenic and induce disrupted balance between Treg and Th17 cells [39]. This further indicated that exploring the molecular mechanisms of miR-183-5p in SLE progression provides new insights into SLE etiology and could help identify novel therapeutic targets.

This study had several limitations. Firstly, the sample size was relatively small, and larger trials are warranted for the validation of these findings. Secondly, other autoimmune diseases should be assessed to confirm the specificities and sensitivities of these biomarkers. Finally, further functional studies are required to clarify the mechanism of these miRNAs in SLE.

5. Conclusion

miRNA expression profiling in PBMCs from SLE cases was significantly altered in comparison with healthy controls. We identified miR-183-5p as a potential diagnostic biomarker of SLE. miR-183-5p amounts showed positive associations with SLEDAI and anti-dsDNA antibody, implying that miR-183-5p is linked to SLE disease activity. Meanwhile, Foxo1, a miR-183-5p target, was markedly downregulated in SLE cases, indicating that miR-183-5p regulates the pathogenic mechanisms and activity of SLE by inhibiting the expression of Foxo1. Further studies are required to uncover the functions of these miRNAs in SLE, which would eventually improve the diagnosis and treatment of SLE.

Data Availability

The data generated or analyzed in this study are available from the corresponding author upon reasonable request.

Conflicts of Interest

The authors declare that there are no conflicts of interest.

Authors' Contributions

Shaolan Zhou, Jing Zhang, and Pengfei Luan contributed equally to this work.

Acknowledgments

This research was supported by grants of the National Natural Science Foundation of China (82060301 and 81960306) and the Natural Science Foundation of Ningxia Province of China (2020AAC03116).

Supplementary Materials

Supplementary 1. Supplementary Table 1: reverse transcription and PCR primer sequences.

Supplementary 2. Supplementary Table 2: the differentially expressed miRNAs between SLE cases and healthy controls.










References

- [1] D. Deafen, A. Escalante, L. Weinrib et al., "A revised estimate of twin concordance in systemic lupus erythematosus," *Arthritis and Rheumatism*, vol. 35, no. 3, pp. 311–318, 1992.
- [2] D. Alarcón-Segovia, M. E. Alarcón-Riquelme, M. H. Cardiel et al., "Familial aggregation of systemic lupus erythematosus, rheumatoid arthritis, and other autoimmune diseases in 1,177 lupus patients from the GLADEL cohort," *Arthritis and Rheumatism*, vol. 52, no. 4, pp. 1138–1147, 2005.
- [3] M. Teruel and M. E. Alarcón-Riquelme, "The genetic basis of systemic lupus erythematosus: what are the risk factors and what have we learned," *Journal of Autoimmunity*, vol. 74, pp. 161–175, 2016.
- [4] Y. Deng and B. P. Tsao, "Updates in lupus genetics," *Current rheumatology reports*, vol. 19, no. 11, p. 68, 2017.
- [5] L. Chen, D. L. Morris, and T. J. Vyse, "Genetic advances in systemic lupus erythematosus: an update," *Current Opinion in Rheumatology*, vol. 29, no. 5, pp. 423–433, 2017.
- [6] K. Liu and C. Mohan, "What do mouse models teach us about human SLE?," *Clinical immunology*, vol. 119, no. 2, pp. 123–130, 2006.
- [7] J. C. Crispin, S.-N. C. Liossis, K. Kis-Toth et al., "Pathogenesis of human systemic lupus erythematosus: recent advances," *Trends in Molecular Medicine*, vol. 16, no. 2, pp. 47–57, 2010.
- [8] D. H. Kono and A. N. Theofilopoulos, "Genetics of SLE in mice," *Springer Seminars in Immunopathology*, vol. 28, no. 2, pp. 83–96, 2006.
- [9] M. A. Jeffries and A. H. Sawalha, "Epigenetics in systemic lupus erythematosus: leading the way for specific therapeutic agents," *International Journal of Clinical Rheumatology*, vol. 6, no. 4, pp. 423–438, 2011.
- [10] T. Hughes and A. H. Sawalha, "The role of epigenetic variation in the pathogenesis of systemic lupus erythematosus," *Arthritis research & therapy*, vol. 13, no. 5, p. 245, 2011.
- [11] D. P. Bartel, "MicroRNAs: target recognition and regulatory functions," *Cell*, vol. 136, no. 2, pp. 215–233, 2009.
- [12] L. Zhang, H. Wu, M. Zhao, C. Chang, and Q. Lu, "Clinical significance of miRNAs in autoimmunity," *Journal of Autoimmunity*, vol. 109, p. 102438, 2020.
- [13] D. Baltimore, M. P. Boldin, R. M. O'Connell, D. S. Rao, and K. D. Taganov, "MicroRNAs: new regulators of immune cell development and function," *Nature Immunology*, vol. 9, no. 8, pp. 839–845, 2008.
- [14] R. M. O'Connell, D. S. Rao, A. A. Chaudhuri, and D. Baltimore, "Physiological and pathological roles for microRNAs in the immune system," *Nature Reviews. Immunology*, vol. 10, no. 2, pp. 111–122, 2010.
- [15] K. D. Taganov, M. P. Boldin, and D. Baltimore, "MicroRNAs and immunity: tiny players in a big field," *Immunity*, vol. 26, no. 2, pp. 133–137, 2007.
- [16] C. Xiao and K. Rajewsky, "MicroRNA control in the immune system: basic principles," *Cell*, vol. 136, no. 1, pp. 26–36, 2009.
- [17] C. G. Vinuesa, R. J. Rigby, and D. Yu, "Logic and extent of miRNA-mediated control of autoimmune gene expression," *International Reviews of Immunology*, vol. 28, no. 3–4, pp. 112–138, 2009.
- [18] M. P. Gantier, A. J. Sadler, and B. R. G. Williams, "Fine-tuning of the innate immune response by microRNAs," *Immunology and Cell Biology*, vol. 85, no. 6, pp. 458–462, 2007.
- [19] S. Zhao, Y. Wang, Y. Liang et al., "MicroRNA-126 regulates DNA methylation in CD4+ T cells and contributes to systemic lupus erythematosus by targeting DNA methyltransferase 1," *Arthritis and Rheumatism*, vol. 63, no. 5, pp. 1376–1386, 2011.
- [20] E. Stagakis, G. Bertsias, P. Verginis et al., "Identification of novel microRNA signatures linked to human lupus disease activity and pathogenesis: miR-21 regulates aberrant T cell responses through regulation of PDCD4 expression," *Annals of the Rheumatic Diseases*, vol. 70, no. 8, pp. 1496–1506, 2011.
- [21] S.-W. Kim, K. Ramasamy, H. Bouamar, A. P. Lin, D. Jiang, and R. C. T. Aguiar, "MicroRNAs miR-125a and miR-125b constitutively activate the NF- κ B pathway by targeting the tumor necrosis factor alpha-induced protein 3 (TNFAIP3, A20)," *Proceedings of the National Academy of Sciences of the United States of America*, vol. 109, no. 20, pp. 7865–7870, 2012.
- [22] I. Alevizos and G. G. Illei, "MicroRNAs as biomarkers in rheumatic diseases," *Nature reviews. Rheumatology*, vol. 6, no. 7, pp. 391–398, 2010.
- [23] A. Gallo, M. Tandon, I. Alevizos, and G. G. Illei, "The majority of microRNAs detectable in serum and saliva is concentrated in exosomes," *PLoS one*, vol. 7, no. 3, article e30679, 2012.
- [24] H. Zhang, X. Huang, L. Ye et al., "B cell-related circulating microRNAs with the potential value of biomarkers in the differential diagnosis, and distinguishment between the disease activity and lupus nephritis for systemic lupus erythematosus," *Frontiers in Immunology*, vol. 9, p. 1473, 2018.
- [25] M. C. Hochberg, "Updating the American College of Rheumatology revised criteria for the classification of systemic lupus erythematosus," *Arthritis and rheumatism*, vol. 40, no. 9, p. 1725, 1997.
- [26] D. D. Gladman, D. Ibañez, and M. B. Urowitz, "Systemic lupus erythematosus disease activity index 2000," *The Journal of Rheumatology*, vol. 29, no. 2, pp. 288–291, 2002.
- [27] P. J. Chien, J. H. Yeh, H. C. Chiu et al., "Inhibition of peripheral blood natural killer cell cytotoxicity in patients with myasthenia gravis treated with plasmapheresis," *European Journal of Neurology*, vol. 18, no. 11, pp. 1350–1357, 2011.

- [28] Q. Zhou, S. Haupt, J. T. Kreuzer et al., "Decreased expression of miR-146a and miR-155 contributes to an abnormal Treg phenotype in patients with rheumatoid arthritis," *Annals of the Rheumatic Diseases*, vol. 74, no. 6, pp. 1265–1274, 2015.
- [29] W. Duan, W. Zhang, J. Jia, Q. Lu, and M. Eric Gershwin, "Exosomal microRNA in autoimmunity," *Cellular & Molecular Immunology*, vol. 16, no. 12, pp. 932–934, 2019.
- [30] Y.-Q. Xie, H.-D. Ma, and Z.-X. Lian, "Epigenetics and primary biliary cirrhosis: a comprehensive review and implications for autoimmunity," *Clinical Reviews in Allergy & Immunology*, vol. 50, no. 3, pp. 390–403, 2016.
- [31] D. Qian, K. Chen, H. Deng et al., "MicroRNA-374b suppresses proliferation and promotes apoptosis in T-cell lymphoblastic lymphoma by repressing AKT1 and Wnt-16," *Clinical cancer research : an official journal of the American Association for Cancer Research*, vol. 21, no. 21, pp. 4881–4891, 2015.
- [32] S. Garcia-Rodriguez, J.-L. Callejas-Rubio, N. Ortego-Centeno et al., "Altered AKT1 and MAPK1 gene expression on peripheral blood mononuclear cells and correlation with T-helper-transcription factors in systemic lupus erythematosus patients," *Mediators of Inflammation*, vol. 2012, Article ID 495934, 14 pages, 2012.
- [33] J. Shi, S. Chi, J. Xue, J. Yang, F. Li, and X. Liu, "Emerging role and therapeutic implication of Wnt signaling pathways in autoimmune diseases," *Journal of Immunology Research*, vol. 2016, Article ID 9392132, 18 pages, 2016.
- [34] G.-C. Li, X.-Y. Cao, Y.-N. Li et al., "MicroRNA-374b inhibits cervical cancer cell proliferation and induces apoptosis through the p38/ERK signaling pathway by binding to JAM-2," *Journal of Cellular Physiology*, vol. 233, no. 9, pp. 7379–7390, 2018.
- [35] K. Ichiyama and C. Dong, "The role of miR-183 cluster in immunity," *Cancer Letters*, vol. 443, pp. 108–114, 2019.
- [36] J. Thiel, C. Alter, S. Luppus et al., "MicroRNA-183 and microRNA-96 are associated with autoimmune responses by regulating T cell activation," *Journal of autoimmunity*, vol. 96, pp. 94–103, 2019.
- [37] C. Wan, C. Y. Ping, X. Y. Shang et al., "MicroRNA 182 inhibits CD4CD25Foxp3 Treg differentiation in experimental autoimmune encephalomyelitis," *Clinical immunology*, vol. 173, pp. 109–116, 2016.
- [38] X. Yang, Q. He, Z. Guo et al., "MicroRNA-425 facilitates pathogenic Th17 cell differentiation by targeting forkhead box O1 (Foxo1) and is associated with inflammatory bowel disease," *Biochemical and Biophysical Research Communications*, vol. 496, no. 2, pp. 352–358, 2018.
- [39] K. Ichiyama, A. Gonzalez-Martin, B.-S. Kim et al., "The microRNA-183-96-182 cluster promotes T helper 17 cell pathogenicity by negatively regulating transcription factor Foxo1 expression," *Immunity*, vol. 44, no. 6, pp. 1284–1298, 2016.

Research Article

IL-13 Augments Histone Demethylase JMJD2B/KDM4B Expression Levels, Activity, and Nuclear Translocation in Airway Fibroblasts in Asthma

Khuloud Bajbouj ^{1,2}, Mahmood Y. Hachim ³, Rakhee K. Ramakrishnan ^{1,2},
Huwaida Fazel ¹, Jumana Mustafa ¹, Shahed Alzaghari ¹, Mahmoud Eladl ¹,
Jasmin Shafarin ², Ronald Olivenstein⁴, and Qutayba Hamid ^{1,2,4}

¹College of Medicine, University of Sharjah, Sharjah, UAE

²Sharjah Institute for Medical Research, University of Sharjah, Sharjah, UAE

³College of Medicine, Mohammed Bin Rashid University of Medicine and Health Sciences, Dubai, UAE

⁴Meakins-Christie Laboratories, McGill University, Montreal, QC, Canada

Correspondence should be addressed to Khuloud Bajbouj; kbajbouj@sharjah.ac.ae and Qutayba Hamid; qalheialy@sharjah.ac.ae

Received 15 November 2020; Revised 8 February 2021; Accepted 12 February 2021; Published 22 February 2021

Academic Editor: Xianfeng Wang

Copyright © 2021 Khuloud Bajbouj et al. This is an open access article distributed under the Creative Commons Attribution License, which permits unrestricted use, distribution, and reproduction in any medium, provided the original work is properly cited.

Purpose. Asthma is one of the most common obstructive pulmonary diseases worldwide. Epigenetic alterations, including DNA methylation and histone modifications, have been reported to contribute to asthma pathogenesis. Since the inflammation mediator and remodeling trigger, IL-13, is known to play a central role in the pathophysiology of asthma, this study was aimed to identify novel IL-13-regulated epigenetic modifiers in asthma that may contribute to subepithelial fibrosis. **Methods.** Publicly available transcriptomic datasets from Gene Expression Omnibus (GEO) were used to identify differentially expressed genes on an epigenetic level upon IL-13 exposure in lung fibroblasts. Bronchial fibroblasts isolated from healthy and asthmatic individuals were assessed for the gene and protein expression levels of the identified gene at baseline and upon IL-13 treatment using qRT-PCR and western blotting, respectively. Its subcellular localization and tissue distribution were examined in bronchial fibroblasts as well as bronchial biopsies by immunofluorescence and immunohistochemical analysis, respectively. **Results.** Bioinformatic analysis revealed the differential expression of the histone demethylase JMJD2B/KDM4B, a well-known epigenetic modulator that leads to the demethylation of different lysine residues on histones, in IL-13-treated lung fibroblasts. The baseline expression levels of JMJD2B were higher in asthmatic fibroblasts and in bronchial biopsies in comparison to healthy ones. There was also an increase in JMJD2B activity as evidenced by the demethylation of its downstream target, H3K36me3. Furthermore, IL-13 stimulation induced JMJD2B expression and further demethylation of H3K36me3 in asthmatic fibroblasts. This was accompanied by increased translocation of JMJD2B into the nucleus. **Conclusion.** This study highlights the novel pathological involvement of the histone demethylase JMJD2B/KDM4B in asthmatic airway fibroblasts that are regulated by IL-13. **Clinical implications.** Given that there is no single therapeutic medicine to effectively treat the various subtypes of asthma, this study provides promising insights into JMJD2B as a new therapeutic target that could potentially improve the treatment and management of asthma.

1. Introduction

Asthma is an inflammatory disease of the airways, characterized by different degrees of obstruction that results from airway remodeling. An inflammatory immune response is

triggered by the exposure of asthmatic airways to allergens, resulting in the activation of T helper type 2 (Th2) lymphocytes. These Th2 cells release cytokines such as interleukin-(IL-) 4, IL-5, IL-9, and IL-13 that in turn regulate both airway inflammation as well as airway remodeling. IL-13 in

particular plays a pivotal role in the regulation of the allergic diathesis.

Subepithelial fibrosis is a feature of airway remodeling that is associated with an aberrant fibroblast phenotype. There are reported differences in the morphology and cytoskeletal architecture between asthmatic and nonasthmatic fibroblasts. In contrast with nonasthmatic normal fibroblasts, the asthmatic fibroblasts form thick and aligned ventral stress fibers that are accompanied by focal adhesions [1]. Asthmatic fibroblasts also exhibit a synthetic phenotype with increased expression of extracellular matrix components, such as type 1 collagen, proteoglycans, versican, hyaluronan, fibronectin, decorin, and tenascin C, and their increased secretion into the surrounding environment. Many studies have shown the increased potential of asthmatic fibroblasts to differentiate into myofibroblasts in comparison to nonasthmatic fibroblasts [2, 3]. IL-13 is an important contributor to subepithelial fibrosis by exerting its action on fibroblasts. It modulates the remodeling of the subepithelial basement membrane by stimulating increased fibroblast proliferation, myofibroblastic differentiation, and extensive collagen deposition leading to thickening and narrowing of the airways [2, 3].

Epigenetic processes, including DNA methylation, histone acetylation, microRNA expression, and chromatin alterations, alter gene transcription without a change in the DNA nucleotide sequence. Epigenetic modulations have been implicated to play a role in the pathogenesis of respiratory diseases. When the normal epigenetic regulation is disturbed by environmental exposures, Th1/Th2 balance can be affected and can thereby contribute to the pathogenesis of asthma and COPD [4]. Some of these environmental triggers linked with the epigenetics of asthma, and specifically with DNA methylation, include low birth weight [5], gestational folate levels [6], socioeconomic position [7], and smoking [8], to name a few. IL-13 is known to induce epigenetic changes in asthmatic airways and to alter transcriptional gene regulation [9]. Even a single exposure of IL-13 may induce DNA methylation changes in airway epithelial cells and contribute to fibrosis and asthmatic phenotype [10]. Further, the epigenetic regulation of IL-13-mediated collagen deposition by fibroblasts suggests an epigenetic fibrotic response of fibroblasts to IL-13 exposure [11]. Since the involvement of IL-13-mediated epigenetic regulation of subepithelial fibrosis in asthma is not clearly understood, we employed bioinformatics to identify novel IL-13 regulated epigenetic modifiers in asthma.

Jumonji C (JmjC) is a group of histone demethylases that regulates gene transcription epigenetically. Different JmjC domain-containing proteins have been shown to play a role in cancer regulation and progression and have been used as biomarkers in some types of cancer [12]. JMJD2B, formerly known as KDM4B, is a member of the JmjC protein family that activates gene expression through demethylation of di- and trimethylated histones, such as H3K9me2/me3, H3K36me2/me3, and H3K4 me2/me3 histones. It has been shown to play a role in the progression of both lung cancer and bladder cancer cell proliferation [12, 13]. The activation of the histone demethylase JMJD2B, a gene that is expressed in fibroblasts, leads to the demethylation of different lysine

residues on histones that may activate genes responsible for fibrosis [12].

Asthma is a multifactorial disease that involves subepithelial fibrosis and associated narrowing of the airways. Here, we have identified the novel pathological involvement of the histone demethylase JMJD2B/KDM4B in asthmatic airway fibroblasts that is further regulated by IL-13. We show that the disease pathology occurs at the molecular (IL-13 expression), genetic (JMJD2B activation), epigenetic (H3K36me3 demethylation), and cellular (fibroblast activation) levels.

2. Materials and Methods

2.1. Identifying Core Differentially Expressed Genes in IL-13 Treated versus Untreated Adult Lung Fibroblasts. The publicly available transcriptomic datasets from Gene Expression Omnibus (GEO) were filtered to search for a dataset that includes primary lung fibroblasts treated with IL-13 versus control without IL-13 stimulation. One dataset (GSE43515) included the needed setting, where adult lung fibroblasts were treated with or without IL-13. Raw CEL files were extracted and subjected to Preprocessing Quality Control, normalization, and filtering. Differentially expressed genes (DEGs) were then identified based on Gene Set Enrichment Analysis (GSEA). To filter out nonvariant genes between IL-13-treated and vehicle controls-treated fibroblasts, a combination of noise and variance filtering was applied. Only probes with a value of 100 or higher in the MAS5 dataset in all 12 samples were selected. The probes that passed the first filter, then, are subjected to the coefficient of variation (CV) filter using their gcRMA expression intensities. Probes with a CV value of 10-50% across all samples were considered to be variant and thus selected. CV was calculated as the mean/standard deviation of each gene across all samples.

2.2. In Silico Validation of Initially Identified DEGs in a Different Dataset. To confirm that these identified genes are differentially expressed in response to IL-13 in lung fibroblasts, another independent dataset (GSE56338) was used for *in silico* validation. In this setting, human fibroblasts were stimulated with IL-13 and compared to media and pretreatment controls. 2 cell passages were employed with each including 2 independent experiments.

2.3. Identifying Regulatory Programs on the Epigenetic Level for the Identified DEGs. We used Enrichr: a comprehensive gene set enrichment analysis web server library which contains extensive processed ChIP seq data from Roadmap Epigenomics Project to associate detected peaks near genes to identify gene regulatory programs on the epigenetic level. The DEGs identified earlier were uploaded to Enrichr online tool (<https://maayanlab.cloud/Enrichr/enrich#>), and Epigenomics Roadmap HM ChIP-seq results were downloaded. Only sets with adjusted *p*-value < 0.05 were selected that were related to fibroblasts.

2.4. Enriched Ontology Clustering for the Identified Genes. Enriched Ontology Clustering for the identified genes was performed using Metascape (<http://metascape.org/gp/index.html#/main/step1>) [12–15].

2.5. Cell Culture and IL-13 Stimulation. Human-derived fibroblasts from healthy and asthma subjects were maintained in DMEM medium supplemented with 2 µg/mL of insulin, 1 mM of sodium pyruvate, 1 mM of nonessential amino acids, 4 mM of glutamine, 10% fetal calf serum, and antibiotics (penicillin/streptomycin) at 37°C and 5% CO₂. Cells were seeded at 0.5 – 1 × 10⁵ cells/mL in 25 cm² flasks. At ~70% confluency, cells were stimulated with 20 ng/ml of IL-13 (ProSpec). Control cell cultures were either left untreated or treated with equal volumes of DMSO as vehicle.

2.6. Western Blotting Analysis. Cells were lysed in ice-cold RIPA buffer (Abcam) containing protease inhibitor cocktail tablets (Sigma). Whole cell lysate protein concentrations were quantified using the standard Bradford method (Bio-Rad). Lysate aliquots containing 30–50 µg of protein were separated by 12% sodium dodecyl sulfate–polyacrylamide gel electrophoresis (SDS-PAGE) and transferred onto a nitrocellulose membrane (Bio-Rad). The membrane was then blocked by 5% skimmed milk powder for 1 h at room temperature, washed with TBST, and reacted with primary immunoglobulin G (IgG) unlabeled primary antibodies; anti-JMJD2B (Abcam), various modified and total histones (Cell signaling), β-actin (Sigma), at 1:1000 dilution overnight at 4°C. The secondary (anti-mouse and anti-rabbit) antibodies (Cell Signaling) were then reacted with the membrane at 1:1000 dilution for 1 h at room temperature. Chemiluminescence was detected using the ECL kit (Thermo Scientific Pierce). Protein band quantification was carried out using the Bio-Rad Image Lab software (ChemiDoc™ Touch Gel and Western Blot Imaging System; Bio-Rad). β-Actin was used as a normalization control.

2.7. Quantitative Real-Time PCR. The cDNA was synthesized from 1 µg of total RNA using the QuantiTect Reverse Transcription Kit (Qiagen) according to the manufacturer's protocol. qPCR was performed using 1:1 of complementary DNA (cDNA), specific primers for each gene, SYBR® Green I, and an iCycler Thermal Cycler. Expression levels of target human gene JMJD2B (F:5'-GGACTGACGGCAACCTCTAC-3', R:5'-CGTCCTCAAACCTCCACCTG-3') was normalized to GAPDH expression (F:5'-CCAGGTGGTCTCCTCTGAC TTC-3', R:5'-TCATACCCAGGAAATGAGCTTGACA-3').

2.8. Immunofluorescence Staining. Cells were seeded at 10⁴ cells/ml on sterile poly-L-lysine-coated glass cover slips in 6-well culture plates and cultured overnight. Cells were starved for 12 hr prior to IL-13 stimulation as described previously. Cells on cover slips were then washed with PBS and fixed with 4% paraformaldehyde for 15 min at room temperature and treated with 0.1% Triton X-100 for 10 min. Fixed and permeabilized cells were blocked with BSA at 3% for 1 hr, rinsed with 1X PBS and incubated with unlabeled JMJD2B primary antibody (Abcam) overnight at 4°C. Cells were then washed with 1X PBS and reacted with the Alexafluor® 488- or Alexafluor® 680-labeled secondary antibody (Abcam) for 1 hr at 37°C. Genomic DNA was stained with 4',6'-diamidino-2-phenylindole (DAPI) (Invitrogen) according to manufacturer's instructions. Slides were visual-

ized by fluorescence microscopy using an Olympus BX51 fluorescence microscope (Olympus Corporation, Tokyo, Japan).

2.9. Immunohistochemical Staining. Immunohistochemistry was performed as previously described [14]. Briefly, the bronchial biopsy sections were deparaffinized using xylene, and antigen retrieval was performed in Tris-EDTA buffer with pH9. JMJD2B primary antibody (Cell signaling Technology) was used at a dilution of 1:50, followed by the corresponding biotinylated secondary antibody. Color development was achieved using HRP/DAB Detection IHC kit (abcam). Counterstaining was done using hematoxylin, and the slides were rinsed and mounted with DPX mounting medium.

2.10. Statistical Analysis. All graphical data was analyzed using GraphPad Prism 5 (GraphPad Software Inc., La Jolla, CA, USA), and unpaired *t*-test was used to generate *p*-values for comparisons between groups in each data set.

3. Results

3.1. Bioinformatic Analysis Revealed Differential Expression Pattern of JMJD2B upon IL-13 Stimulation. 1362 genes were identified to be variable between the IL-13-treated and untreated groups of fibroblasts indicating their role in the response of lung fibroblasts to IL-13. These genes were further processed to identify their shared pathways and common regulators.

3.1.1. The Identified Genes Are Regulated or Affected by Histone (H2 and H3) Modification. The identified genes showed overlap with gene sets that are regulated or affected by histone modifications as studied in IMR90 (normal lung fibroblast cell line from a human female). Histone (H2 and H3) modifications (H2BK12ac, H2BK20ac, H2BK120ac, H2BK15ac, H3K9ac, H4K8ac, H3K18ac, and H3K27ac) were detected as shown in table (Supplementary (available here)).

3.1.2. Four DEGs (JMJD2B, JMJD2C, PTDSR, and JMJD3) Were Involved in Histone Trimethylation and or Demethylation. As our results showed that the DEGs between IL-13-treated and IL-13-untreated fibroblasts are related to histone modifications, we then searched which among these genes are related to histone modifications in their Biological Process (GO) using a metascape database. 4 genes were found to be involved in histone trimethylation and or demethylation, namely JMJD2B, JMJD2C, PTDSR, and JMJD3 (Table 1).

3.1.3. IL-13 Upregulated JMJD2B Expression in Adult Lung Fibroblasts. To understand the effect of IL-13 on the expression of JMJD2B, JMJD2C, JMJD3, and PTDSR in lung fibroblasts, another dataset (GSE56338) was used for *in silico* validation of earlier results. We extracted the normalized gene expression value for the 4 genes and compared the fibroblasts treated with IL-13 with those left untreated. Compared to media-treated cells, IL-13-treated fibroblasts showed upregulation of JMJD2B expression (Figure 1).

TABLE 1: DEGs involved in histone trimethylation and or demethylation.

MyList	Description	Biological process (GO)
JMJD2B	Lysine demethylase 4B	GO:0070544 histone H3-K36 demethylation; GO:0033169 histone H3-K9 demethylation; GO:0070076 histone lysine demethylation
JMJD2C	Lysine demethylase 4C	GO:1900113 negative regulation of histone H3-K9 trimethylation; GO:0070544 histone H3-K36 demethylation; GO:1900112 regulation of histone H3-K9 trimethylation
JMJD3	Lysine demethylase 6B	GO:0071557 histone H3-K27 demethylation; GO:0060992 response to fungicide; GO:0070076 histone lysine demethylation
PTDSR	Jumonji domain containing 6, arginine demethylase and lysine hydroxylase	GO:0018395 peptidyl-lysine hydroxylation to 5-hydroxy-L-lysine; GO:0070077 histone arginine demethylation; GO:0070078 histone H3-R2 demethylation

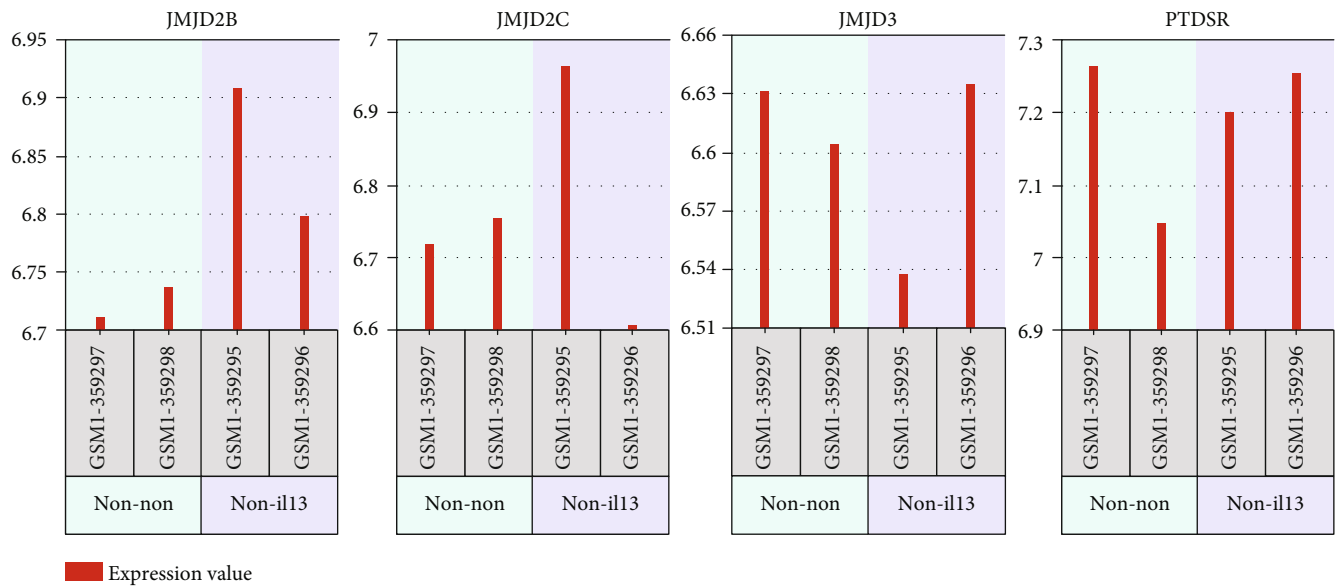


FIGURE 1: Normalized gene expression of four DEGs genes (JMJD2C, JMJD2B, PTDSR, and JMJD3) was involved in histone trimethylation and or demethylation as extracted from GSE56338 dataset. Adult lung fibroblasts (passage 6) treated with IL-13 (non-il13) compared to the same cells treated with media only (non-non).

3.2. JMJD2B Expression and Activity Is Higher in Asthmatic-Derived Airway Fibroblasts. In order to compare the gene expression levels of JMJD2B in the fibroblasts obtained from the airway submucosa of healthy and asthmatic individuals, quantitative real-time PCR was carried out. The gene expression of JMJD2B was higher in asthmatic-derived airway fibroblasts than in healthy airway fibroblasts (Figure 2(a)). This further validated in part the results of the bioinformatic analysis indicating a pathological role of JMJD2B in asthmatic fibroblasts.

Consequently, a western blot was run and developed, comparing JMJD2B and the trimethylated histone H3 at lysine residues K4, K9, K27, K36, and K79, together with housekeeping gene β -actin, in both healthy and asthmatic fibroblasts. In agreement with the gene expression levels, increased protein expression of JMJD2B was observed in the asthmatic fibroblasts (Figure 2(b)). Considering the demethylation potential of JMJD2B, western blotting revealed that H3K36me3 levels were significantly reduced in correlation with higher JMJD2B in asthmatic fibroblasts

(Figure 2(c)). No significant H3 demethylation was detected at positions K4, K9, K27, and K79 in asthmatic fibroblasts when compared to healthy. These results indicate the presence of increased JMJD2B expression and activity levels in the asthmatic airway fibroblasts than in the healthy airway fibroblasts.

3.3. IL-13 Augmented JMJD2B Expression and Activity in Asthmatic Fibroblasts. Bioinformatic analysis suggested IL-13 mediated epigenetic regulation of lung fibroblasts through JMJD2B expression. Furthermore, IL-13 is known to induce fibrosis by increasing the activity of fibroblasts, and we investigated if this involved promoting the expression of the JMJD2B gene in asthmatic fibroblasts. Therefore, the fibroblasts were stimulated with IL-13, and the subsequent expression of JMJD2B was measured through quantitative real-time PCR and western blotting, and the activity of JMJD2B was measured through western blotting. In comparison to the healthy fibroblasts, the increased gene expression of JMJD2B in asthmatic fibroblasts was further boosted in the presence

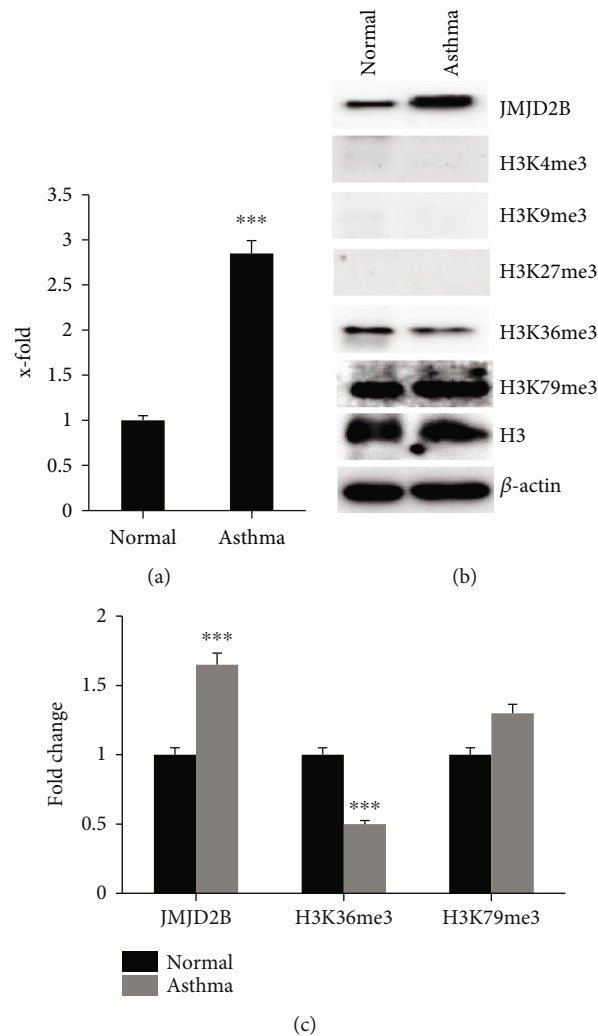


FIGURE 2: Baseline differential levels of histone demethylase JMJD2B and downstream targets in healthy and asthmatic fibroblasts. (a) qRT-PCR analysis of JMJD2B expression levels. (b) Western blot analysis showing JMJD2B and trimethylated histones H3 lysine residues at K4, K9, K27, K36, and K79 protein levels in the fibroblasts. (c) Calculated mean \pm SD fold change in protein-expression levels in normal and asthma fibroblasts based on two separate experiments. *** $p < 0.01$, determined using unpaired two-tailed Student *t*-test. Representative immunoblots depicting protein levels normal and asthma fibroblasts where β -actin was used as loading control.

of IL-13 (Figure 3(a)). After IL-13 stimulation, the increase in JMJD2B gene expression was more pronounced in asthmatic fibroblasts as compared to healthy ones (Figures 3(a) and 3(b)). A slight increase was also evident in JMJD2B protein levels of asthma cells incubated with IL-13 when compared to the control counterparts (Figure 3(c)). Moreover, since this gene codes for a demethylase enzyme, the levels of methylated histones were measured before and after IL-13 stimulation in both cell lines. A significant decline in H3 methylation was noted at position K36 in asthmatic fibroblasts upon incubation with IL-13 (Figure 3(d)). These results suggest the possibility of IL-13 to enhance JMJD2B expression and subsequent demethylation activity to a significant extent in asthmatic fibroblasts than in healthy fibroblasts.

3.4. IL-13 Enhanced JMJD2B Nuclear Translocation. Considering its histone demethylation activity, JMJD2B mostly has a nuclear localization. It tends to concentrate more in the

nucleus when its activity increases. Immunofluorescence staining of both healthy and asthmatic fibroblasts was performed before and after incubation with IL-13 to detect the subcellular localization of JMJD2B. In addition to increased JMJD2B immunoreactivity in the asthmatic fibroblasts, JMJD2B concentrated more in the nucleus following IL-13 stimulation, reflecting increased activity in asthmatic fibroblasts (Figures 4(a) and 4(b)). The change in subcellular localization was less evident in healthy fibroblasts.

3.5. Enhanced Nuclear JMJD2B Expression in Asthmatic Bronchial Biopsies. In order to validate our results thus far, we performed immunohistochemical staining of endobronchial biopsy tissue from asthmatic and healthy individuals, which further confirmed the nuclear localization of JMJD2B in asthmatic samples. In accordance with the above results, intense immunostaining of JMJD2B was observed in the epithelial and submucosal compartments of asthmatic

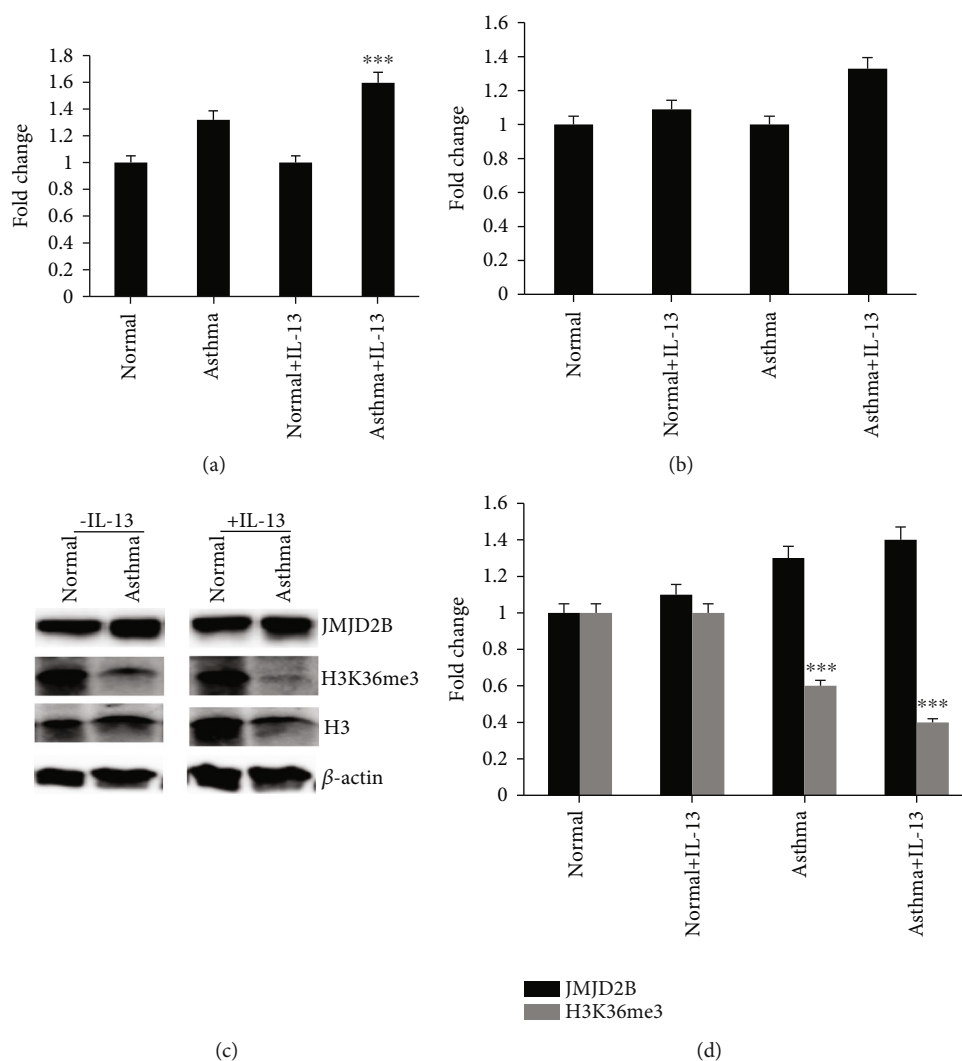


FIGURE 3: JMJD2B and its downstream target levels after IL-13 stimulation in normal and asthmatic fibroblasts. (a) qRT-PCR analysis of JMJD2B expression levels upon IL-13 stimulation in normal and asthma fibroblasts. (b) qRT-PCR analysis of JMJD2B expression levels comparing fibroblasts with or without IL-13 stimulation in normal and asthma fibroblasts. (c) Western blot analysis showing JMJD2B and trimethylated histones H3 lysine residue at K36 protein levels in the fibroblasts upon IL-13 stimulation. (d) Calculated mean \pm SD fold change in protein-expression levels comparing fibroblasts with or without IL-13 stimulation in normal and asthma fibroblasts based on two separate experiments. Graphical data are represented as mean \pm SEM. *** $p < 0.01$, determined using unpaired two-tailed Student t -test. Representative immunoblots depicting protein levels normal and asthma fibroblasts where β -actin was used as loading control.

specimens when compared to control. Furthermore, nuclear staining of JMJD2B can be observed in both the ciliated epithelium as well as in fibroblasts in the asthmatic tissue specimen when compared to the control tissue (Figure 5).

4. Discussion

Our study identified the dysregulation of a novel gene, JMJD2B, in asthmatic fibroblasts. Bioinformatic analysis suggested the differential expression of JMJD2B/KDM4B, a histone demethylase, in lung fibroblasts upon IL-13 stimulation. This was validated in asthmatic fibroblasts and bronchial biopsies, where JMJD2B expression levels were elevated in asthmatic specimens at baseline in contrast to their healthy counterparts. This was found to be further enhanced upon

IL-13 stimulation. IL-13 stimulation also resulted in increased JMJD2B translocation into the nucleus and further demethylation of H3K36me3, reflecting its possibly increased activity in asthmatic fibroblasts.

IL-13 is a well-known mediator of subepithelial fibrosis and inducer of epigenetic changes in asthmatic airways. Since IL-13 plays a central role in the pathogenesis of asthma, we used bioinformatics to identify novel IL-13-regulated epigenetic modifiers in asthma. Our analysis identified the involvement of a novel gene, namely JMJD2B/KDM4B, in the pathogenesis of subepithelial fibrosis in asthma that is responsive to IL-13 stimulation.

In order to validate our bioinformatic findings, we used primary bronchial fibroblasts from asthmatic and healthy individuals. Our results demonstrated the increased expression

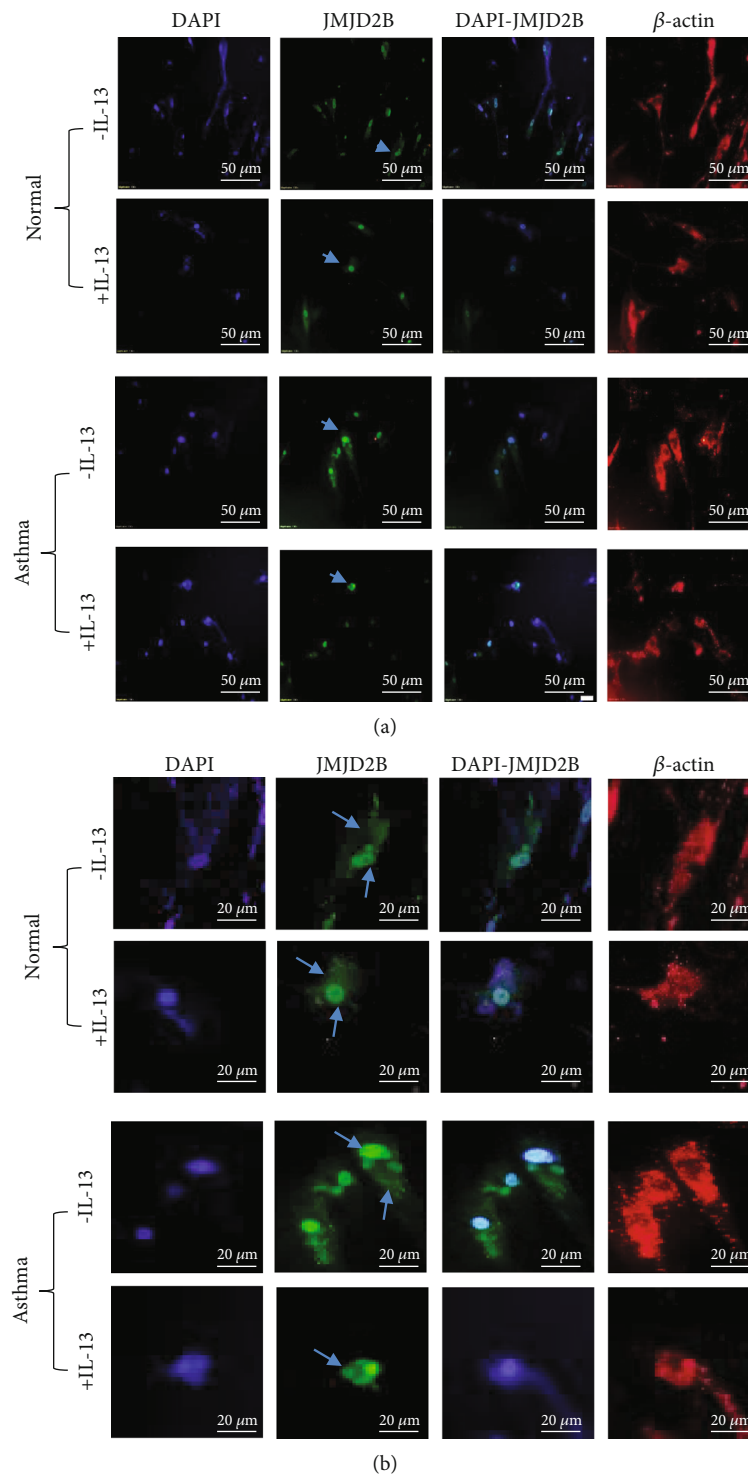


FIGURE 4: JMJD2B subcellular localization after IL-13 stimulation in normal and asthmatic fibroblasts. Immunofluorescence staining of in normal and asthmatic fibroblasts stimulated with IL-13 that were stained for DNA (DAPI; blue), JMJD2B (green), β -actin (red). The images were observed under a microscope at 20x magnification (a) and at 40x magnification (b). Arrows indicate subcellular localization of JMJD2B in fibroblasts.

and activity of JMJD2B at baseline in asthmatic fibroblasts compared to its healthy counterparts, which was evidenced by the demethylation of its downstream target H3K36me3 (Figure 2(b)). While upregulated JMJD2B expression has been

implicated in the pathogenesis of non-small cell lung carcinoma cells [15] and pulmonary hypertension [16], literature is scarce in the fields of asthma and COPD. The increased activity of JMJD2B has been reported in literature to

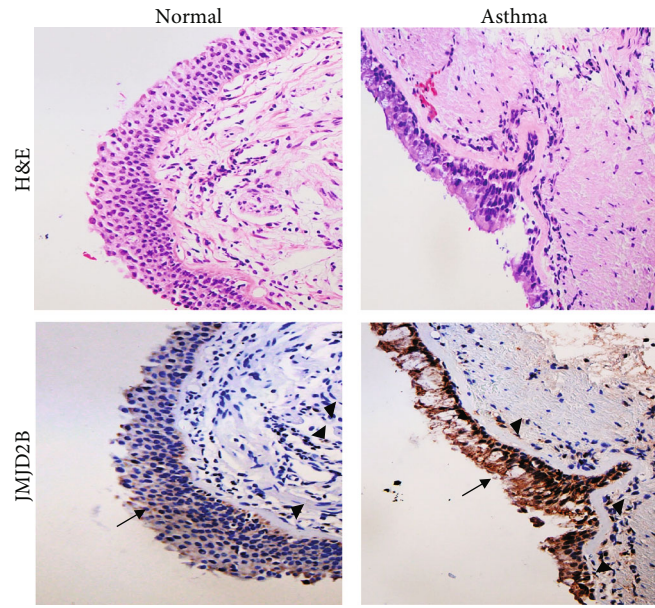


FIGURE 5: JMJD2B expression in asthmatic bronchial biopsy tissues. Representative bronchial biopsy sections from healthy control showing weak and asthmatic showing moderate to strong JMJD2B protein expression. Representative images for H&E staining taken at 10x magnification and IHC for JMJD2B taken at 20x magnification showing developed with 3,3'-diaminobenzidine (brown). Nuclei were counterstained with hematoxylin (blue). Arrows refer to bronchial epithelium. Arrowheads refer to fibroblasts.

epigenetically regulate endothelial-to-mesenchymal transition (EndMT), an important process in wound healing after tissue injury, where the affected endothelial cells become fibroblast-like, leading to tissue fibrosis [12]. Further, suppression of JMJD2B prevented EndMT-induced reduction of H3K9me3 and subsequent expression of EndMT-related genes. This indicates an important role of JMJD2B in promoting a profibrotic phenotype. In our findings, the elevated expression and activity of JMJD2B at baseline in asthmatic fibroblasts may indicate an aberrant fibroblast phenotype in asthma and ongoing fibrosis even in the absence of active or apparent inflammation clinically. This signifies a potential translational use in the form of early inhibition of the activity of JMJD2B to slow down, or even prevent, fibrosis in the airways of asthmatic individuals.

IL-13 is a key pathogenic player in asthma that is known to induce mononuclear and eosinophilic inflammation, mucus hyperplasia with cellular metaplasia, and fibrosis in the subepithelial layers of the airways, eventually ending up with airway obstruction [17]. In addition to its increased baseline expression in asthmatic fibroblasts, JMJD2B levels were further induced in asthmatic airway fibroblasts upon exposure to IL-13 (Figure 3(a)). IL-13 also augmented the demethylation of histone H3, suggesting a potential mechanism involving JMJD2B in IL-13-mediated activation of fibroblasts which plays an important role in promoting fibrosis as well as inflammatory processes in asthma. It is interesting to note here that our literature search has shown no previous literature demonstrating any direct relation between IL-13 levels and JMJD2B. This is, therefore, one of the first reports indicating the involvement of IL-13-mediated JMJD2B expression in the pathogenesis of asthma.

Despite the well-recognized immunopathobiology of IL-13 in asthma, clinical trials of anti-IL-13 monoclonal anti-

bodies (mAbs) in patients with severe asthma have been largely ineffective. For instance, the STRATOS1 and STRATOS2 phase 3 clinical trials that assessed the safety and efficacy of Tralokinumab for the treatment of severe, uncontrolled asthma did not show significant improvement in asthma outcomes [18]. Further, another mAb, GSK679586, although well-tolerated, did not demonstrate clinically meaningful improvements in patients with severe asthma [19]. Although JMJD2B expression was induced by IL-13, the elevated baseline expression of this enzyme in asthmatic fibroblasts suggests constitutively high expression of JMJD2B in asthmatic fibroblasts. In this context, JMJD2B may serve as a potential therapeutic target downstream of IL-13. Therefore, targeting JMJD2B may help alleviate IL-13-mediated biological responses in asthma. Our study also showed increased JMJD2B activity in the nucleus of asthmatic fibroblasts compared to their healthy counterparts. This further indicated a link between the nuclear translocation of JMJD2B and asthma pathogenesis. Hypoxic conditions, as seen in the asthmatic airways [20], have previously been reported to induce increased nuclear localization and activity of JMJD2B in pulmonary arterial smooth muscle cells [16]. This study also identified potential biological processes targeted by JMJD, which included proliferation, apoptosis, metabolism, and inflammation, all of which are dysregulated in asthmatic fibroblasts. This further reinforces the pathogenic role of increased JMJD2B activity in promoting airway remodeling.

Increasing evidence suggests an important role of environmental epigenetic regulation in shaping the different asthmatic phenotypes. Importantly, the reversibility of these epigenetic modifications is an attractive feature that may be exploited for the development of novel epigenetic drugs. It

would be interesting to explore the use of epigenome-modifying tools in targeting the various hallmark features of asthma, including airway remodeling and airway inflammation.

In an era where the importance of epigenetic alterations in fibrosis and inflammation is increasingly being appreciated, we demonstrate here a novel epigenetic control of fibrosis mediated by JMJD2B in asthmatic airways. Increased activity of histone demethylase JMJD2B is induced by IL-13-mediated profibrotic and proinflammatory conditions.

Data Availability

The datasets used in the present study are available from the corresponding authors upon reasonable request.

Conflicts of Interest

The authors declare that there is no conflict of interest.

Authors' Contributions

QH and KB performed the conceptualization; KB, MH, RKR, and RO performed the data curation; KB, MH, HF, JM, SA, MA, JS, RKR, and QH did the investigation; KB and QH did the supervision; KB, RKR, MH, HF, JM, SA, and MA wrote the original draft; KB, RKR, MH, and QH wrote, reviewed, and edited the manuscript. Mahmood Y. Hachim and Rakhee K. Ramakrishnan contributed equally to this work.

Acknowledgments

We would like to acknowledge the generous support of the Sharjah Institute for Medical Research (SIMR), University of Sharjah, UAE. We would like to acknowledge Mr. Abdalla Eltayeb for his contribution in staining the lung tissues. All authors agree to be accountable for all aspects of the work. This work was supported by the University of Sharjah Competitive grant, Ref. number: 1901090263. The abstract of this paper was presented at the CHEST Annual virtual Meeting, October 18–22, 2020, Chicago, IL, USA, as an online abstract with interim findings. The abstract was published in “e-Abstracts” supplement in the CHEST Journal, ALLERGY AND AIRWAY| VOLUME 158, ISSUE 4, SUPPLEMENT, A42-A43, OCTOBER 01, 2020 (DOI: 10.1016/j.chest.2020.08.076). [https://journal.chestnet.org/article/S0012-3692\(20\)32262-5/fulltext](https://journal.chestnet.org/article/S0012-3692(20)32262-5/fulltext).

Supplementary Materials

Supplementary Figure: original whole blot of Figure 3(c). Western blot analysis showing JMJD2B and trimethylated histones H3 lysine residue at K36 protein levels in the normal and asthmatic fibroblasts upon IL-13 stimulation. Supplementary Table: gene sets that are regulated or affected by histone modification with overlap with the identified DEGs using Enrichr online tool (<https://maayanlab.cloud/Enrichr/enrich#>) Epigenomics Roadmap HM ChIP-seq. Only sets with adjusted p value < 0.05 were selected that were related to fibroblasts. (*Supplementary Materials*)

References

- [1] M. Sarna, K. A. Wojcik, P. Hermanowicz et al., “Undifferentiated bronchial fibroblasts derived from asthmatic patients display higher elastic modulus than their non-asthmatic counterparts,” *PLoS One*, vol. 10, no. 2, article e0116840, 2015.
- [2] R. Firszt, D. Francisco, T. D. Church, J. M. Thomas, J. L. Ingram, and M. Kraft, “Interleukin-13 induces collagen type-1 expression through matrix metalloproteinase-2 and transforming growth factor- β 1 in airway fibroblasts in asthma,” *The European respiratory journal*, vol. 43, no. 2, pp. 464–473, 2014.
- [3] A. Saito, H. Okazaki, I. Sugawara, K. Yamamoto, and H. Takizawa, “Potential action of IL-4 and IL-13 as fibrogenic factors on lung fibroblasts in vitro,” *International archives of allergy and immunology*, vol. 132, no. 2, pp. 168–176, 2003.
- [4] W. Karmaus, A. H. Ziyab, T. Everson, and J. W. Holloway, “Epigenetic mechanisms and models in the origins of asthma,” *Current opinion in allergy and clinical immunology*, vol. 13, no. 1, pp. 63–69, 2013.
- [5] E. W. Tobi, B. T. Heijmans, D. Kremer et al., “DNA methylation of IGF2, GNASAS, INSIGF and LEP and being born small for gestational age,” *Epigenetics*, vol. 6, no. 2, pp. 171–176, 2014.
- [6] C. E. Boeke, A. Baccarelli, K. P. Kleinman et al., “Gestational intake of methyl donors and global LINE-1 DNA methylation in maternal and cord blood: prospective results from a folate-replete population,” *Epigenetics*, vol. 7, no. 3, pp. 253–260, 2014.
- [7] N. Borghol, M. Suderman, W. McArdle et al., “Associations with early-life socio-economic position in adult DNA methylation,” *International journal of epidemiology*, vol. 41, no. 1, pp. 62–74, 2012.
- [8] L. P. Breitling, R. Yang, B. Korn, B. Burwinkel, and H. Brenner, “Tobacco-smoking-related differential DNA methylation: 27K discovery and replication,” *American journal of human genetics*, vol. 88, no. 4, pp. 450–457, 2011.
- [9] A. T. Ooi, S. Ram, A. Kuo et al., “Identification of an interleukin 13-induced epigenetic signature in allergic airway inflammation,” *American journal of translational research*, vol. 4, no. 2, pp. 219–228, 2012.
- [10] J. Nicodemus-Johnson, K. A. Naughton, J. Sudi et al., “Genome-wide methylation study identifies an IL-13-induced epigenetic signature in asthmatic airways,” *American journal of respiratory and critical care medicine*, vol. 193, no. 4, pp. 376–385, 2016.
- [11] S. O'Reilly, M. Ciechomska, N. Fullard, S. Przyborski, and J. M. van Laar, “IL-13 mediates collagen deposition via STAT6 and microRNA-135b: a role for epigenetics,” *Scientific Reports*, vol. 6, no. 1, p. 25066, 2016.
- [12] S. F. Glaser, A. W. Heumüller, L. Tombor et al., “The histone demethylase JMJD2B regulates endothelial-to-mesenchymal transition,” *Proceedings of the National Academy of Sciences of the United States of America*, vol. 117, no. 8, pp. 4180–4187, 2020.
- [13] K. E. Leon and K. M. Aird, “Jumonji C demethylases in cellular senescence,” *Genes*, vol. 10, no. 1, 2019.
- [14] T. Ichikawa, A. Panariti, S. Audusseau et al., “Effect of bronchial thermoplasty on structural changes and inflammatory mediators in the airways of subjects with severe asthma,” *Respiratory Medicine*, vol. 150, pp. 165–172, 2019.

- [15] L. Duan, R. E. Perez, P. D. Chastain 2nd, M. T. Mathew, D. R. Bijukumar, and C. G. Maki, "JMJD2 promotes acquired cisplatin resistance in non-small cell lung carcinoma cells," *Oncogene*, vol. 38, no. 28, pp. 5643–5657, 2019.
- [16] C. Muecke, S. Dabral, W. Seeger, and S. S. Pullamsetti, "Role and regulation of Jumonji C domain-containing histone demethylases 1A and 2B in pulmonary hypertension," *European Respiratory Journal*, vol. 48, article PA5092, suppl 60, 2016.
- [17] J. A. Elias, Z. Zhu, G. Chupp, and R. J. Homer, "Airway remodeling in asthma," *The Journal of clinical investigation*, vol. 104, no. 8, pp. 1001–1006, 1999.
- [18] R. A. Panettieri Jr., U. Sjöbring, A. Péterffy et al., "Tralokinumab for severe, uncontrolled asthma (STRATOS 1 and STRATOS 2): two randomised, double-blind, placebo-controlled, phase 3 clinical trials," *The Lancet Respiratory medicine*, vol. 6, no. 7, pp. 511–525, 2018.
- [19] E. H. De Boever, C. Ashman, A. P. Cahn et al., "Efficacy and safety of an anti-IL-13 mAb in patients with severe asthma: a randomized trial," *The Journal of allergy and clinical immunology*, vol. 133, no. 4, pp. 989–996.e4, 2014.
- [20] T. Ahmad, M. Kumar, U. Mabalirajan et al., "Hypoxia response in asthma: differential modulation on inflammation and epithelial injury," *American journal of respiratory cell and molecular biology*, vol. 47, no. 1, pp. 1–10, 2012.

Research Article

Identification of a New Prognostic Risk Signature of Clear Cell Renal Cell Carcinoma Based on N⁶-Methyladenosine RNA Methylation Regulators

Yan Zhang,^{1,2} Yao Yao,¹ Xiaochen Qi,³ Jianyi Li,⁴ Meihong Liu,⁵ Xiangyu Che ,³ Yingkun Xu ,⁶ and Guangzhen Wu ³

¹Department of Laboratory, The First Affiliated Hospital of Dalian Medical University, Dalian, China

²Department of Clinical Laboratory, The First People's Hospital of Linhai, Taizhou, China

³Department of Urology, The First Affiliated Hospital of Dalian Medical University, Dalian, China

⁴Organ Transplant Center, The First Affiliated Hospital, Sun Yat-sen University, Guangzhou, China

⁵Department of Respiratory Medicine, The First Affiliated Hospital of Dalian Medical University, Dalian, China

⁶Department of Urology, Shandong Provincial Hospital, Cheeloo College of Medicine, Shandong University, Jinan, China

Correspondence should be addressed to Xiangyu Che; dalianchexiangyu@163.com, Yingkun Xu; yingkunxu@hotmail.com, and Guangzhen Wu; wuguang0613@hotmail.com

Received 13 December 2020; Revised 15 January 2021; Accepted 27 January 2021; Published 12 February 2021

Academic Editor: Xianfeng Wang

Copyright © 2021 Yan Zhang et al. This is an open access article distributed under the Creative Commons Attribution License, which permits unrestricted use, distribution, and reproduction in any medium, provided the original work is properly cited.

As the most prevalent internal eukaryotic modification, N⁶-methyladenosine (m⁶A) is installed by methyltransferases, removed by demethylases, and recognized by readers. However, there are few studies on the role of m⁶A in clear cell renal cell carcinoma (ccRCC). In this study, we researched the RNA-seq transcriptome data of ccRCC in the TCGA dataset and used bioinformatics analyses to detect the relationship between m⁶A RNA methylation regulators and ccRCC. First, we compared the expression of 18 m⁶A RNA methylation regulators in ccRCC patients and normal tissues. Then, data from ccRCC patients were divided into two clusters by consensus clustering. LASSO Cox regression analysis was used to build a risk signature to predict the prognosis of patients with ccRCC. An ROC curve, univariate Cox regression analysis, and multivariate Cox regression analysis were used to verify this risk signature's predictive ability. Then, we internally validated this signature by random sampling. Finally, we explored the role of the genes in the signature in some common pathways. Gene distribution between the two subgroups was different; cluster 2 was gender-related and had a worse prognosis. IGF2BP3, IGF2BP2, HNRNPA2B1, and METTL14 were chosen to build the risk signature. The overall survival of the high- and low-risk groups was significantly different ($p = 7.47e - 12$). The ROC curve also indicated that the risk signature had a decent predictive significance (AUC = 0.72). These results imply that the risk signature has a potential value for ccRCC treatment.

1. Introduction

As one of the most common types of kidney cancer in adults, renal cell carcinoma (RCC) accounts for nearly 3% of adult malignant tumors in the US [1]. Clear cell renal cell carcinoma (ccRCC) is the most common histological subtype of RCC [2]. The exact cause of ccRCC is uncertain, but smoking and several genetic predisposition conditions may be related to its development. ccRCC has the worst prognosis among all renal epithelial tumors. At present, surgery is considered an

effective treatment, but there are still 20%–40% of patients with postoperative metastasis or recurrence [3]. Therefore, we aimed to find a way to evaluate the prognosis of ccRCC (to make specific judgments of prognoses), determine accurate biomarkers for patients, and reduce mortality.

N⁶-Methyladenosine (m⁶A) is a modified adenosine residue, methylated at position N⁶ [4]. It is involved in a series of mRNA metabolism processes, such as mRNA stability, splicing, transport, and translation, and plays an important role in the fate of mRNA. m⁶A is mainly located

within the consensus sequence RRACH (R = G or A; H = A, C, or U) [5, 6]. This sequence is enriched near 3'-untranslated regions as well as in stop codon regions of protein-encoded mRNAs [7, 8]; in addition, when present in the 5'-UTR, mRNAs can be translated in a cap-independent manner [9]. m⁶A is the most common and abundant internal transcriptional modification found in RNAs in eukaryotic cells [4, 10, 11]. There have been many recent studies on m⁶A, and results indicate that m⁶A methylation contributes to the pathogenesis and progression of tumors [12, 13] [14, 15] and even those cancer responses to treatments are related to m⁶A [16–18].

The dynamic process of m⁶A modification is orchestrated by writers (methyltransferase complexes), erasers (demethylases), and readers (Figure 1(a)). Writers, such as METTL14, WTAP, and KIAA1429, catalyze the adenylate mRNA m⁶A modification, whereas the complex composed of METTL3, METTL14, and KIAA1429 causes the m⁶A methylated group to be written into RNA [19]. Erasers, such as FTO and ALKBH5, cause the demethylation of the base [10, 20, 21]. Finally, readers play an important role in RNA metabolism; they recognize the base modified by m⁶A, bind to the methylation site, and activate the downstream physical process [22–24]; proteins from the YTH domain family, together with IGF2BP1-3 and HNRNPA2B1, belong to the group of reader proteins. Some studies have mentioned that m⁶A regulators could be used as prognostic biomarkers in ccRCC, but these studies only analyzed some m⁶A regulators and did not make a complete risk signature. In this study, we collected data from 539 patients with ccRCC from The Cancer Genome Atlas (TCGA) and used bioinformatics analysis to determine the connection between m⁶A regulators and ccRCC in an attempt to identify a risk signature to predict the prognosis of patients with ccRCC.

2. Materials and Methods

2.1. Ethics Statement. This study was approved by the Ethics Committee of the First Affiliated Hospital of Dalian Medical University and conducted in accordance with the principles expressed in the Declaration of Helsinki. All datasets were retrieved from published literature, and all written informed consent was verified.

2.2. Data Acquisition. We systematically searched for RNA-seq transcriptome data of ccRCC in the TCGA dataset (<https://cancergenome.nih.gov/>) and downloaded all the matching clinical information data. During the processing of the clinical data in TCGA, we discounted patient samples with missing clinical information. As the lymph node metastasis status of most data is unknown, this factor was later removed from the analysis.

We used the data from the cBioPortal (<https://www.cbioportal.org/>) to verify the correlation between METTL14 and YTHDC1. To further understand the biological functions of these regulators, we used KOBAS (<http://kobas.cbi.pku.edu.cn/index.php>) to analyze the data obtained from GO, KEGG, and Reactome. We also searched the data on GSCALite (<http://bioinfo.life.hust.edu.cn/web/GSCALite/>)

to identify those pathways in which the 18 regulators used in this study are active and those drugs to which they are sensitive to, and to further detect the roles of the four chosen genes in cell signaling pathways.

2.3. Bioinformatics Analyses. First, we used the Perl package to merge all the data and extract the information of the 18 m⁶A RNA methylation regulators for further study.

We then used R (version 3.5) software to compare the expression levels of the regulators in 539 patients with ccRCC and 72 normal kidney tissues and construct a cluster analysis tree, followed by a vioplot to clearly visualize differential expression. We also analyzed the correlation between these 18 regulators.

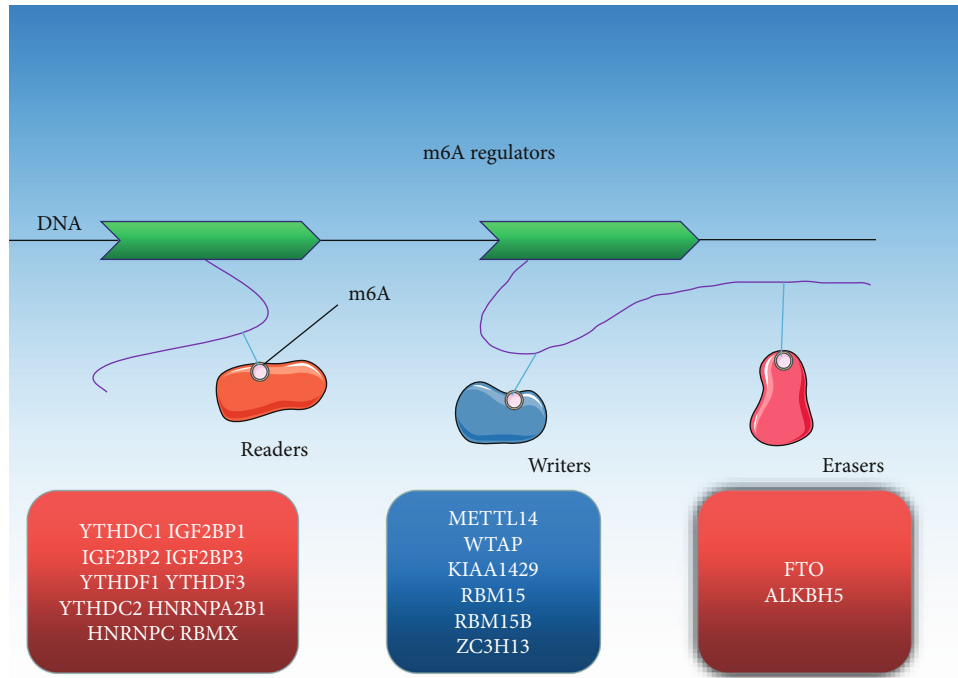
The consistent clustering algorithm was used to determine the clustering number of samples under the following classification parameters: (1) the growth rate of the cumulative distribution function (CDF) value was slow; (2) no small clusters were allowed; (3) the data in a cluster needed to have good clustering, implying a high correlation within the cluster. Then, we performed principal component analysis (PCA) to verify the clustering results.

Aiming to build a proper risk signature using m⁶A RNA methylation regulators in ccRCC, we used the least absolute shrinkage and selection operator (LASSO) Cox regression algorithm to choose the appropriate risk factors. The association between regulators and survival was first identified. Then, the coefficient was determined using the minimum standard. The best penalty parameter λ was selected to obtain the final risk score. Then, we used the risk signature to divide the patients into two subgroups and compared the overall survival (OS) of these two subgroups. Then, the receiver operating characteristic (ROC) curve was estimated, and univariate and multivariate Cox regression analyses were performed to verify the predictive ability of the risk signature. Finally, we use the GSE22541 dataset in the GEO database for external verification and random internal verification on the ccRCC dataset in the TCGA database. All these were also executed using R software package.

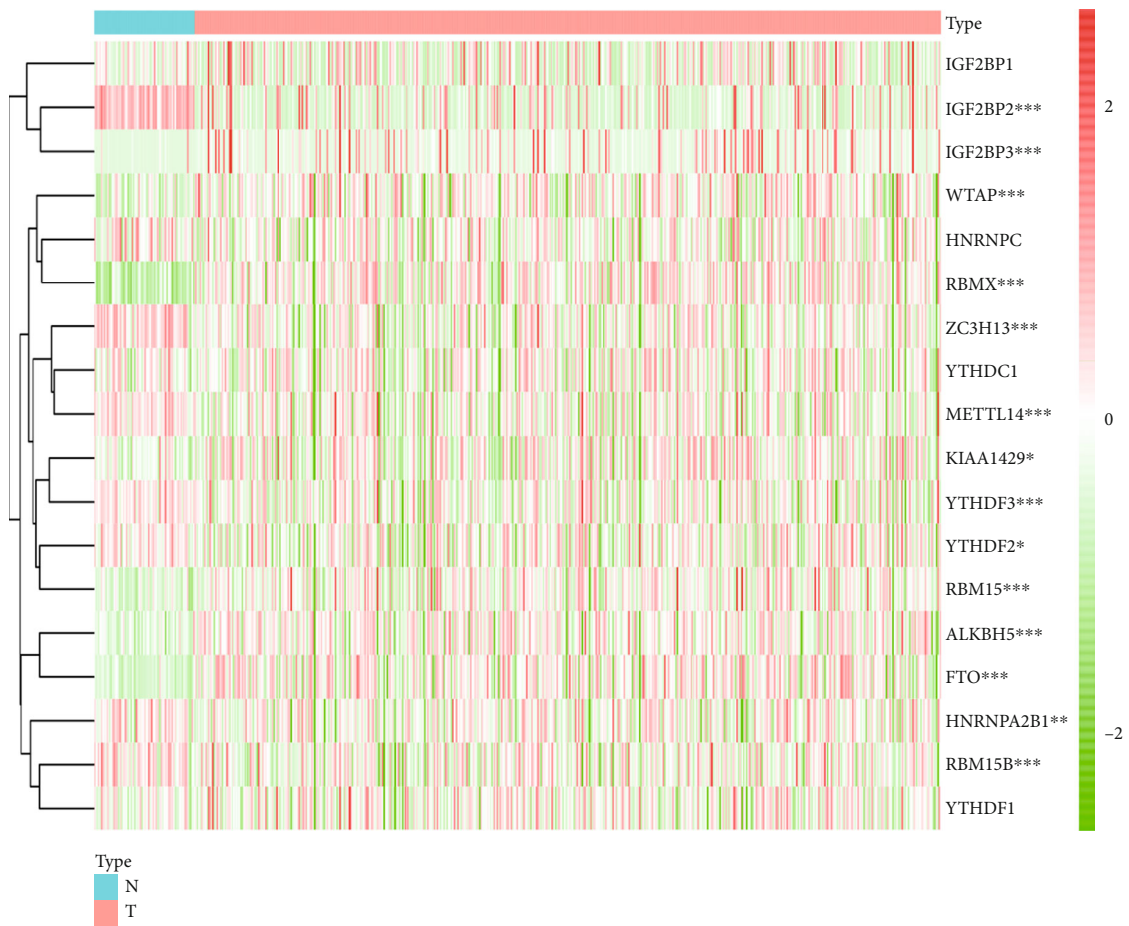
2.4. Statistical Analyses. The expression of m⁶A RNA methylation regulators in tumor tissues and normal tissues was compared by one-way ANOVA. Kaplan-Meier analysis was used to obtain survival curves [25]. *t*-tests were used to compare the expression levels in ccRCC for different clinical characteristics. We obtained the optimal cut-off value of each risk score in the training group using R software to build the risk signature. Cox regression analysis was used to evaluate the association between the risk score, other clinical characteristics, and OS. The log-rank tests were used to perform survival analyses. In all our analyses, $p < 0.05$ was considered statistically significant.

3. Results

3.1. The Panorama of m⁶A RNA Methylation Regulators in ccRCC. First, we compared the expression of the 18 m⁶A RNA methylation regulators in 539 ccRCC cancer tissues against the expression in 72 normal kidney tissues obtained

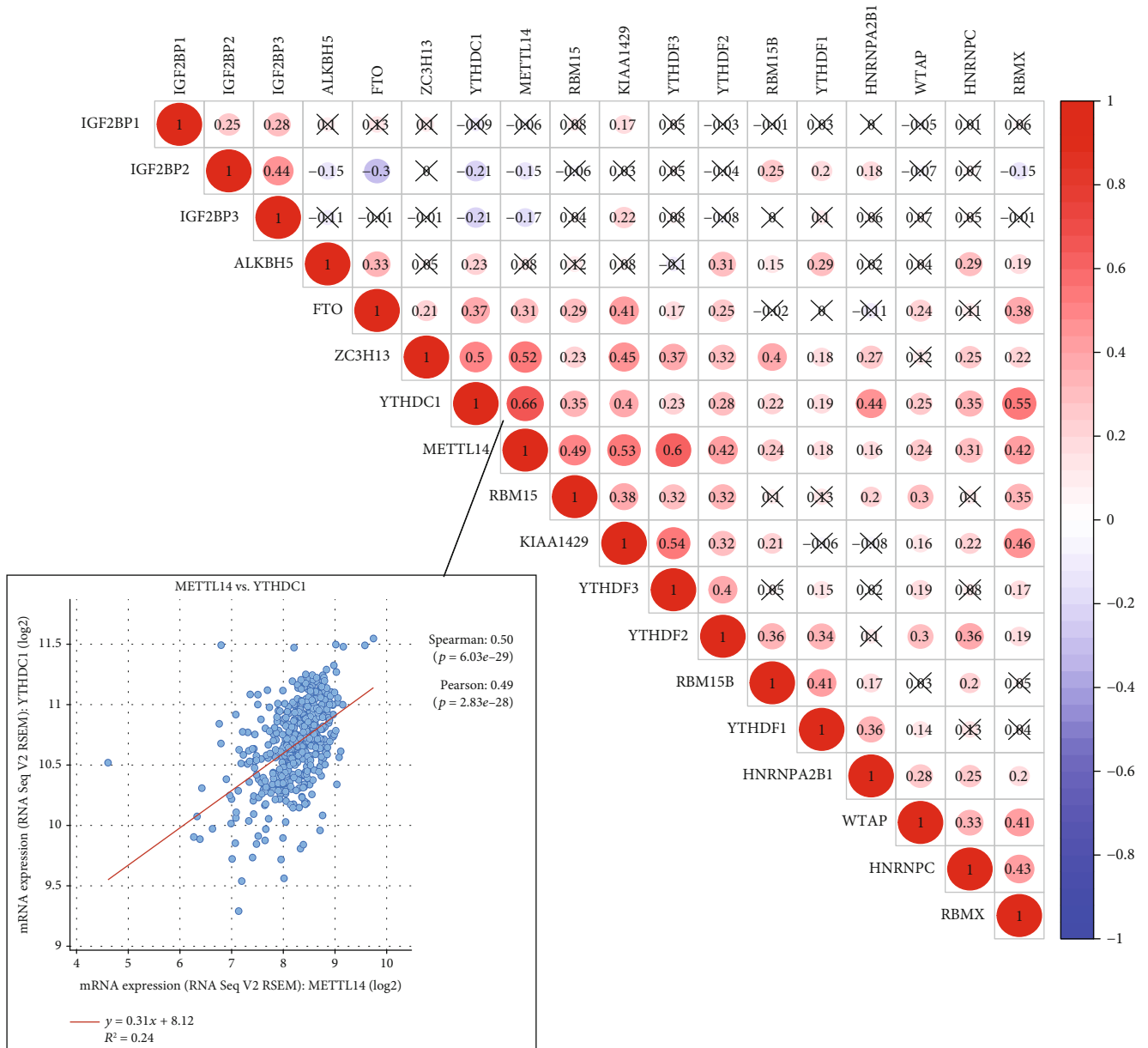


(a)



(b)

FIGURE 1: Continued.



(c)

FIGURE 1: Continued.

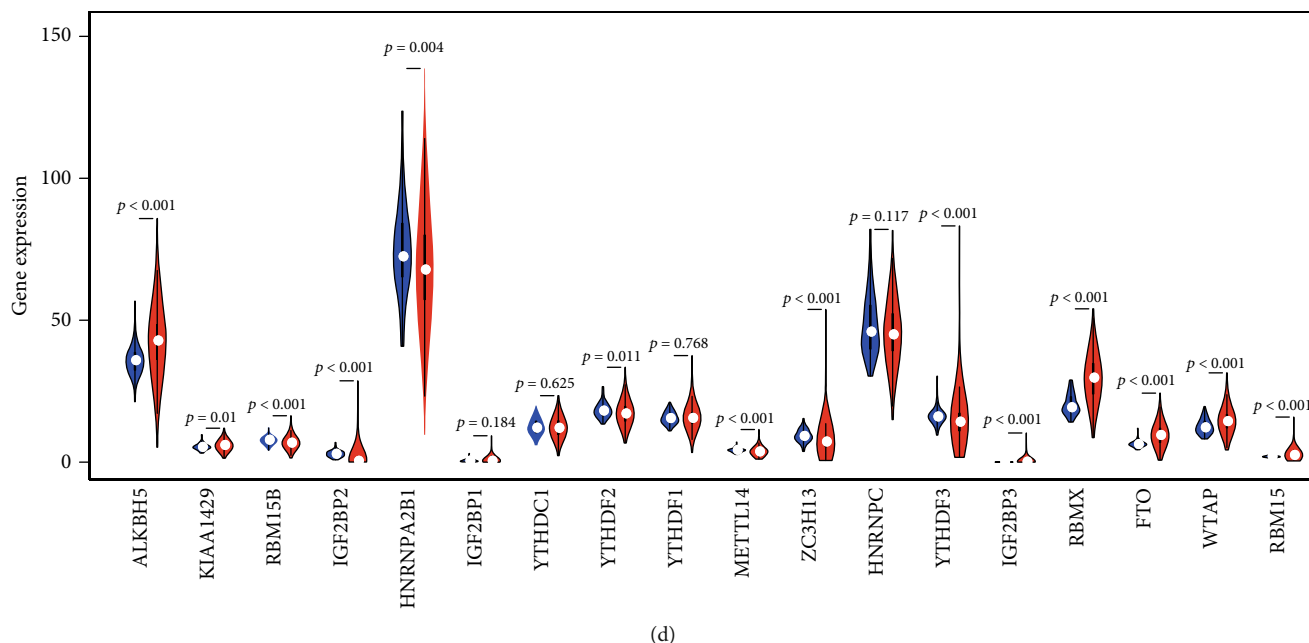


FIGURE 1: The panorama of m^6A RNA methylation regulators in ccRCC. (a) The m^6A RNA methylation process and the regulators involved. (b) Expression levels of 18 m^6A RNA methylation regulators in ccRCC and normal tissues. The upper tree diagram represents grouping results for the samples, whereas the tree on the left represents cluster analysis results for regulators. Highly expressed genes are represented by a red-colored gradient: the highest the expression, the darker the red tone. In contrast, lowly expressed genes are represented by a green-colored gradient, being the genes with the lowest expression the darker ones. (c) Spearman correlation analysis of the 18 m^6A RNA methylation regulators in ccRCC and verification of the correlation between YTHDC1 and RBM15. (d) Violin plot visualizing differentially expressed m^6A RNA methylation regulators in ccRCC. The x-axis represents different genes, the y-axis represents gene expression, blue represents normal kidney tissue, and red represents ccRCC tissue. * $p < 0.05$, ** $p < 0.01$, and *** $p < 0.001$.

from the TCGA database. Compared with normal tissues, the expression of ALKBH5, KIAA1429, RBM15B, IGF2BP2, HNRNPA2B1, YTHDF2, METTL4, ZC3H13, YTHDF3, IGF2BP3, RBMX, FTO, WTAP, and RBM15 showed significant statistical differences (Figures 1(b) and 1(d)). Next, we further explored the interactions between the 18 m^6A RNA methylation regulators and found that such interactions could be positive, negative, or irrelevant (Figure 1(c)). We found that the two most relevant regulators were YTHDC1 and RBM15, with a mutual reinforcement correlation. To verify this conclusion, we explored the cBioPortal data and found that these two regulators had a strong expression correlation.

3.2. Consensus Clustering of m^6A RNA Methylation Regulators Identified Two Clusters of ccRCC. Next, we used consensus clustering to group the 539 ccRCC tissues. According to Figures 2(b) and 2(c), $k=2$ or $k=3$ values would be acceptable; however, after dividing the samples into 3 groups, some data could not be well clustered; therefore, we decided to separate our data into 2 groups. The matrix shown in Figure 2(a) represents the consensus for $k=2$ and indicates a well-defined 2-block structure. Then, we used PCA to verify whether the grouping was appropriate (Figure 2(d)). As there were little overlapping area between clusters 1 and 2, and the data in each group gathered well, we concluded that grouping by m^6A RNA methylation regulator expression was appropriate ($k=2$).

3.3. Groups Determined by Consensus Clustering Are Closely Related to the Prognosis of ccRCC and Clinicopathological Features. According to consensus clustering, we compared the expression levels of m^6A RNA methylation regulators between clusters 1 and 2. Other factors such as gender, age, tumor grade, fustat, cancer stage status, and T, M, and N status were also taken into account for the comparison. We found that the expression levels of m^6A RNA methylation regulators in clusters 1 and 2 were indeed different, and that cluster 2 was correlated with gender (Figure 3(a)). The detailed information of gene expression in clusters 1 and 2 is summarized in Supplementary Material Table S1. As shown in Figure 3(b), the OS of cluster 2 is shorter than that of cluster 1, indicating a worse clinical outcome.

3.4. The Role of m^6A RNA Methylation Regulators in Various Physiological Processes or Signaling Pathways and Drug Sensitivities of m^6A Methylation Regulators. To better understand the function of m^6A RNA methylation regulators, we analyzed the 18 regulators using KOBAS and visualized the results using R language. Relevant data was obtained from Gene Ontology (GO), KEGG, and Reactome (Figures 3(c) and 3(d)) databases. According to the results from pathway enrichment, studied regulators are mainly involved in RNA regulation and metabolism processes, such as RNA binding, poly(A) RNA binding, and gene expression.

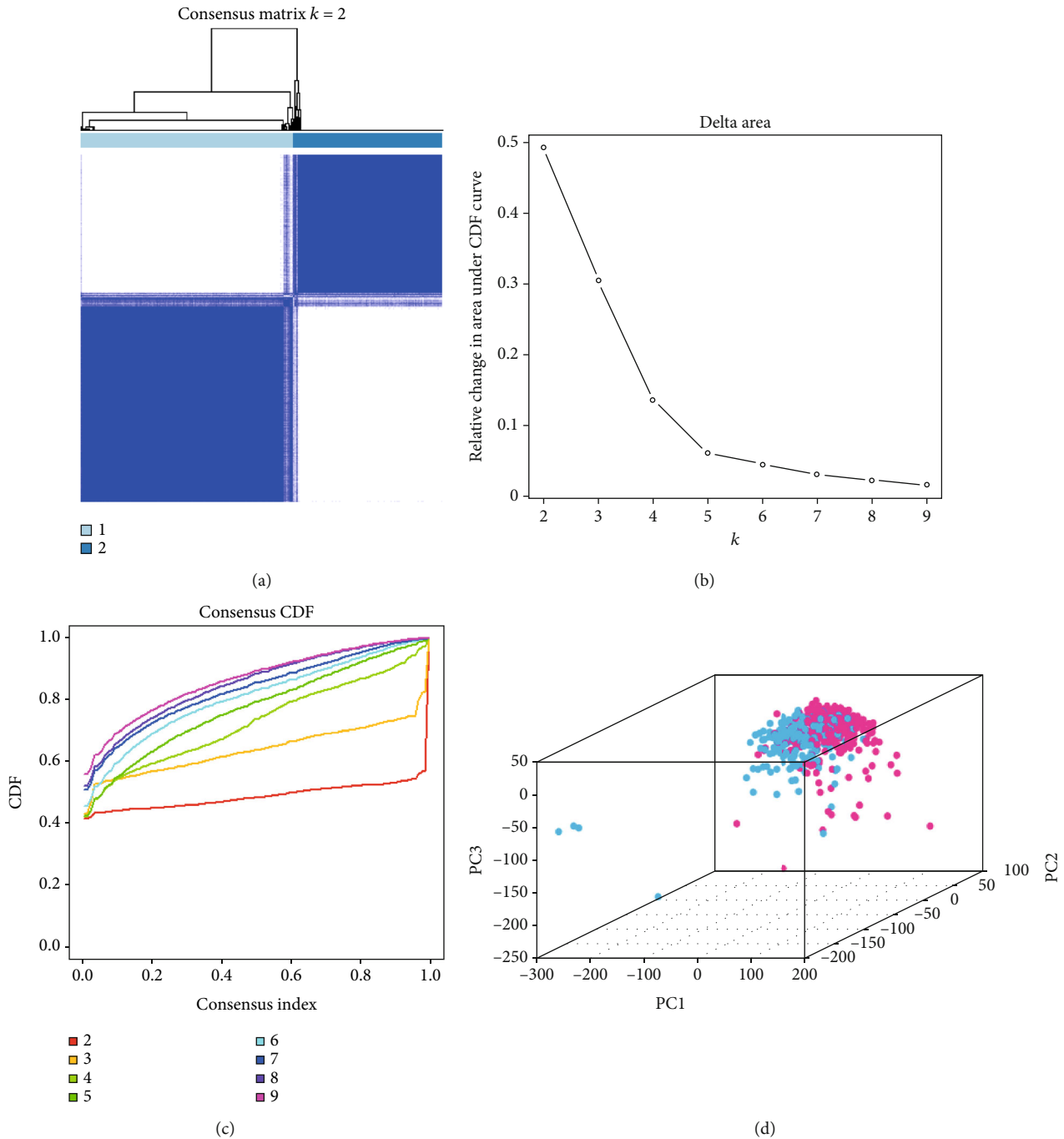
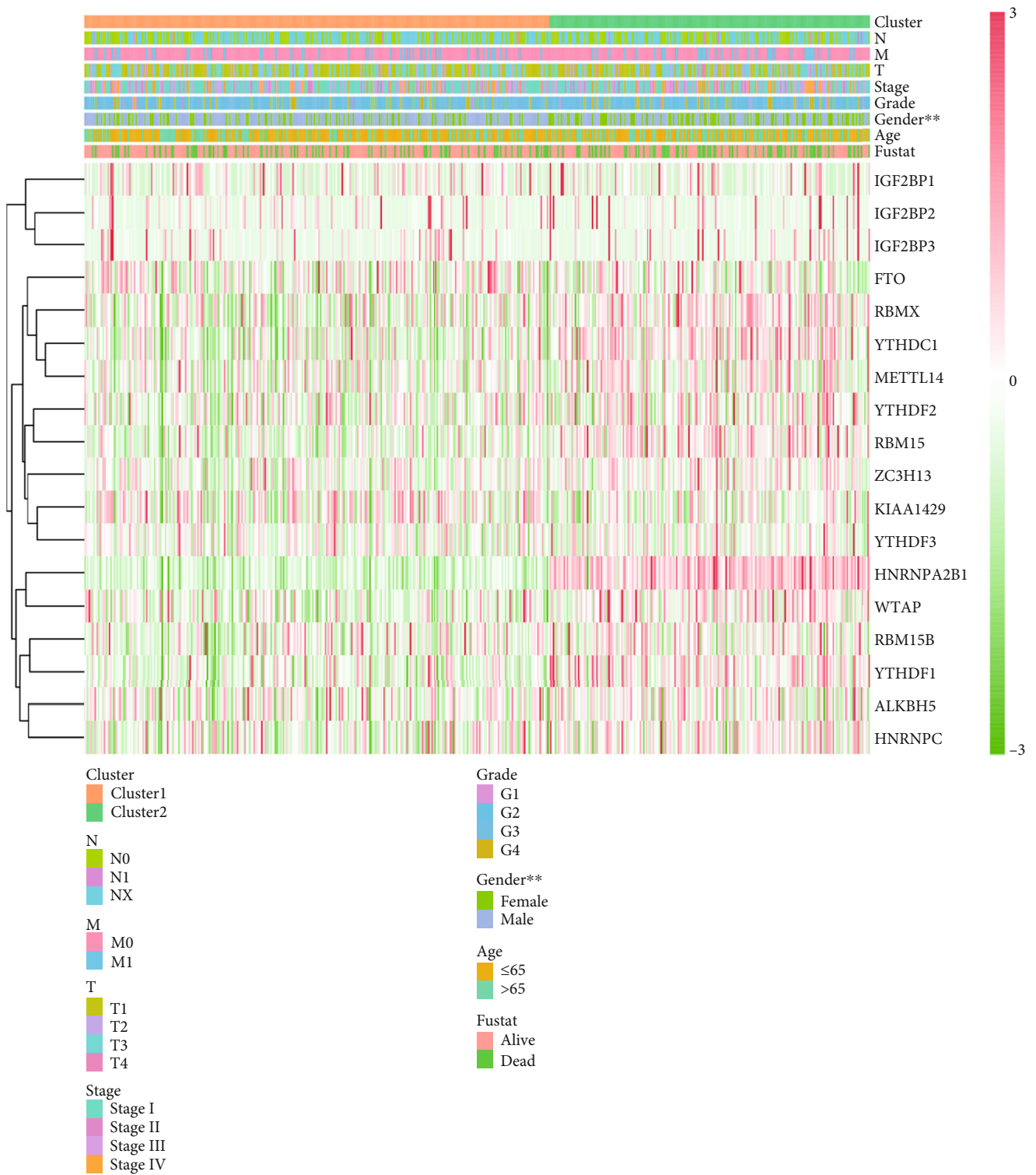


FIGURE 2: Identification of consensus clusters by m⁶A RNA methylation regulators. (a) When $k = 2$: correlation between groups. (b) Relative change in the area under the cumulative distribution function (CDF) curve for k values from 2 to 9. (c) Consensus clustering CDF when k value ranges from 2 to 9. (d) Principal component analysis of the total RNA expression profile in the TCGA dataset (cluster 1 is marked in red and cluster 2 in blue).

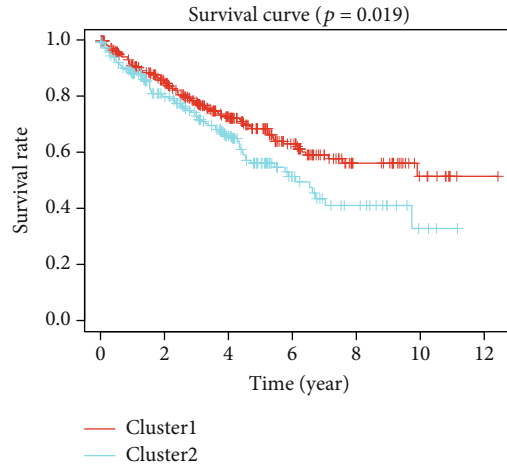
Then, we analyzed the data on GSCALite and found that m⁶A RNA methylation regulators play important roles in many cell signaling pathways and physiological activities. HNRNPA2B1, for example, can activate apoptosis and DNA damage response, and it is also engaged in the cell cycle (Figures 4(a) and 4(b)). In addition, m⁶A RNA methylation regulators are sensitive targets for common chemotherapy drugs and targeted agents (Figure 4(c)).

3.5. A Risk Signature Built with Four Regulators to Evaluate Clinical Outcomes. We tried to determine whether m⁶A methylation regulators can play a prognostic role in ccRCC. Therefore, we performed a univariate Cox regression analysis on the expression levels of these regulators. As shown in Figure 5(a), patients with high expression of KIAA1429 (hazard ratio [HR] = 0.869, 95% confidence interval [CI] = 0.80 – 0.95), YTHDC1 (HR = 0.922, 95%CI

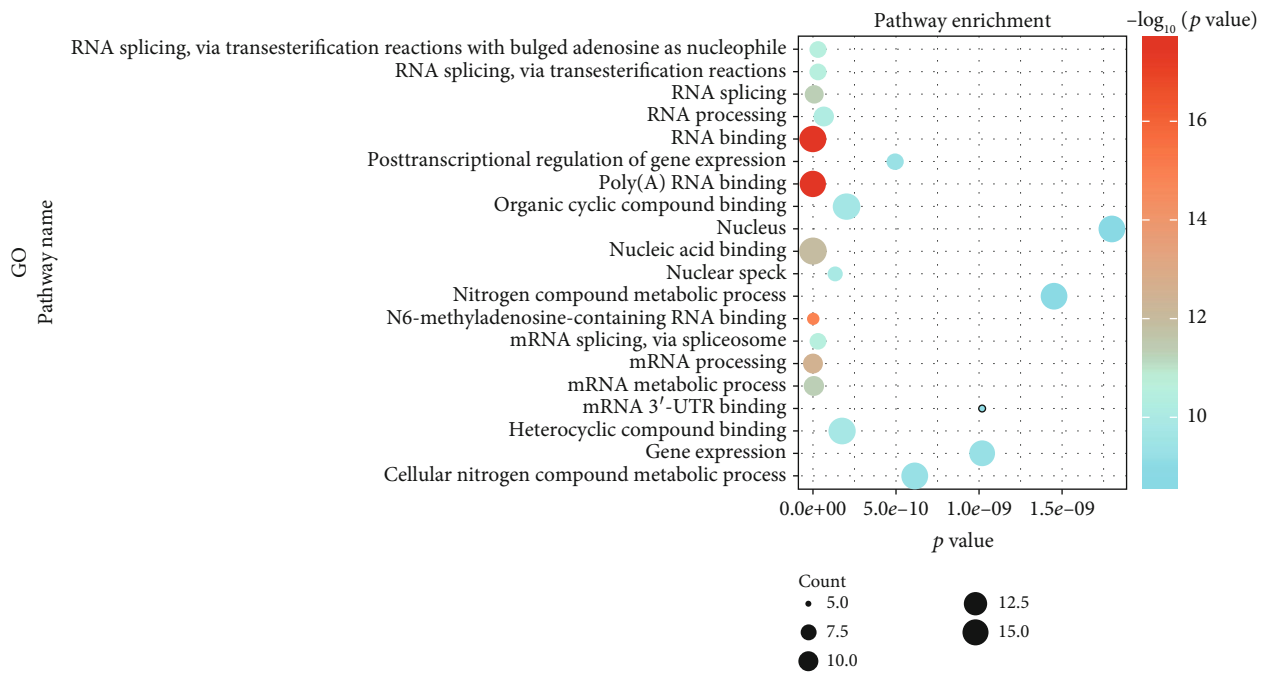


(a)

FIGURE 3: Continued.



(b)



(c)

FIGURE 3: Continued.

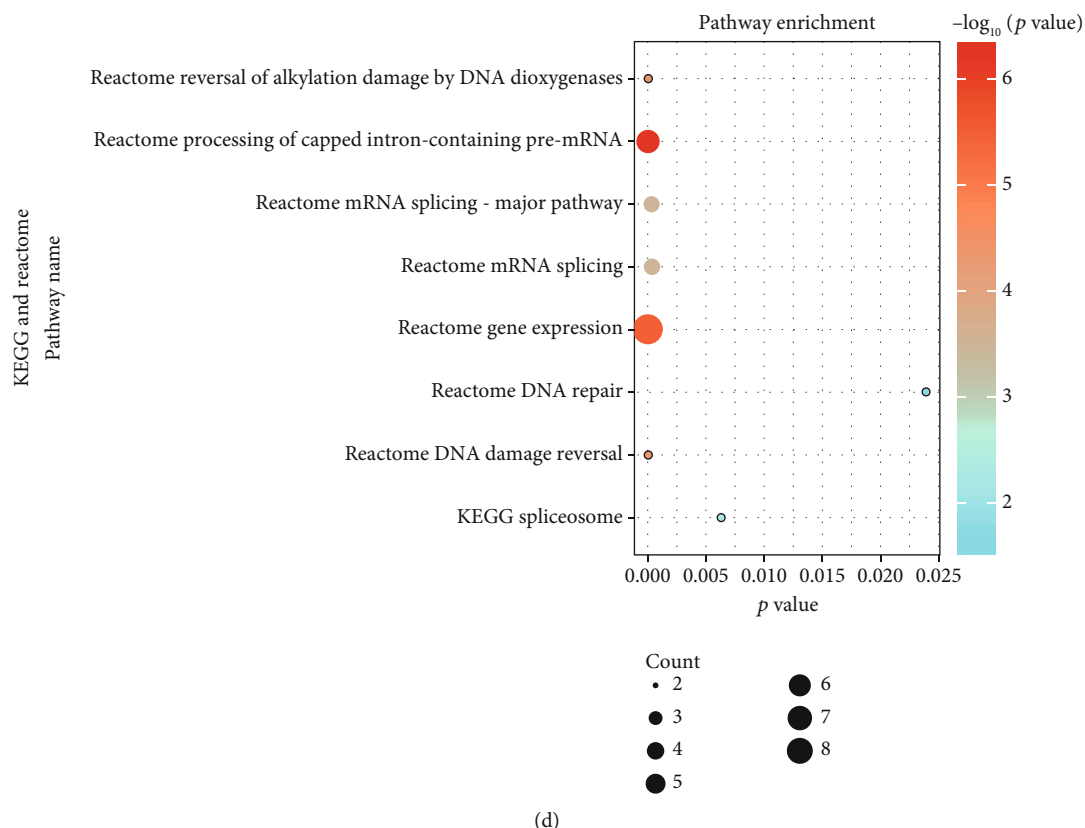


FIGURE 3: Prognosis and clinicopathological features of ccRCC. (a) The heat map and clinicopathological features of the two clusters were identified by m^6A RNA methylation regulators. (b) Kaplan-Meier overall survival (OS) rate curve of patients with ccRCC (cluster 1 patients: red; cluster 2 patients: blue). (c, d) Results from pathway enrichment of the data using Gene Ontology (GO), KEGG, and Reactome. The size of each dot represents the pathway count. High p values are represented by a red-colored dot: the highest the value, the darker the red tone. In contrast, low p values are represented by a blue-colored dot, being the lowest values the darker ones. * $p < 0.05$, ** $p < 0.01$, and *** $p < 0.001$.

= 0.88 – 0.96), YTHDF2 (HR = 0.955, 95%CI = 0.92 – 0.99), METTL14 (HR = 0.662, 95%CI = 0.58 – 0.76), ZC3H13 (HR = 0.892, 95%CI = 0.84 – 0.95), YTHDF3 (HR = 0.953, 95%CI = 0.92 – 0.99), RBMX (HR = 0.971, 95%CI = 0.95 – 0.99), and FTO (HR = 0.945, 95%CI = 0.91 – 0.99) have a better prognosis than patients with high expression of IGF2BP2 (HR = 1.087, 95%CI = 1.06 – 1.12), HNRNPA2B1 (HR = 1.016, 95%CI = 1.01 – 1.02), IGF2BP1 (HR = 1.14, 95%CI = 1.02 – 1.28), and IGF2BP3 (HR = 1.415, 95%CI = 1.27 – 1.58).

Next, we used the LASSO Cox regression algorithm to analyze the 18 regulators in the TCGA dataset and chose four of them, IGF2BP3, IGF2BP2, METTL14, and HNRNPA2B1, to build the risk signature. Selection was based on the minimum criteria and the coefficients obtained from the LASSO algorithm that were used to calculate the risk score for the TCGA dataset (Figures 5(b) and 5(c)).

To verify the prognostic ability of the four-regulator risk signature, we graded the data in the TCGA dataset and divided them into two groups according to the risk signature, the high-risk and low-risk groups, and drew the corresponding survival curves. We found that the clinical outcomes of the high-risk group were significantly worse than those of the low-risk group (Figure 5(d)).

3.6. The Prognostic Value of the Risk Signature Built with Four m^6A RNA Methylation Regulators. We compared the expression of the four selected regulators between the low-risk and the high-risk groups. We also compared the expression considering several characteristics, such as T and M statuses, the clinical stage and grade of the tumor, the patients' age, gender, and fustat, and the cluster (1 or 2) to which the regulators belonged. After noticing that most of the data in the TCGA dataset were NX, we decided not to consider this factor in our analysis. We found that there was a high expression of IGF2BP3, IGF2BP2, and HNRNPA2B1 and a low expression of METTL14 in the high-risk group. The high-risk group also showed stronger correlations with M and T statuses, tumor stage and grade, fustat, and cluster of origin than the low-risk group (Figure 6(a)).

Receiver operating characteristic (ROC) curves were used to test the accuracy and specificity of the four-gene risk signature. The AUC = 0.72 indicated that the risk score could efficiently predict the 5-year survival of patients with ccRCC (Figure 6(b)). Then, we performed univariate and multivariate Cox regression analyses of the data from the TCGA dataset to determine whether the risk signature could be useful as an independent factor to predict the clinical outcome (Figures 6(c) and 6(d)). Results from the univariate Cox

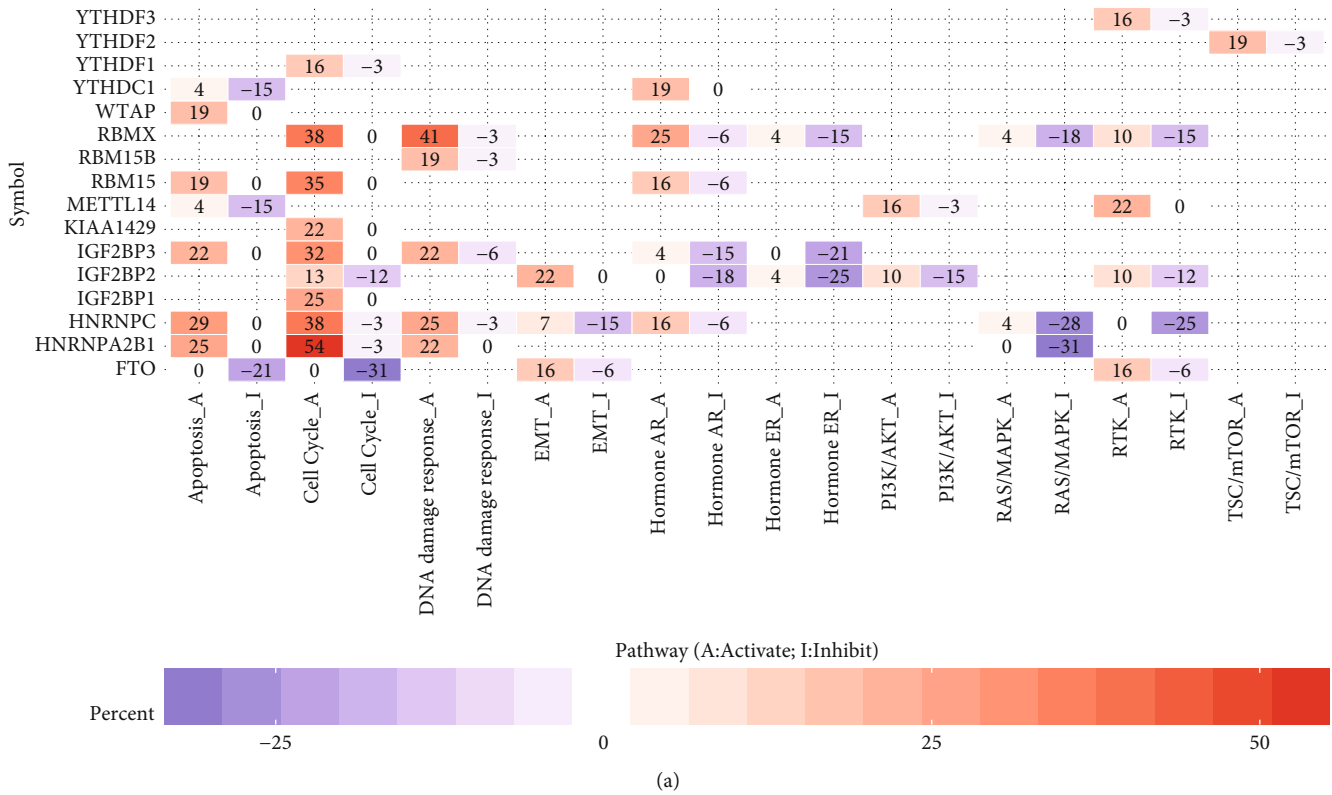
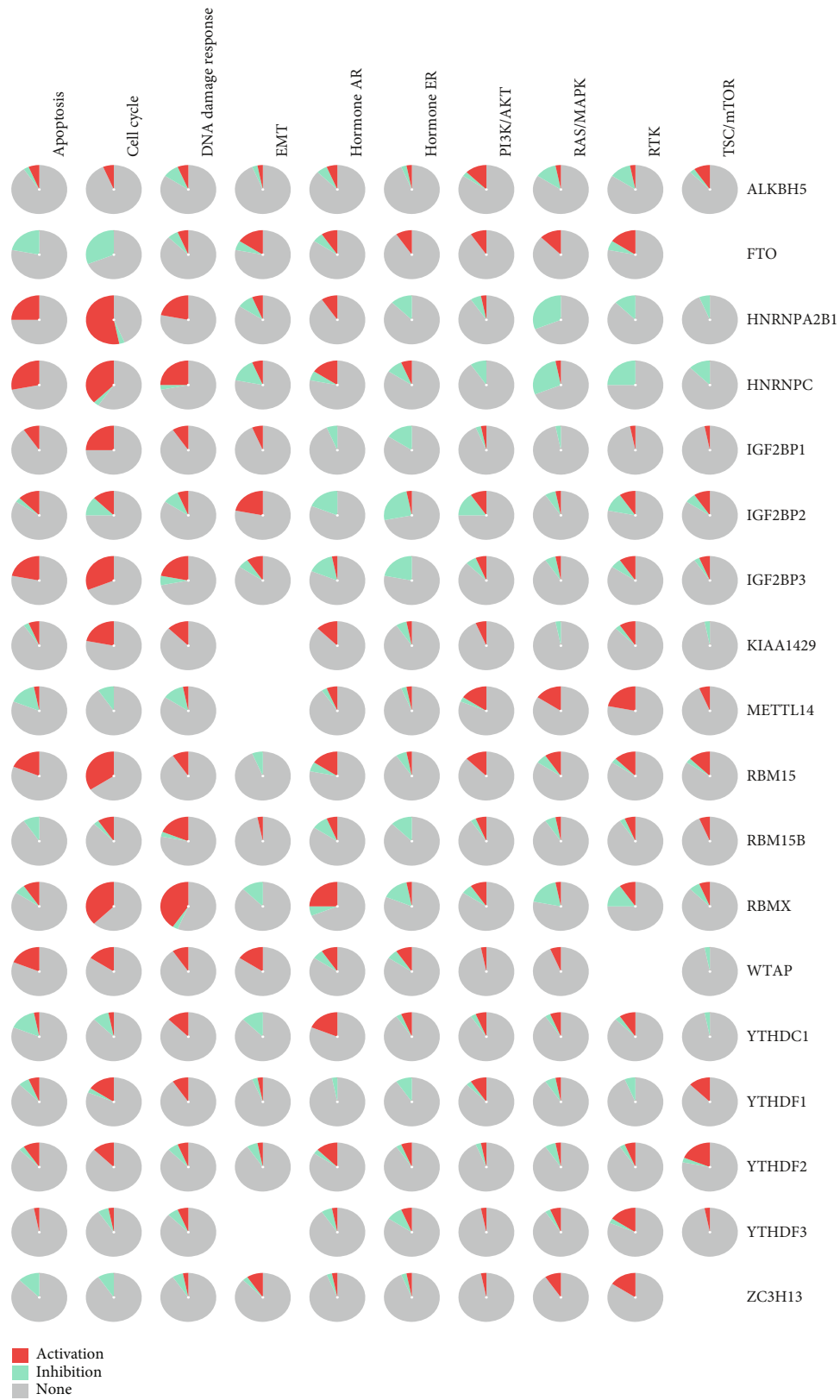
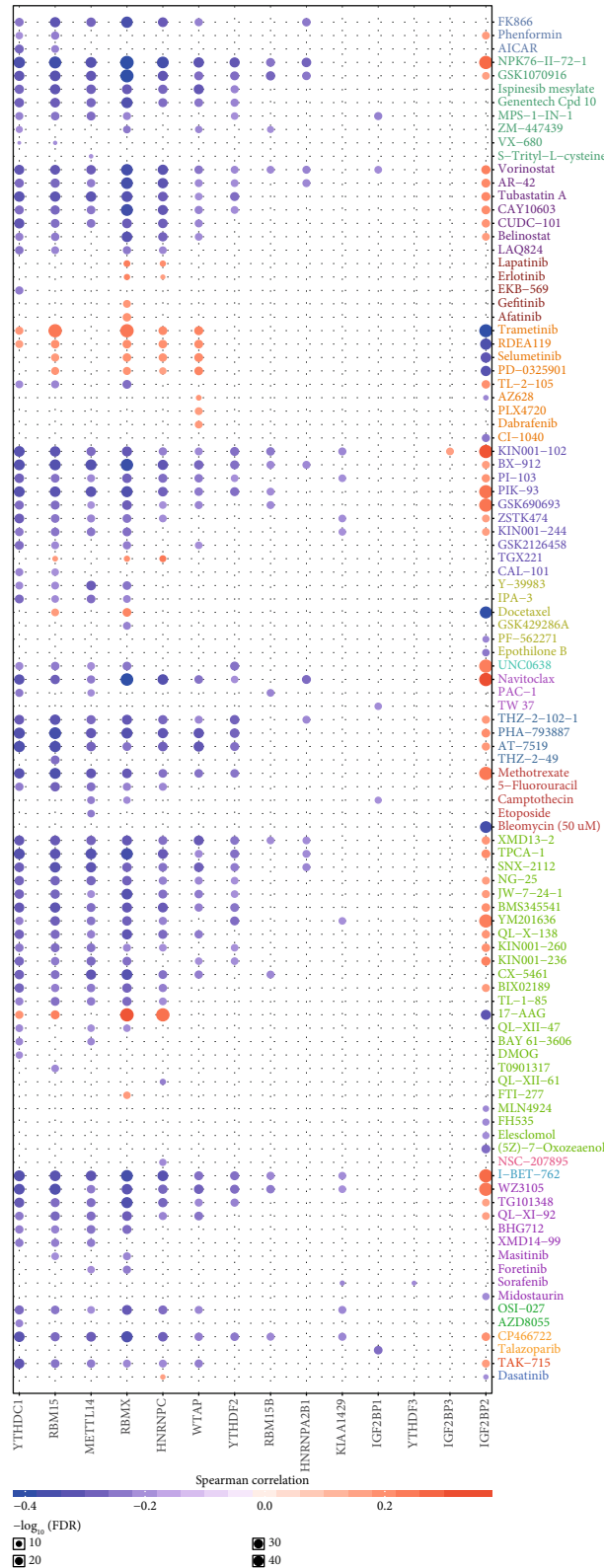


FIGURE 4: Continued.



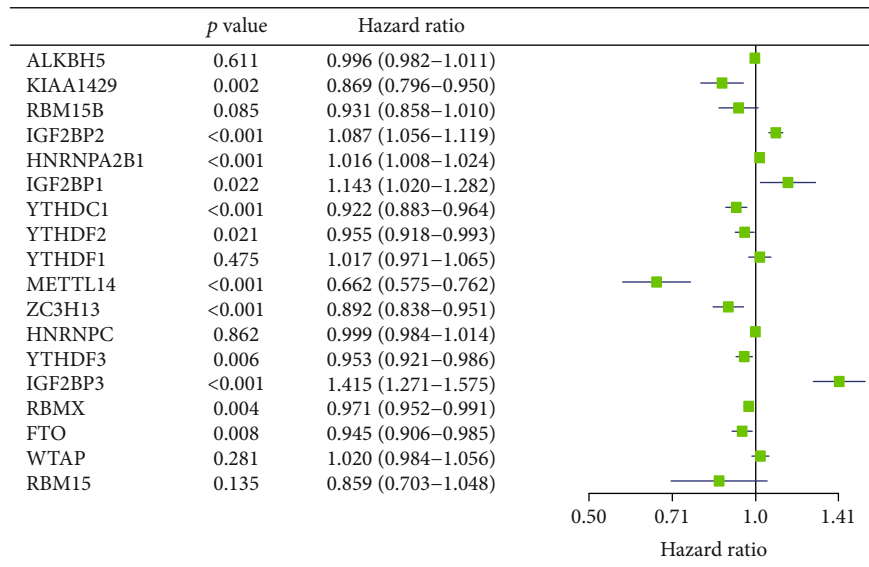
(b)

FIGURE 4: Continued.

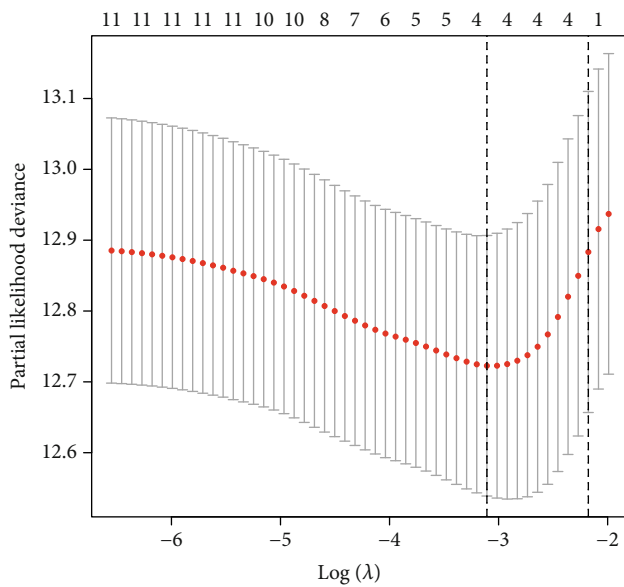


(c)

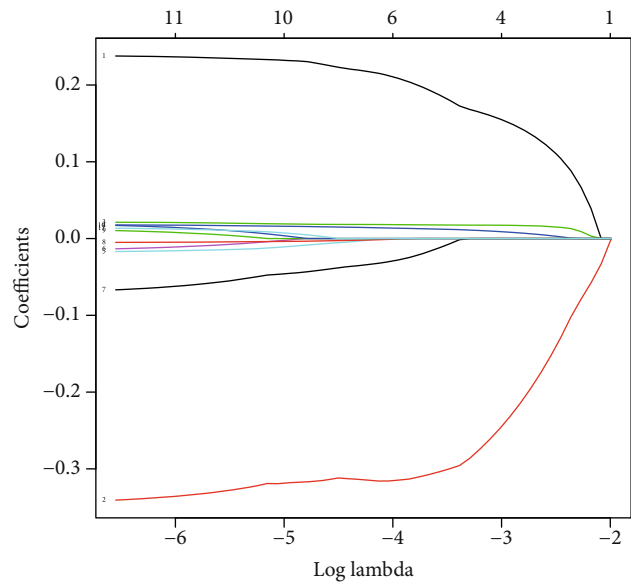
FIGURE 4: Physiological processes, signaling pathways, and drug sensitivities relevant to m⁶A methylation regulators. (a) Effect of m⁶A methylation regulators on physiological processes and signaling pathways. A: active; I: inhibited; the darker the color, the stronger the inhibition (blue) or activation (red). If a regulator activates a process or a pathway, the activation index is higher than the inhibition index. On the contrary, if the inhibition index has the highest value, then the process is inhibited. (b) Pie chart showing the results from (a) (red: activation; green: inhibition). (c) Drug sensitivities of m⁶A methylation regulators (ordinate axis: various drugs; abscissa axis: regulators).



(a)



(b)



(c)

FIGURE 5: Continued.

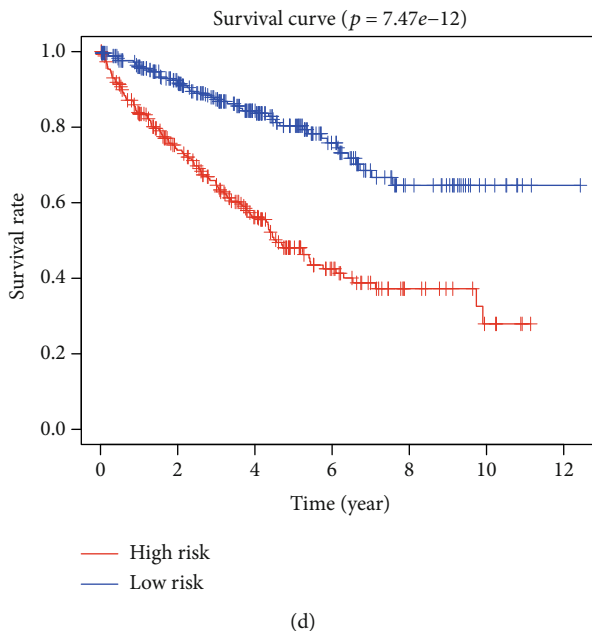


FIGURE 5: Risk signature for ccRCC. (a) Hazard ratios (HRs) and 95% confidence intervals (CIs) were calculated using univariate Cox regression. (b, c) Coefficients calculated by the least absolute shrinkage and selection operator (LASSO) multivariate Cox regression algorithm. (d) Kaplan-Meier overall survival (OS) rate curve for high-risk (red) and low-risk (blue) groups of patients.

regression analysis showed that age (HR = 1.031, 95%CI = 1.02 – 1.05), grade (HR = 2.296, 95%CI = 1.87 – 2.82), stage (HR = 1.865, 95%CI = 1.63 – 2.13), T status (HR = 1.893, 95%CI = 1.60 – 2.24), M status (HR = 4.407, 95%CI = 3.22 – 6.03), and risk score (HR = 2.209, 95%CI = 1.85 – 2.64) correlated with OS. In addition, results from the multivariate Cox regression analysis indicated that age (HR = 1.037, 95%CI = 1.02 – 1.05) and risk score (HR = 1.88, 95%CI = 1.51 – 2.25) were associated with OS. Therefore, we can conclude that the risk signature can predict the prognosis of patients with ccRCC independently and in combination with other risk factors (Figures 6(c) and 6(d)).

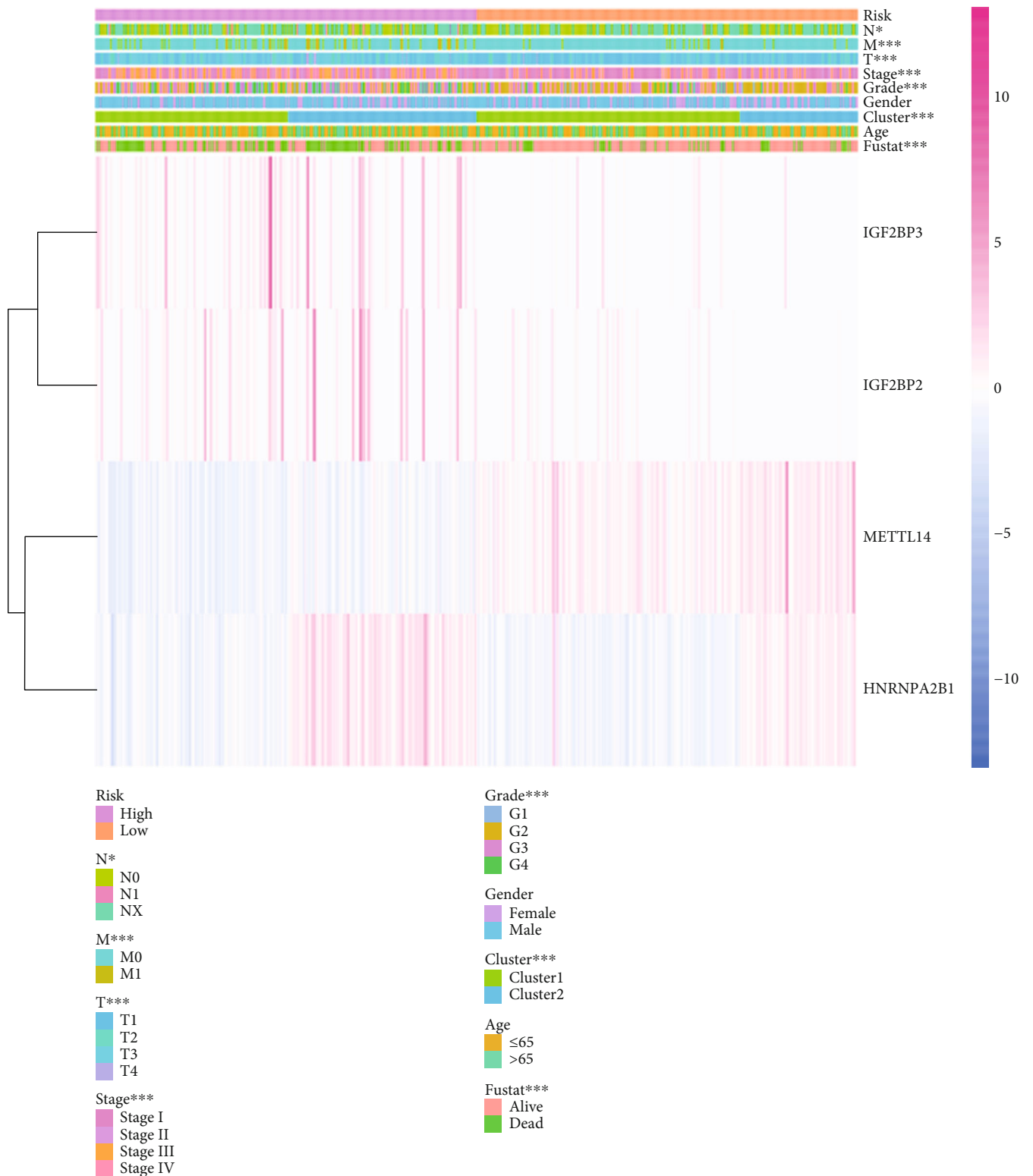
3.7. Random Sampling Verification and External Verification Based on the Signature. To verify the accuracy of the signature, we tested it over randomly sampled data from TCGA. Survival curves indicated that the OS of the high-risk group was lower than the low-risk group (Figure 7(a)). Figure 7(b) shows the expression levels of the four genes in the chosen samples. The high-risk group contained 24 samples, and the low-risk group contained 26 samples. Compared with the low-risk group, the high-risk group had lower expression of METTL14 and higher expression of IGF2BP3, IGF2BP2, and HNRNPA2B1. To further extend the performance of the risk signature, we made a nomogram to take other clinicopathological factors into account. By using this nomogram, we could calculate the 5-year survival, 7-year survival, and 10-year survival of the patients (Figure 8). Then, we used GSE22541 for external verification. Since this dataset only contained patient DFS information and not OS information, we verified the DFS of the risk model and the four genes in ccRCC and drew the corresponding survival curve (Supplementary Materials Figure S1(A–E)). Surprisingly, we found

that the external verification results also support the results obtained through the TCGA database in the early stage.

3.8. GSEA Pathway Analysis of the Four Genes. We selected five signaling pathways for evaluating changes in the expression of the four genes belonging to the newly described signature. An open-up parabola indicates that the gene activates the pathway, whereas an open-down parabola indicates that the gene can inhibit the pathway (Figures 9(a)–9(d)). For instance, IGF2BP3 has a positive regulatory effect on the calcium signaling pathway, glycosaminoglycan degradation, P53 signaling pathway, and steroid biosynthesis; however, high levels of IGF2BP3 can inhibit glycerolipid metabolism. Finally, in order to show the process of this research more clearly, we draw a corresponding flow chart (Figure 10).

4. Discussion

Evidence shows that m⁶A RNA methylation has various functions in the occurrence, development, and proliferation of cancer [26, 27]. It may also affect cancer stem cell pluripotency and cell differentiation [16, 28], promote cancer cell migration [29], and contribute to tumor immunity [30]. m⁶A RNA methylation regulators include three major elements: writers, erasers, and readers. Writers catalyze the formation of m⁶A, erasers remove m⁶A from RNAs, and readers recognize and bind m⁶A sites. As writers, the complex formed by METTL14 and METTL3 recognizes the substrate [31], WTAP ensures that the complex is located exactly on the nuclear speckle [32], RBM15 attaches to the WTAP-METTL3 complex and engages it to specific RNA sites [33], ZC3H13 mediates the combination of WTAP and Spentito [34], and KIAA1429 is related to the selectivity



(a)

FIGURE 6: Continued.

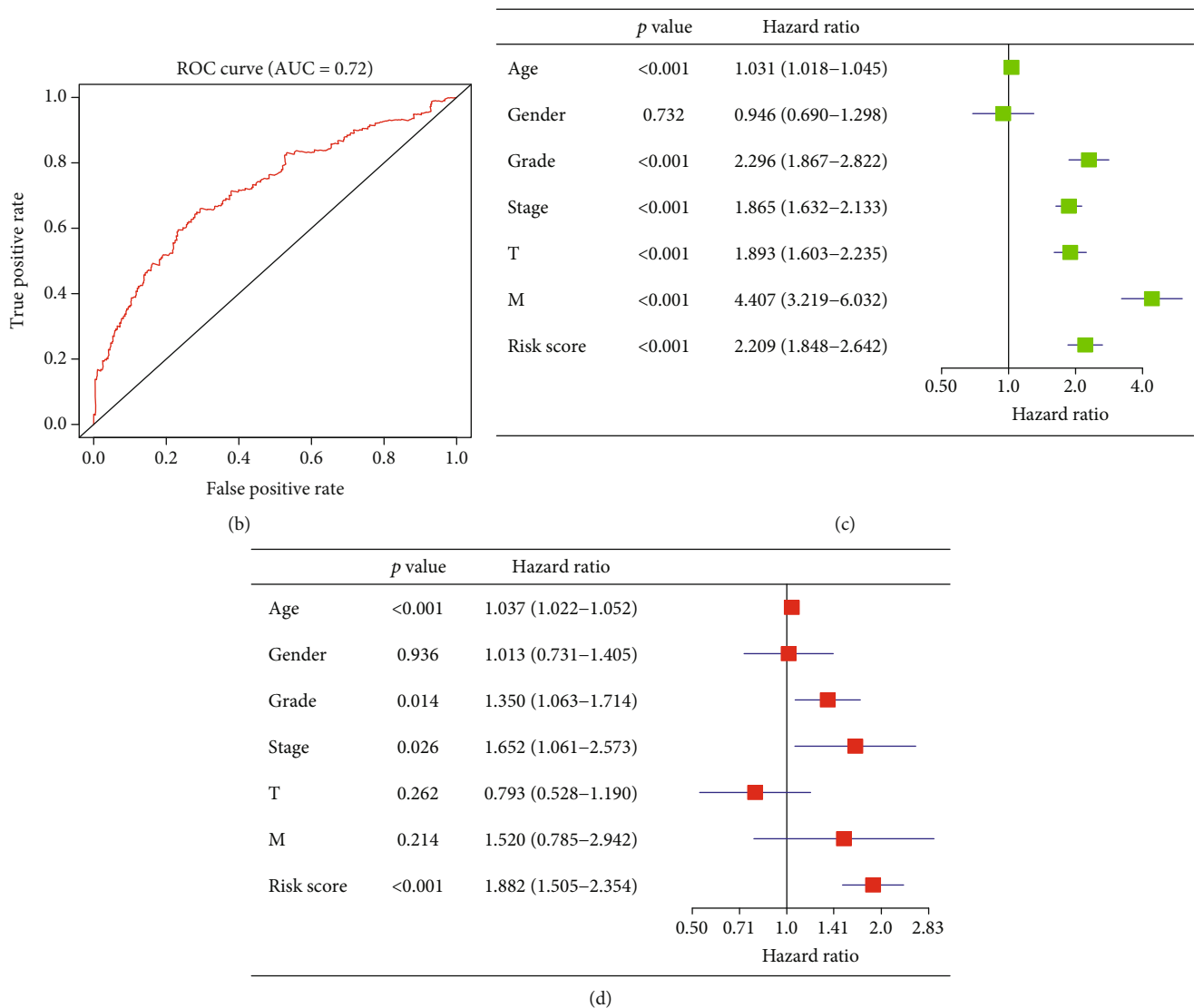
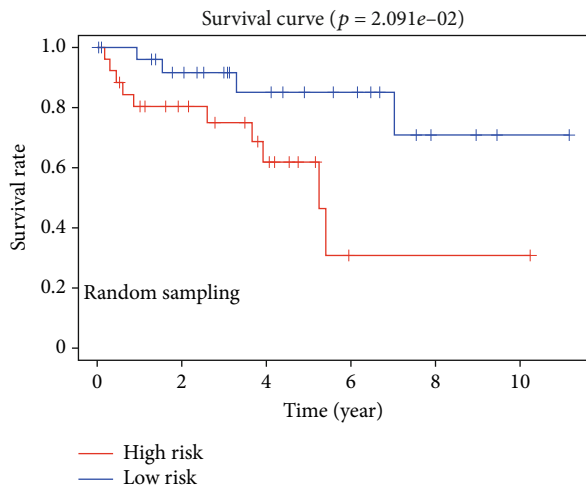


FIGURE 6: Prognosis value and accuracy of the risk signature. (a) Comparison of clinicopathological characteristics and expression of IGF2BP3, IGF2BP2, HNRNPA2B1, and METTL14 between the two groups defined by the risk signature. (b) ROC curve representing the efficiency and accuracy of the risk signature: the ROC curve for 5-year survival prediction by risk signature (data from TCGA). (c) Univariate Cox regression analysis of the association between clinicopathological factors, risk score, and overall survival of patients from TCGA datasets. (d) Multivariate Cox regression analysis of the association between clinicopathological factors, risk score, and overall survival of patients from TCGA datasets. * $p < 0.05$, ** $p < 0.01$, and *** $p < 0.001$.

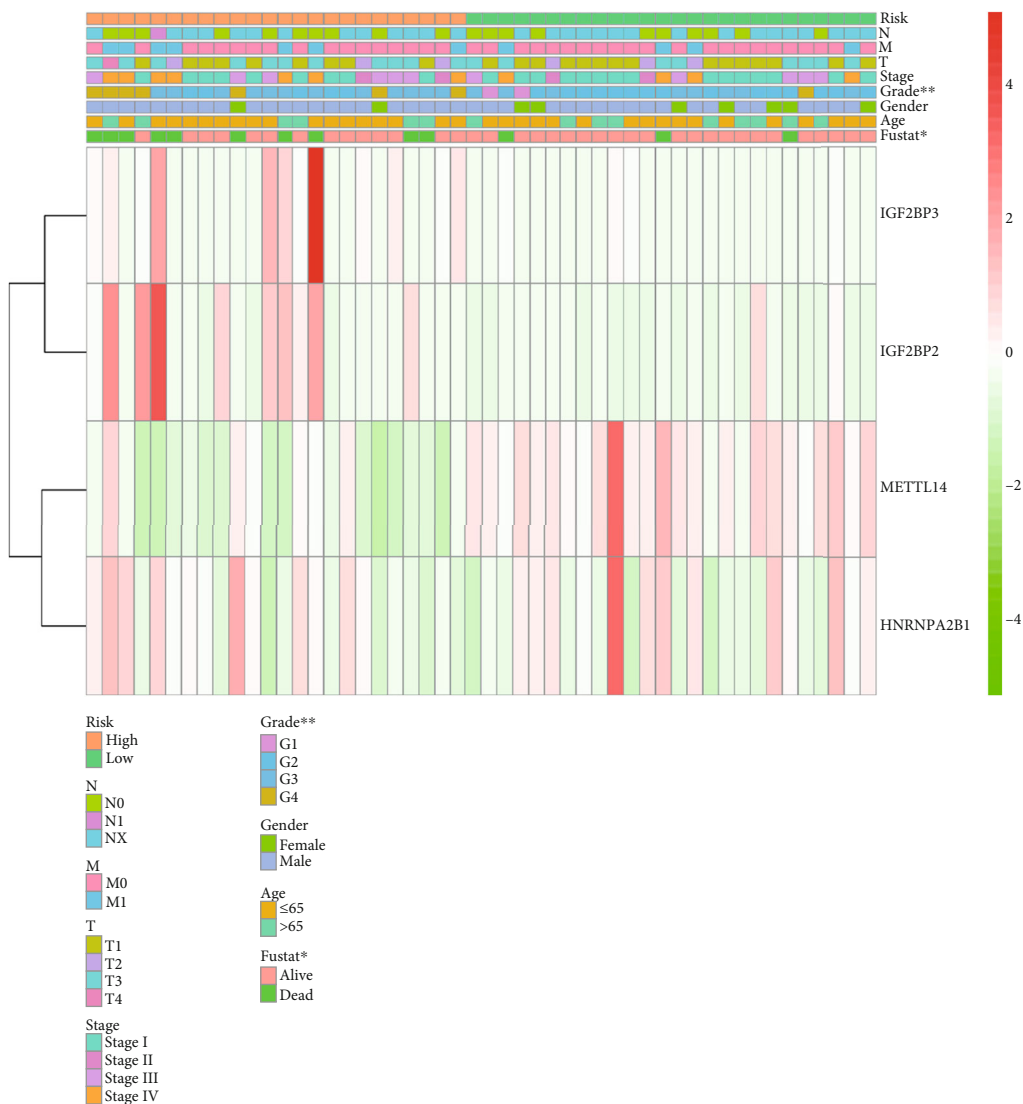
of m⁶A modified sites [35]. As erasers, FTO controls mRNA splicing and regulates adipogenesis [36], and ALKBH5 participates in the process of splicing and the production of longer 3'-UTR mRNAs [37]. Finally, as readers, YTH domain family members are the first to recognize m⁶A [38], IGF2BPs bind to m⁶A and enhance RNA stability of the target mRNA [23], HNRNPA2B1 mediates the splicing of RNAs and enhances primary miRNA processing [39], and HNRNPC and RBMX regulate the processing of m⁶A-containing RNA transcripts indirectly [40] [41].

In the United States, the estimated number of new patients with kidney and renal pelvis cancer in 2019 was 73,820 (44,120 males and 29,700 females), whereas the estimated death toll was 14,770 (9,820 males and 4,950 females)

[1]. Compared with data from previous years, morbidity and mortality have increased. In China, the number of new patients with renal cancer in 2014 was about 6.8×10^4 (4.3×10^4 males and 2.6×10^4 females) and the estimated death toll was 2.6×10^4 (1.6×10^4 males and 0.9×10^4 females) [42]. At present, the main treatment for kidney cancer is surgery, and an adjuvant therapy, including immunotherapy and chemotherapy, can be chosen according to the disease stage. However, there is a possibility of recurrence to the surgical treatment and some patients are initially refractory to immunotherapy and chemotherapy [43]. Among renal cancers, ccRCC is the main histological subtype, accounting for 75% of all cases [44]. However, compared with other cancers, there are few studies on ccRCC. In



(a)



(b)

FIGURE 7: Random sampling of data in TCGA to validate the accuracy of the signature. (a) Kaplan-Meier overall survival (OS) rate curve of high-risk (red) and low-risk (blue) patients with ccRCC. Data was obtained by random sampling from TCGA. (b) Heat map of clinicopathological features and expression levels of IGF2BP3, IGF2BP2, HNRNPA2B1, and METTL14 genes in the randomly sampled data.

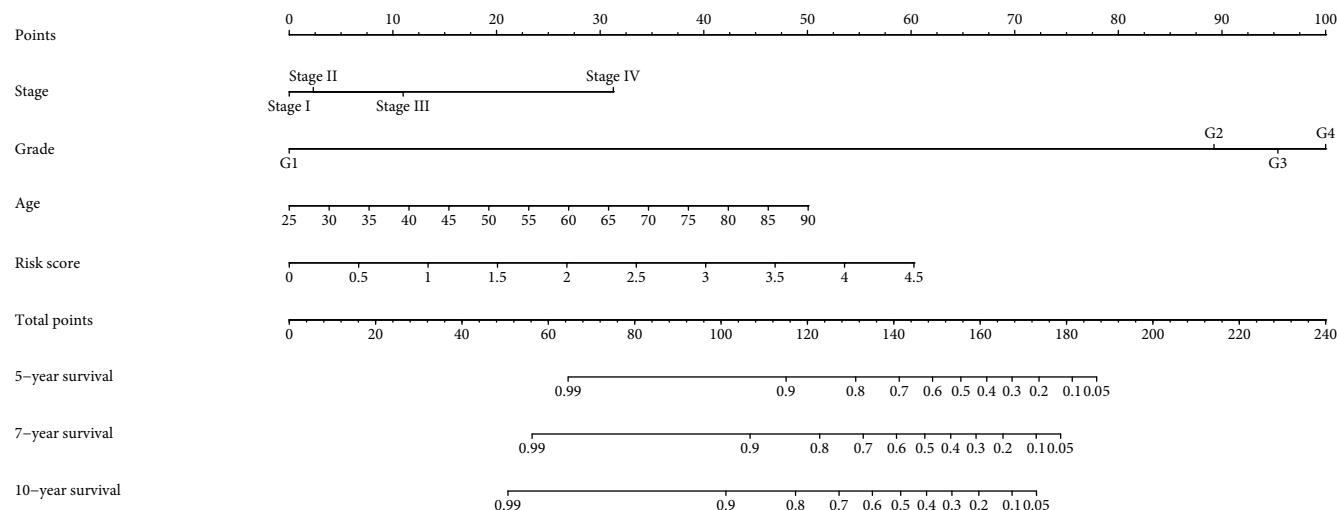


FIGURE 8: Nomogram to predict 5-year, 7-year, and 10-year OS of ccRCC patients.

addition, there are few articles on bioinformatics analyses of ccRCC. In this study, we analyzed a dataset of ccRCC patients from TCGA, grouped the data by consensus clustering, and built a risk signature with m⁶A RNA methylation regulators to predict the prognosis of patients with ccRCC. We hope that this can suggest ideas for future research.

Considering the close relationship between m⁶A and cancer, we wanted to explore the linkage between m⁶A RNA methylation regulators and ccRCC. In this study, 18 m⁶A RNA methylation regulators were chosen. To better understand the important role of m⁶A RNA methylation regulators in ccRCC, we first compared the expression of these regulators in normal and tumor tissues and found that most of them are differentially expressed among both kinds of tissues. Besides, correlation analyses revealed that these 18 regulators interact with each other. Therefore, it is suggested that these 18 m⁶A RNA methylation regulators could either act independently or interactively to play a role in the occurrence and development of ccRCC. To further determine the effects of m⁶A RNA methylation regulators on the clinicopathological characteristics and prognosis of the patients, we separated our data into two groups by consistent clustering. The expression levels of m⁶A RNA methylation regulators in the two clusters were different, and most of the regulators had a higher expression in cluster 2. Moreover, a survival curve showed that cluster 2 had a significantly worse prognosis than cluster 1.

Next, we tried to determine the function of these regulators in ccRCC by integrating their functions in GO, KEGG, and Reactome. We found that they can play roles in DNA repair, RNA splicing, and other physiological processes such as apoptosis, cell cycle, and epithelial mesenchymal transformation (EMT), and even inhibit or activate cell signaling pathways, including the PI3K/Akt pathway. Therefore, we proposed that these regulators affect the occurrence and development of ccRCC by intervening in the above processes. We also determined the drug sensitivities of these regulators, aiming to provide some ideas for future targeted drug research for ccRCC.

To build a risk signature, we used the LASSO Cox regression algorithm over the 18 regulators in the TCGA dataset. We then chose four regulators (IGF2BP3, IGF2BP2, METTL14, and HNRNPA2B1) to build the signature, and separated patients into high-risk and low-risk groups according to it. Characteristically, patients from the high-risk group had a worse prognosis, having increased expression levels of IGF2BP3, IGF2BP2, and HNRNPA2B1 and decreased expression levels of METTL14 compared to those in normal tissues.

The risk signature can be used independently or combined with other indicators to predict patient prognosis. To determine this, the signature was tested against randomly sampled data from TCGA. In these random samples, the prognosis predicted by the signature was found to be in accordance with the actual prognosis of the patients, and the expression levels of the four chosen genes were also consistent with previous results. All these results show that the risk signature can effectively judge the prognosis of patients with ccRCC. We believe that this risk signature can be used to predict the five-year survival rate of patients in the clinical practice. Finally, we enriched the function of the four signature genes in five different pathways; similar to previous results, we found that in patients with ccRCC, these genes play a positive or negative role in many physiological processes.

According to other studies, IGF2BP2 and IGF2BP3 belong to the IGF2BP protein family, formed by IGF2BP1-3. As readers, IGF2BPs recognize GGC sequences and target thousands of mRNA transcripts; they can regulate the stability, translation, and storage of RNA, thereby affecting the expression of genes (recognition of RNA N⁶-methyladenosine by IGF2BP proteins enhances mRNA stability and translation). Huang et al. found that in pancreatic ductal adenocarcinoma, the expression of IGF2BP2 was upregulated and led to a poor outcome [45]. In addition, in patients with acute myelocytic leukemia, the overexpression of IGF2BP2 indicates poor survival, and IGF2BP2 expression is associated with mutations in FLT3-ITD and IDH1, which are also indicators of poor prognosis [46]. These results are consistent with our

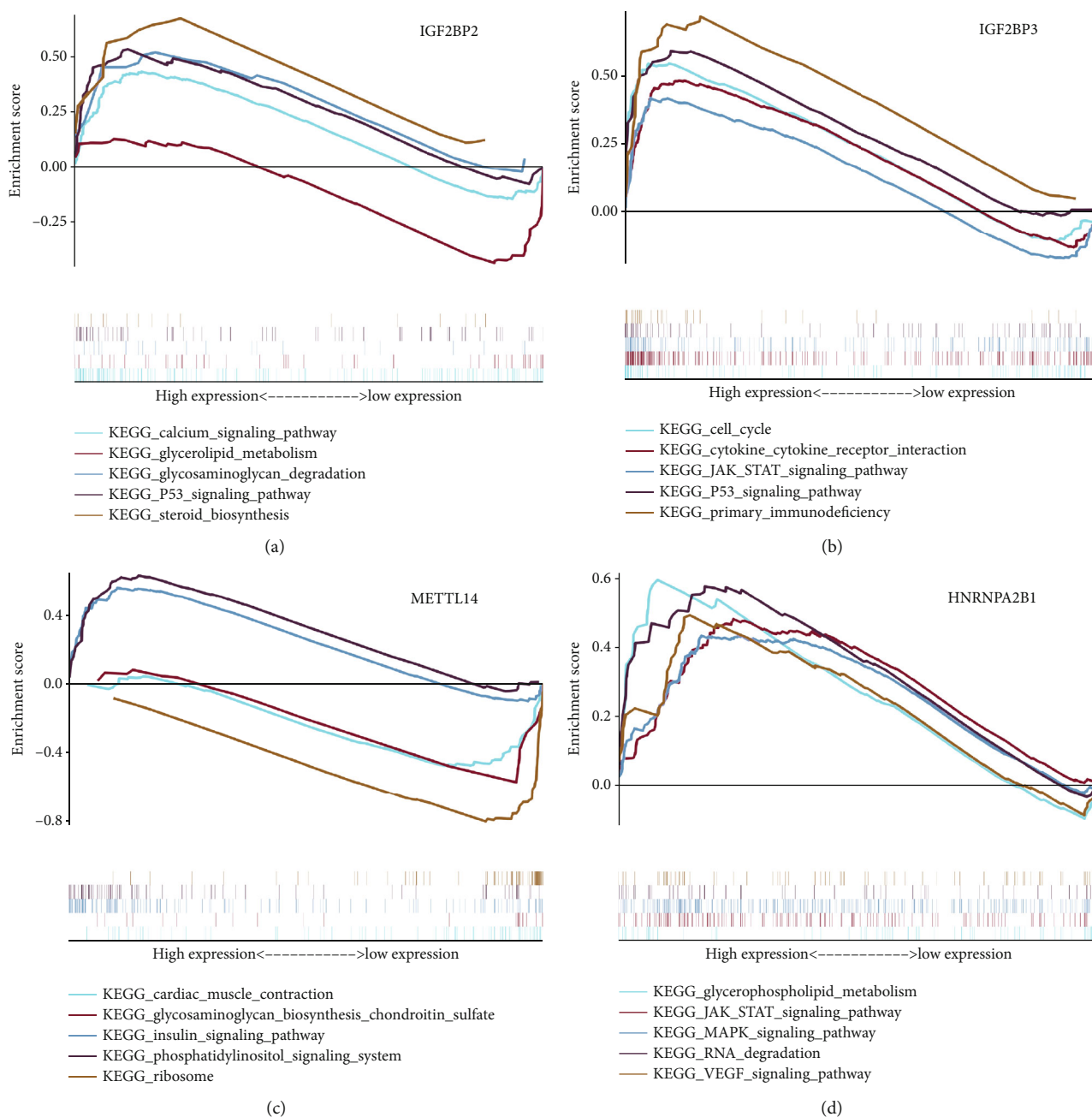


FIGURE 9: GSEA pathway analysis of IGF2BP3, IGF2BP2, HNRNPA2B1, and METTL14 genes. (a–d) An upward parabola indicates that the indicated gene promotes the pointed pathway; otherwise, the pathway is suppressed.

results, that is, IGF2BP2 and IGF2BP3 play a positive regulatory role in the process of tumor occurrence and development. These conclusions are urging us to carry out relevant research to verify whether inhibiting the expression of IGF2BP2 and IGF2BP3 can inhibit the growth of the tumor.

HNRNPA2B1 binds m⁶A-containing sites on nuclear RNAs. HNRNPA2B1 can also regulate alternative splicing of exons in a set of transcripts, similar to METTL3; consequently, METTL3 depletion together with a diminishment in HNRNPA2B1 concentration may have a close correlated impact in the cell [47]. Previous studies have shown that HNRNPA2B1 is overexpressed in breast cancer tissue, and that its encoded protein can activate the STAT3 and

ERK1/2 signaling pathways, thereby promoting the tumorigenic potential of cancer cells. Here, we found that the expression of HNRNPA2B1 in the high-risk group was also significantly increased, and that the prognosis of the group with high levels of this regulator is worse than that of the group with low levels. Therefore, studying the pathways related to this reader and finding possible inhibitors could also be a breach in the treatment of ccRCC.

As a writer, METTL14 plays a role by tightly combining with METTL3. Studies have revealed that METTL14 and ALKBH5 control the expression of each other and inhibit the expression of YTHDF3, thereby blocking RNA demethylation to degrade cancer cells [48]. Compared with studies

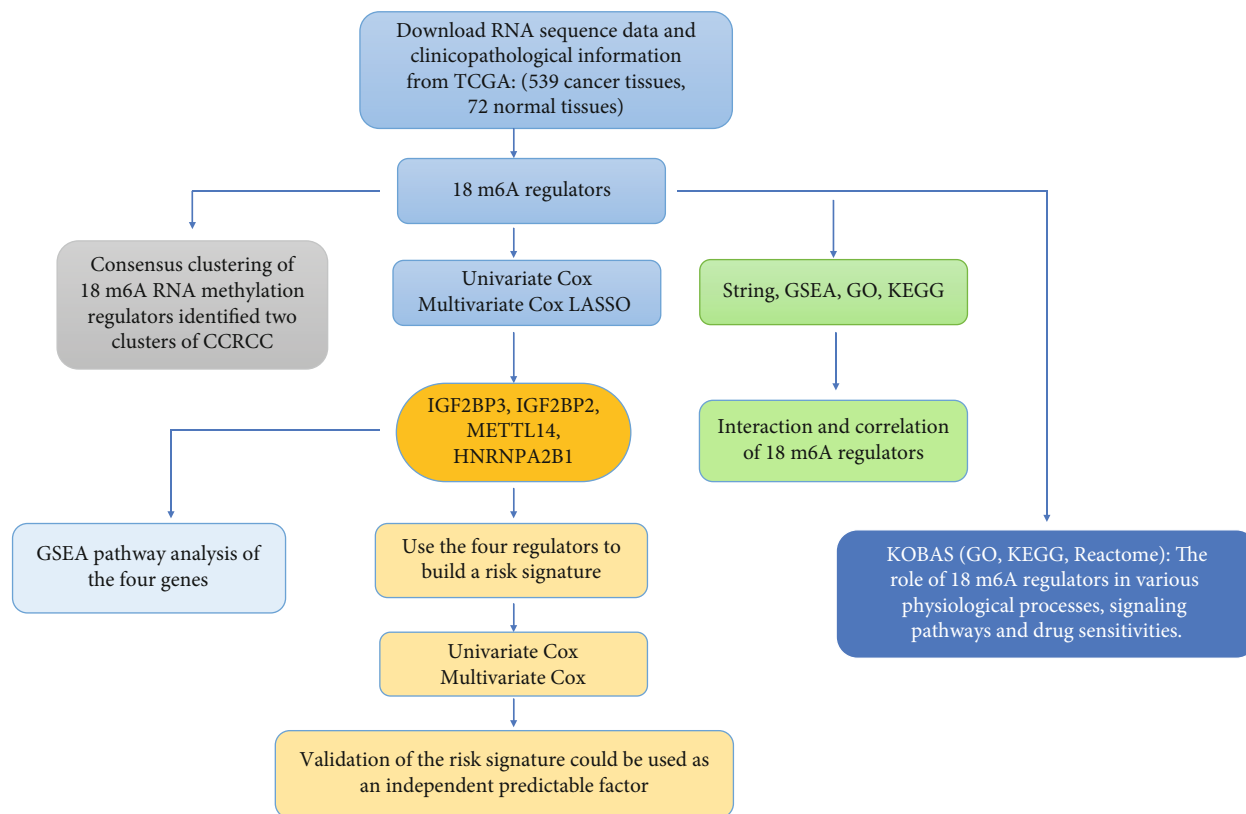


FIGURE 10: The flowchart of this study.

focused in METTL3, research on METTL14 has only been gradually carried out in the last ten years. However, many articles have reported that METTL14 can mediate the self-renewal of HSCs (hematopoietic stem cells) by upregulating the expression of regulators such as BMI-1 and PRDM16 [49]. A study on leukemia also found that METTL14 can block myeloid differentiation and promote the self-renewal of normal HSPCs and LSCs/LICs (leukemia stem cells/leukemia-induced cells) [50]. In addition, downregulation of METTL14 can promote metastasis of liver cancer cells, whereas its overexpression significantly reduces tumor invasion and metastasis (METTL14 suppresses the metastatic potential of hepatocellular carcinoma by modulating N⁶-methyladenosine-dependent primary microRNA processing). These data are consistent with our results that suggest that a high expression of METTL14 can inhibit tumor growth or other harmful physiological processes. Therefore, improving the expression of METTL14 could be an effective therapeutic strategy to treat some diseases.

Although there are few studies on ccRCC and m⁶A, a high expression of IGF2BP2 and IGF2BP3 has been reported in many kinds of tumors. Consequently, it is thought that IGF2BP2 and IGF2BP3 are closely related to the occurrence and development of tumors. In addition, there are few studies about HNRNPA2B1, but according to our results and those from breast cancer studies, we believe that it is also an important regulator that promotes tumorigenesis. METTL14 may inhibit tumor development and metastasis. Compared with normal tissues, its expres-

sion is significantly reduced in tumor tissues; therefore, invasion and metastasis of the tumor are more likely to occur. In the future, we will further explore the relationship between these regulators and the occurrence and development of ccRCC, trying to identify the specific mechanisms that underlie this disease.

This study has some limitations. For example, it only discusses data at the gene and mRNA levels. Overcoming technical problems around the complexity of protein expression modification is needed to further analyze the relation between the selected m⁶A regulators and ccRCC at the protein level. Additionally, the AUC value of the ROC curve just exceeded 0.7; the sample size needs to be increased in the future to further confirm the sensitivity and specificity of this signature. However, we believe that the establishment of this signature will play a great role in predicting the five-year survival rate of patients with ccRCC and improving their treatment. This signature may also be a good starting point for new studies on ccRCC.

5. Conclusion

m⁶A RNA methylation regulators are closely related to the occurrence and development of ccRCC. The newly defined risk signature can predict the prognosis of patients with ccRCC. Regulators used to build the risk signature may also become targets for the diagnosis and treatment of ccRCC.

Abbreviations

RCC:	Renal cell carcinoma
ccRCC:	Clear cell renal cell carcinoma
TCGA:	The Cancer Genome Atlas
ALKBH5:	ALKB homolog 5, RNA demethylase
RBM15B:	RNA-binding motif protein 15B
IGF2BP2:	Insulin-like growth factor 2 mRNA-binding protein 2
HNRNPA2B1:	Heterogeneous nuclear ribonucleoprotein A2/B1
YTHDF2:	YTH N ⁶ -methyladenosine RNA-binding protein 2
METTL4:	Methyltransferase-like 4
ZC3H13:	Zinc finger CCCH-type-containing 13
YTHDF3:	YTH N ⁶ -methyladenosine RNA-binding protein 3
IGF2BP3:	Insulin-like growth factor 2 mRNA-binding protein 3
RBMX:	X-linked RNA-binding motif protein
FTO:	FTO alpha-ketoglutarate-dependent dioxygenase
WTAP:	WT1-associated protein
RBM15:	RNA-binding motif protein 15
YTHDC1:	YTH domain-containing 1
METTL14:	Methyltransferase-like 14
IGF2BP1:	Insulin-like growth factor 2 mRNA-binding protein 1
OS:	Overall survival
DFS:	Disease-free survival.

Data Availability

All data included in this study are available upon request by contact with the corresponding author.

Disclosure

Yan Zhang and Yao Yao are co-first authors. The results (published or shown) here are in whole or part based upon data generated by the TCGA Research Network: <https://www.cancer.gov/tcga>.

Conflicts of Interest

The authors declare that there is no conflict of interests.

Authors' Contributions

Yan Zhang and Yao Yao contributed equally to this work. Guangzhen Wu, Yingkun Xu, and Xiangyu Che conceived and designed this study and revised the manuscript. Yan Zhang and Yao Yao performed the statistical analysis and data interpretation and were major contributors in writing the manuscript. Jianyi Li, Meihong Liu, and Xiaochen Qi revised the manuscript. All authors read and approved the final manuscript.

Acknowledgments

We thank the TCGA project for providing us the data. In addition, Yingkun Xu would also like to thank Jiayi Li for suggestions and assistance in the research process. This project is supported by the Scientific Research Fund of Liaoning Provincial Education Department (No. LZ2020071).

Supplementary Materials

Figure S1: external verification based on the GSE22541 dataset. Table S1: expression of 18 m⁶A RNA methylation regulators between clusters 1 and 2. (*Supplementary Materials*)

References

- [1] R. L. Siegel, K. D. Miller, and A. Jemal, "Cancer statistics, 2019," *CA: a Cancer Journal for Clinicians*, vol. 69, no. 1, pp. 7–34, 2019.
- [2] B. C. Leibovich, C. M. Lohse, P. L. Crispen et al., "Histological subtype is an independent predictor of outcome for patients with renal cell carcinoma," *The Journal of Urology*, vol. 183, no. 4, pp. 1309–1316, 2010.
- [3] L. C. Harshman, T. K. Choueiri, C. Drake, and F. Stephen Hodi, "Subverting the B7-H1/PD-1 pathway in advanced melanoma and kidney cancer," *Cancer Journal*, vol. 20, no. 4, pp. 272–280, 2014.
- [4] R. Desrosiers, K. Friderici, and F. Rottman, "Identification of methylated nucleosides in messenger RNA from Novikoff hepatoma cells," *Proceedings of the National Academy of Sciences of the United States of America*, vol. 71, no. 10, pp. 3971–3975, 1974.
- [5] S. Ke, E. A. Alemu, C. Mertens et al., "A majority of m6A residues are in the last exons, allowing the potential for 3' UTR regulation," *Genes & Development*, vol. 29, no. 19, pp. 2037–2053, 2015.
- [6] K. D. Meyer, Y. Saletore, P. Zumbo, O. Elemento, C. E. Mason, and S. R. Jaffrey, "Comprehensive analysis of mRNA methylation reveals enrichment in 3' UTRs and near stop codons," *Cell*, vol. 149, no. 7, pp. 1635–1646, 2012.
- [7] T. Csepany, A. Lin, C. J. Baldick Jr., and K. Beemon, "Sequence specificity of mRNA N⁶-adenosine methyltransferase," *The Journal of Biological Chemistry*, vol. 265, no. 33, pp. 20117–20122, 1990.
- [8] C. M. Wei and B. Moss, "Nucleotide sequences at the N⁶-methyladenosine sites of HeLa cell messenger ribonucleic acid," *Biochemistry*, vol. 16, no. 8, pp. 1672–1676, 1977.
- [9] K. D. Meyer, D. P. Patil, J. Zhou et al., "5' UTR m⁶A promotes cap-independent translation," *Cell*, vol. 163, no. 4, pp. 999–1010, 2015.
- [10] C. R. Alarcon, H. Lee, H. Goodarzi, N. Halberg, and S. F. Tavazoie, "N⁶-methyladenosine marks primary microRNAs for processing," *Nature*, vol. 519, no. 7544, pp. 482–485, 2015.
- [11] D. P. Patil, C. K. Chen, B. F. Pickering et al., "m⁶A RNA methylation promotes XIST-mediated transcriptional repression," *Nature*, vol. 537, no. 7620, pp. 369–373, 2016.
- [12] L. P. Vu, B. F. Pickering, Y. Cheng et al., "The N⁶-methyladenosine (m⁶A)-forming enzyme METTL3 controls myeloid differentiation of normal hematopoietic and leukemia cells," *Nature Medicine*, vol. 23, no. 11, pp. 1369–1376, 2017.

- [13] M. Chen, L. Wei, C. T. Law et al., "RNA N⁶-methyladenosine methyltransferase-like 3 promotes liver cancer progression through YTHDF2-dependent posttranscriptional silencing of SOCS2," *Hepatology*, vol. 67, no. 6, pp. 2254–2270, 2018.
- [14] J. Liu, D. Ren, Z. Du, H. Wang, H. Zhang, and Y. Jin, "m⁶A demethylase FTO facilitates tumor progression in lung squamous cell carcinoma by regulating MZF1 expression," *Biochemical and Biophysical Research Communications*, vol. 502, no. 4, pp. 456–464, 2018.
- [15] R. Su, L. Dong, C. Li et al., "R-2HG exhibits anti-tumor activity by targeting FTO/m⁶A/MYC/CEBPA signaling," *Cell*, vol. 172, no. 1–2, pp. 90–105.e23, 2018.
- [16] C. Zhang, D. Samanta, H. Lu et al., "Hypoxia induces the breast cancer stem cell phenotype by HIF-dependent and ALKBH5-mediated m⁶A-demethylation of NANOG mRNA," *Proceedings of the National Academy of Sciences of the United States of America*, vol. 113, no. 14, pp. E2047–E2056, 2016.
- [17] Q. Cui, H. Shi, P. Ye et al., "m⁶A RNA methylation regulates the self-renewal and tumorigenesis of glioblastoma stem cells," *Cell Reports*, vol. 18, no. 11, pp. 2622–2634, 2017.
- [18] J. Zhang, H. Tsoi, X. Li et al., "Carbonic anhydrase IV inhibits colon cancer development by inhibiting the Wnt signalling pathway through targeting the WTAP-WT1-TBL1 axis," *Gut*, vol. 65, no. 9, pp. 1482–1493, 2016.
- [19] J. A. Bokar, M. E. Shambaugh, D. Polayes, A. G. Matera, and F. M. Rottman, "Purification and cDNA cloning of the AdoMet-binding subunit of the human mRNA (N⁶-adenosine)-methyltransferase," *RNA*, vol. 3, no. 11, pp. 1233–1247, 1997.
- [20] D. Dai, H. Wang, L. Zhu, H. Jin, and X. Wang, "N⁶-Methyladenosine links RNA metabolism to cancer progression," *Cell Death & Disease*, vol. 9, no. 2, 2018.
- [21] P. J. Batista, "The RNA modification N⁶-methyladenosine and its implications in human disease," *Genomics, Proteomics & Bioinformatics*, vol. 15, no. 3, pp. 154–163, 2017.
- [22] C. Xu, K. Liu, H. Ahmed, P. Loppnau, M. Schapira, and J. Min, "Structural basis for the discriminative recognition of N⁶-methyladenosine RNA by the human YT521-B homology domain family of proteins," *The Journal of Biological Chemistry*, vol. 290, no. 41, pp. 24902–24913, 2015.
- [23] H. Huang, H. Weng, W. Sun et al., "Recognition of RNA N⁶-methyladenosine by IGF2BP proteins enhances mRNA stability and translation," *Nature Cell Biology*, vol. 20, no. 3, pp. 285–295, 2018.
- [24] B. S. Zhao, I. A. Roundtree, and C. He, "Post-transcriptional gene regulation by mRNA modifications," *Nature Reviews. Molecular Cell Biology*, vol. 18, no. 1, pp. 31–42, 2017.
- [25] A. Nagy, A. Lanczky, O. Menyhart, and B. Gyorfy, "Validation of miRNA prognostic power in hepatocellular carcinoma using expression data of independent datasets," *Scientific reports*, vol. 8, no. 1, article 9227, 2018.
- [26] J. Chen, Y. Sun, X. Xu et al., "YTH domain family 2 orchestrates epithelial-mesenchymal transition/proliferation dichotomy in pancreatic cancer cells," *Cell Cycle*, vol. 16, no. 23, pp. 2259–2271, 2017.
- [27] X. Cai, X. Wang, C. Cao et al., "HBXIP-elevated methyltransferase METTL3 promotes the progression of breast cancer via inhibiting tumor suppressor let-7g," *Cancer Letters*, vol. 415, pp. 11–19, 2018.
- [28] H. Bansal, Q. Yihua, S. P. Iyer et al., "WTAP is a novel oncogenic protein in acute myeloid leukemia," *Leukemia*, vol. 28, no. 5, pp. 1171–1174, 2014.
- [29] L. Yang, Y. Ma, W. Han et al., "Proteinase-activated receptor 2 promotes cancer cell migration through RNA methylation-mediated repression of miR-125b," *The Journal of Biological Chemistry*, vol. 290, no. 44, pp. 26627–26637, 2015.
- [30] H. B. Li, J. Tong, S. Zhu et al., "m⁶A mRNA methylation controls T cell homeostasis by targeting the IL-7/STAT5/SOCS pathways," *Nature*, vol. 548, no. 7667, pp. 338–342, 2017.
- [31] P. Wang, K. A. Doxtader, and Y. Nam, "Structural basis for cooperative function of Mettl3 and Mettl14 methyltransferases," *Molecular Cell*, vol. 63, no. 2, pp. 306–317, 2016.
- [32] X. L. Ping, B. F. Sun, L. Wang et al., "Mammalian WTAP is a regulatory subunit of the RNA N⁶-methyladenosine methyltransferase," *Cell Research*, vol. 24, no. 2, pp. 177–189, 2014.
- [33] S. Zhang, "Mechanism of N⁶-methyladenosine modification and its emerging role in cancer," *Pharmacology & Therapeutics*, vol. 189, pp. 173–183, 2018.
- [34] P. Knuckles, T. Lence, I. U. Haussmann et al., "Zc3h13/Flacc is required for adenosine methylation by bridging the mRNA-binding factor Rbm15/Spenito to the m⁶A machinery component Wtap/Fl(2)d," *Genes & Development*, vol. 32, no. 5–6, pp. 415–429, 2018.
- [35] S. Schwartz, M. R. Mumbach, M. Jovanovic et al., "Perturbation of m⁶A writers reveals two distinct classes of mRNA methylation at internal and 5' sites," *Cell Reports*, vol. 8, no. 1, pp. 284–296, 2014.
- [36] X. Zhao, Y. Yang, B. F. Sun et al., "FTO-dependent demethylation of N⁶-methyladenosine regulates mRNA splicing and is required for adipogenesis," *Cell Research*, vol. 24, no. 12, pp. 1403–1419, 2014.
- [37] C. Tang, R. Klukovich, H. Peng et al., "ALKBH5-dependent m⁶A demethylation controls splicing and stability of long 3' UTR mRNAs in male germ cells," *Proceedings of the National Academy of Sciences of the United States of America*, vol. 115, no. 2, pp. E325–E333, 2018.
- [38] S. Liao, H. Sun, and C. Xu, "YTH domain: a family of N⁶-methyladenosine (m⁶A) readers," *Genomics, Proteomics & Bioinformatics*, vol. 16, no. 2, pp. 99–107, 2018.
- [39] C. R. Alarcon, H. Goodarzi, H. Lee, X. Liu, S. Tavazoie, and S. F. Tavazoie, "HNRNPA2B1 is a mediator of m⁶A-dependent nuclear RNA processing events," *Cell*, vol. 162, no. 6, pp. 1299–1308, 2015.
- [40] N. Liu, K. I. Zhou, M. Parisien, Q. Dai, L. Diatchenko, and T. Pan, "N⁶-Methyladenosine alters RNA structure to regulate binding of a low-complexity protein," *Nucleic Acids Research*, vol. 45, no. 10, pp. 6051–6063, 2017.
- [41] N. Liu, Q. Dai, G. Zheng, C. He, M. Parisien, and T. Pan, "N⁶-Methyladenosine-dependent RNA structural switches regulate RNA-protein interactions," *Nature*, vol. 518, no. 7540, pp. 560–564, 2015.
- [42] W. Chen, K. Sun, R. Zheng et al., "Cancer incidence and mortality in China, 2014," *Chinese Journal of Cancer Research*, vol. 30, no. 1, pp. 1–12, 2018.
- [43] K. Tamura, M. Horikawa, S. Sato, H. Miyake, and M. Setou, "Discovery of lipid biomarkers correlated with disease progression in clear cell renal cell carcinoma using desorption electrospray ionization imaging mass spectrometry," *Oncotarget*, vol. 10, no. 18, pp. 1688–1703, 2019.

- [44] A. Lopez-Beltran, M. Scarpelli, R. Montironi, and Z. Kirkali, "2004 WHO classification of the renal tumors of the adults," *European Urology*, vol. 49, no. 5, pp. 798–805, 2006.
- [45] S. Huang, Z. Wu, Y. Cheng, W. Wei, and L. Hao, "Insulin-like growth factor 2 mRNA binding protein 2 promotes aerobic glycolysis and cell proliferation in pancreatic ductal adenocarcinoma via stabilizing *GLUT1* mRNA," *Acta Biochimica et Biophysica Sinica*, vol. 51, no. 7, pp. 743–752, 2019.
- [46] X. He, W. Li, X. Liang et al., "IGF2BP2 overexpression indicates poor survival in patients with acute myelocytic leukemia," *Cellular Physiology and Biochemistry*, vol. 51, no. 4, pp. 1945–1956, 2018.
- [47] X. Y. Chen, J. Zhang, and J. S. Zhu, "The role of m⁶A RNA methylation in human cancer," *Molecular Cancer*, vol. 18, no. 1, 2019.
- [48] S. Panneerdoss, V. K. Eedunuri, P. Yadav et al., "Cross-talk among writers, readers, and erasers of m⁶A regulates cancer growth and progression," *Science Advances*, vol. 4, no. 10, article eaar8263, 2018.
- [49] Q. J. Yao, L. Sang, M. Lin et al., "Mettl3-Mettl14 methyltransferase complex regulates the quiescence of adult hematopoietic stem cells," *Cell Research*, vol. 28, no. 9, pp. 952–954, 2018.
- [50] H. Weng, H. Huang, H. Wu et al., "METTL14 inhibits hematopoietic stem/progenitor differentiation and promotes leukemogenesis via mRNA m⁶A modification," *Cell Stem Cell*, vol. 22, no. 2, pp. 191–205.e9, 2018.